THE UNIVERSITY
of EDINBURGH

The role of the structural organisation of pericentromeres in chromosome segregation in budding yeast

Flora Paldi

Thesis for the degree of Doctor of Philosophy

The University of Edinburgh

2020

Declaration

I declare that this thesis has been composed by myself and the work presented within is entirely my own unless indicated otherwise by refence or acknowledgement. This work has not been submitted for any other degree or professional qualification.

Flora Paldi
2020

Acknowledgements

First, I would like to acknowledge Wellcome for funding my 4-year PhD at the Wellcome Centre for Cell Biology. I would like to thank Adele for offering me the opportunity to complete my PhD in her lab and entrusting me with this exciting project. It was a pleasure to see this project evolving. I am also grateful for her support and the scientific freedom that I received during my years in the Marston lab.

I would also like to extend my gratitude to Bonnie Alver who did the initial experiments for this project, as well as my collaborators at the University of Sussex, Stephanie Schalbetter, Jon Baxter and Matt Neale, who helped me to get started with Hi-C. I am extremely grateful to Daniel Robertson in our bioinformatics core facility who did all the bioinformatics, and dealt with this project with infinite patience throughout the years. Also thanks to Dave Kelly in COIL who made my life easier by writing a macro for my image analysis.

Thanks must go to all current and former members of the Marston lab who were always supportive, and to all my friends for all the fun we had. I would like to particularly thank my dear bench neighbours, Wera and Rachael, who were always there when I was in need for scientific advice or friendly counselling, as well as Stefan who I missed every day after he left.

I would like to extend my sincere appreciation to my wonderful partner Pierre who supported and encouraged me every single day of this PhD. The infinite discussions in lunch breaks, evenings and weekends were invaluable in driving this project forward and guiding me during my degree. I am also grateful for all the fun we had which helped me to do my best every day.

Last but not least, I am extremely thankful for my entire family for their endless support through my life, I am immensely lucky to be surrounded by so much love. I am particularly grateful to my parents for raising me the way they did, and teaching me what honestly, integrity and hard work meant. Anyu, Apu, Blanki and Mamu, I could have never done this without you.

Abstract

Genome maintenance, function and transmission requires the adequate structural organisation of chromosomes. Central to this is the conserved ring-shaped protein complex, cohesin, that associates with chromosomes. The property to engage more than one DNA fragment simultaneously allows cohesin to structure chromosomes by linking distant chromosomal loci, as well as to provide cohesion during cell division by co-entrapping replicated sister chromatids. Notably, cohesin is concentrated on chromosomes at specialised chromosomal domains flanking centromeres, called pericentromeres. Pericentromeric cohesin enrichment is instrumental for the biorientation of sister chromatids which in turn is a requisite for accurate chromosome segregation. Although the significance of high pericentromeric cohesin density has been widely studied in budding yeast, the structural organisation of pericentromeres and its implications for chromosome segregation are unknown. This study reports the 3D organisation of budding yeast pericentromeres and its function in chromosome segregation. Centromeres along with centromere-flanking convergent gene pairs structure pericentromeres by loading and restricting cohesin to the pericentromere, respectively. Each side of the pericentromere folds into a separate loop which are then extended into a single open loop by microtubules attaching to kinetochores. In the absence of convergent genes cohesin is repositioned, the pericentromere is enlarged and this leads to impairment in chromosome biorientation. Thus, pericentromere structure that makes budding yeast chromosomes competent for their segregation, is defined by the arrangement of transcriptional units and high cohesin density. Importantly, these results indicate that there is a direct, causal relationship between the 3D organization of a specific chromosomal domain and cellular function.

Lay Summary

All form of life relies on self-propagation by cell division. Key to successful cell division is the proper inheritance of genes necessary for life, that are organized into chromosomes. During cell division, chromosomes are duplicated and equally partitioned between the two new cells. To produce healthy cells, it is essential that both cells inherit a single copy of each chromosome. Errors in this process are linked to a range of medical conditions, such as developmental defects or cancer. When chromosomes duplicate, the two copies, called sister chromatids, become linked. This ensures that they stay together until the cellular machinery is ready to distribute them between daughter cells. The linkage is provided by a protein complex called cohesin. Most cohesin on chromosomes is present around centromeres, regions that are physically contacted by the chromosome segregation apparatus. Through structural constraints, cohesin around centromeres facilitates the mechanical coupling of sister chromatids and the chromosome segregation machinery.

In this study, I use budding yeast to map the extent and behavior of cohesin around centromeres, and decipher changes in the structure of chromosomes when the segregation machinery makes contacts with them. Interestingly, I find that in addition to cohesin, genes present on chromosomes contribute to this specific chromosome structure. Genes on chromosomes have an arrangement and a directionality, with a start and an end. Turning genes around (without interfering with their genetic function) changes their directionality on chromosomes, and it was found that this changes the structure of chromosomes. Importantly, we link these changes in structure to alterations in cohesin distribution around centromeres as well as defects during cell division. Altogether this indicates that genes, which are functional elements of chromosomes, are arranged in a specific way so that they support proper chromosome partitioning during cell division.

Abbreviations

APC/C	Anaphase promoting complex / Cyclosome
BSA	Bovine serum albumin
bp	base pair
CEN	centromere
Cdk	Cyclin-dependent kinase
ChIP	Chromatin immunoprecipitation
CPC	Chromosome Passenger Complex
CRAC	UV crosslinking and analysis of cDNA
CRISPR	Clustered regularly interspaced short palindromic repeats
CTCF	CCCTC-binding factor
C-terminal	Carboxy-terminal
DAPI	4',6-diamidino-2-phenylindole
DDK	Dbf4-dependent kinase
DNA	Deoxyribonucleic acid
DTT	Dithioreitol
E. coli	*Escherichia coli*
EDTA	Ethylenediaminetetraacetic acid
GFP	Green Fluorescent Protein

gRNA	Guide RNA
IP	Immunoprecipitate
kb	Kilobase
KMN	KNL-1 Mis12 Ndc80
LB	Luria-Bertani
Mb	Megabase
MBF	Mlu I cell cycle box binding factor
NGS	Next generation sequencing
N-terminal	Amino-terminal
OD	Optical density
ORF	Open reading frame
PBS	Phosphate buffer saline
PCR	Polymerase chain reaction
PEG	Polyethylene glycol
qPCR	Quantitative PCR
rDNA	Ribosomal DNA
RNA	Ribonucleic acid
RPM	Reads per million
S. cerevisiae	*Saccharomyces cerevisiae*
S. pombe	*Schizosaccharomyces pombe*

SAC	Spindle Assembly Checkpoint
SBF	Swi4/6 cell cycle box binding factor
SDS	Sodium dodecyl sulphate
s.e.m.	Standard error of the mean
SMC	Structural Maintenance of Chromosomes
SOC	Super Optimal Broth with Catabolite Repression
SPB	Spindle Pole Body
TAD	Topologically associated domain

Contents

Chapter 1 Introduction

1.1 The cell division cycle

Cell division is a process that provides means for growth and reproduction through all domains of life. Unicellular organisms can reproduce through a single cell division, while in multicellular organisms, cell division underpins growth and maintenance. When cells divide, they undergo the cell cycle, a series of well-orchestrated events that are broadly conserved through evolution. The explicit regulation of the cell cycle ensures that the process runs error-free which is essential for organism survival.

1.1.1 Entering the cell cycle

Cells can exist in replicative and non-replicative states. Quiescence, or G0 phase describes a state outside the replicative cell cycle, from which most cells can re-enter proliferation. Entry to the cell cycle is usually triggered by environmental factors such as nutrient availability, or external stimuli. When a cell enters the mitotic cell cycle it goes through a series of events that produce two identical daughter cells from the parent cell.

Generally, cell division can be divided into well-defined stages that are temporally separated: the duplication of genetic material, its subsequent partitioning into daughter cells, and the intervening gap phases. Cells can enter the cell cycle from a G0 state or directly following the end of the previous cell cycle. Conversely, at the end of the cell cycle, cells can exit the replicative state to go into G0, or proceed directly into the next cell cycle.

However, when cells enter the cell cycle, a commitment is made for progression through the entire length of it. When undergoing the cell cycle, progression is restricted to cells that fulfilled specific requirements to enter the subsequent phase. This is governed by checkpoints, elaborate molecular

mechanisms that ensure the error-free and unidirectional progression of the cell cycle. Reliable and precise coordination of cell cycle events is essential to avoid uncontrolled growth or cell death, both of which are associated with a number of human conditions.

1.1.2 Stages of the mitotic cell cycle

The mitotic cell cycle starts with the G1 phase ('Gap 1'), during which cellular material in synthesised in preparation for the subsequent cell cycle events. Importantly, at the end of G1, cells pass the G1/S checkpoint where they commit to progression through the cell cycle. G1 is followed by S-phase ('Synthesis') which involves the replication of the cell's DNA content that is organised into chromosomes. DNA replication starts simultaneously at multiple replication origins on each chromosome and proceeds bidirectionally. The product of S-phase is two copies of replicated chromosomes called sister chromatids. Generally, S-phase is followed by a second gap phase G2, a period of rapid growth and protein synthesis which prepares cells for mitosis. From G2, progression into mitosis happens on the condition of passing the G2/M checkpoint, which ensures that all chromosomes are intact and no DNA damage persists (reviewed in Morgan, 2007).

During M-phase ('Mitosis'), the final stage of the cell cycle, two major events occur. First, a nuclear division partitions sister chromatids. Sister chromatid segregation is implemented by the mitotic spindle apparatus, a macromolecular machinery composed of microtubules that makes physical contacts with chromosomes. The establishment of correct contacts between sister chromatids and spindle microtubules is monitored by a third major checkpoint, the spindle assembly checkpoint (SAC). When the SAC is satisfied, chromosome segregation is triggered and cytokinesis, the second M-phase event is initiated. During cytokinesis, the cytoplasm is divided, physically separating the cellular content of daughter cells. This completes the cell cycle.

Mitosis, the process of nuclear division, can be further divided into five major stages. Mitosis starts with prophase which is marked by the condensation of

chromosomes. Prophase is followed by metaphase, when chromosomes get captured by spindle microtubules. Subsequently, in anaphase sister chromatids are pulled apart to opposite sides of the cell. Mitosis ends with telophase where the effects of prophase are reversed, and chromosomes decondense (reviewed in Morgan, 2007).

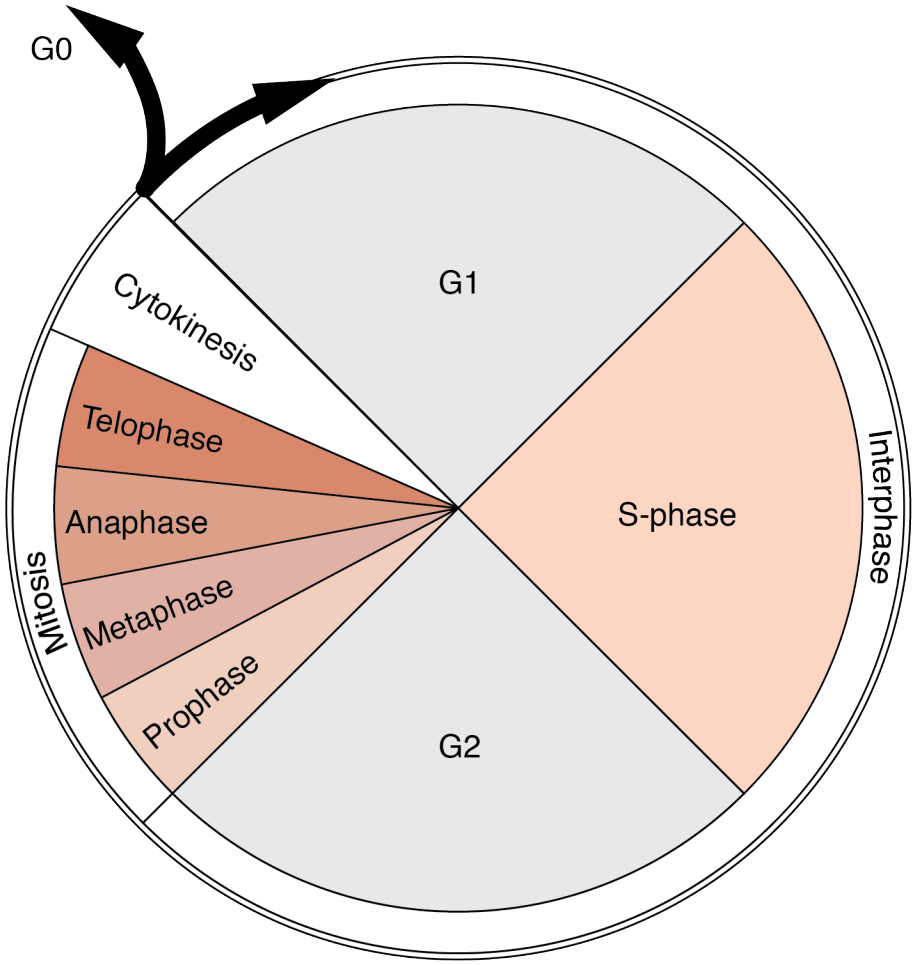

Figure 1.1.2.1 - Stages of the eukaryotic cell cycle - Cell cycle progresses as follows: G1, S-phase, G2 and M-phase. M-phase can be further divided to mitosis and cytokinesis. Mitosis has well-defined sub-stages which are prophase, metaphase, anaphase and telophase. At the end of the cell cycle, nascent cells can either enter the next cell cycle or a quiescent (G0) stage.

1.1.3 Cell cycle regulation

Biochemically, the cell cycle is regulated by the activity of cyclin-dependent kinases (CDKs). Changes in the enzymatic activity of CDKs lead to different phosphorylation and thus activation states of substrates that control cell cycle processes. Substrate specificity and CDK activity is controlled through the orderly synthesis and degradation of a set of regulatory subunits called cyclins. Different cyclin-CDK complex are sequentially formed throughout the cell cycle, each of which is temporarily restricted to a specific stage where it promotes the activation of the next cyclin-CDK complex in sequence. In addition to cyclin availability, CDK activity is further controlled by inhibitory and activating phosphorylation events, as well as changes in CDK inhibitor levels. Overall, these regulatory mechanisms result in a robust and interconnected signalling system that generates switch-like activation and inactivation events at appropriate times, and thereby ensure irreversible and unidirectional progression through the cell cycle.

1.1.3.1 The budding yeast cell cycle

In the unicellular eukaryote, budding yeast (*Saccharomyces cerevisiae*), mitosis provides the means for asexual reproduction. In budding yeast, a single CDK, Cdc28, controls both the G1-S and G2-M transitions. At the beginning of the cell cycle, triggered by nutrient availability and metabolic processes, the synthesis of Cln3 begins leading to the formation of the G1 cyclin-CDK complex, Cln3-Cdc28. Cln3-Cdc28 phosphorylates the inhibitory Whi5, relieving the inhibition of SBF (SCB-binding factor), a transcription factor that binds SCB sequences in the promoters of G1/S cyclins. In parallel, Cln3-Cdc28 activates another transcription factor MBF. These two events lead to the expression of G1/S cyclins Cln1 and Cln2, and S-phase cyclins Clb5 and Clb6, and promote irreversible entry into S-phase (Nasmyth, 1996).

Active G1/S-CDKs promote the duplication of the microtubule-organising centres (called spindle pole bodies (SPBs) in budding yeast), later required for the assembly of the mitotic spindle. Produced already at G1, S-CDKs are held

inactive by the inhibitory protein Sic1. Rising G1/S-CDK activity results in multisite phosphorylation of Sic1 which in turn triggers its degradation, releasing the S-CDKs from inhibition. Importantly, G1/S- and S-CDKs are responsible for the inactivation of the anaphase promoting complex or cyclosome (APC/C) through the phosphorylation of its coactivator subunit, Cdh1. APC/C^{Cdh1} inactivation in G1/S prevents the degradation of mitotic cyclins that are required for later stages of the cell cycle (Nasmyth, 1996).

S-CDKs are responsible for triggering the initiation of DNA replication, further promoting SPB duplication, and inhibiting SBF and MBF to stop the production of G1/S cyclins. Initiation of DNA replication happens through Clb5/Clb6-Cdc28-dependent phosphorylation of preinitiation complexes that assemble on existing pre-replicative complexes (pre-RCs) interspersed on chromosomes. Simultaneously, APC/C^{Cdh1} inactivation result in the gradual accumulation M-phase cyclins. This activates the Mcm1-Fkh transcription factor which in turn activates the expression of mitotic genes including the M-phase cyclins Clb1 and Clb2 (Nasmyth, 1996).

In the budding yeast cell cycle G2 is virtually absent and S-phase is followed directly by M-phase. The activity of M-CDKs rises throughout S-phase and peaks at mid-M-phase. When the cell reaches metaphase, M-CDKs phosphorylate the APC/C which stimulates the binding of its second co-activator Cdc20. The active APC/C^{Cdc20} complex triggers chromosome segregation, as well as the destruction of S- and M-phase cyclins and promotes its own inactivation. This renders APC/C^{Cdc20} inactive by the end of the cell cycle, and the decrease in cyclin-CDK activity restores inhibition by APC/C^{Cdh1}, Sic1 and Whi5 (Nasmyth, 1996).

1.1.3.2 The metazoan cell cycle

Similar principles govern the metazoan cell cycle: although signalling network components do not always share sequence homology, signalling network architecture is strikingly akin to that of budding yeast (Harashima et al., 2013). However, in general while the CDK-cyclin repertoire of yeast is fairly small, in

metazoans this gene family has undergone significant expansion and functional specification. It is thought that the resulting additional regulatory feedback loops and increased complexity might have been necessary to meet novel challenges associated with multicellularity.

1.2 The cohesin complex

1.2.1 The role of cohesin in cell division

The central function of mitosis is the transmission of a full complement of chromosomes to each daughter cell. This is achieved through the linkage of sister chromatids which allows the recognition of replication products as entities to be partitioned between daughter cells. Linkage is provided by the cohesin complex which holds sister chromatids together from their synthesis until their segregation: cohesin loading onto chromosomes is initiated in late G1, and sister chromatid cohesion persist until cohesin removal is triggered at anaphase onset.

1.2.1.1 The cohesin ring

The existence of molecular linkages that hold replicated chromosomes together when cells divide was speculated as early as the 1980s (Koshland and Hartwell, 1987). A decade later, genetic screens for mutants defective in sister chromatid cohesion identified members of the cohesin complex as chromosomal proteins that prevent the premature separation of sister chromatids (Guacci et al., 1997; Michaelis et al., 1997).

Core cohesin proteins assemble into a ring-shaped complex that is composed of two structural maintenance of chromosomes (SMC) proteins Smc1 and Smc3, and a kleisin subunit Scc1 (Figure 1.2.1.1.1). SMC proteins have a conserved domain structure: a globular head domain with ATPase activity composed of the N and C termini, a central hinge domain where the molecule folds back on itself, and a long intramolecular antiparallel coiled-coil that thus forms between the head and the hinge. Importantly, the hinge domains of Smc1 and Smc3 associate to form a V-shaped heterodimer (Haering et al., 2002). Additionally, the kleisin subunit Scc1 interacts with both Smc1 and Smc3, linking the two ATPase head domains. Through these interactions Smc1, Smc3 and Scc1 create the tripartite cohesin ring both *in vitro* (Haering et al., 2002) and *in vivo* (Gruber et al., 2003), where the long stretches of

coiled-coil make up most of the ring circumference. In addition to the interactions that make up the tripartite ring, the SMC heads can also interact. This suggests that two compartments form within the cohesin complex: a large lumen between Smc1 and Smc3 (S compartment), and a small compartment between the SMC heads and the kleisin subunit Scc1 (K compartment) (Chapard et al., 2019).

In the cohesin complex, ATP binding and hydrolysis drive conformational changes that create distinct configurations of the SMC heads. In the ATP-bound state SMC heads are in an engaged (E heads) configuration, while in the absence of ATP, the SMC heads rotate and adopt a juxtaposed (J heads) configuration (Diebold-Durand et al., 2017; Chapard et al., 2019). Although their precise significance is not fully understood, these conformational changes likely underlie certain aspects of cohesin behaviour.

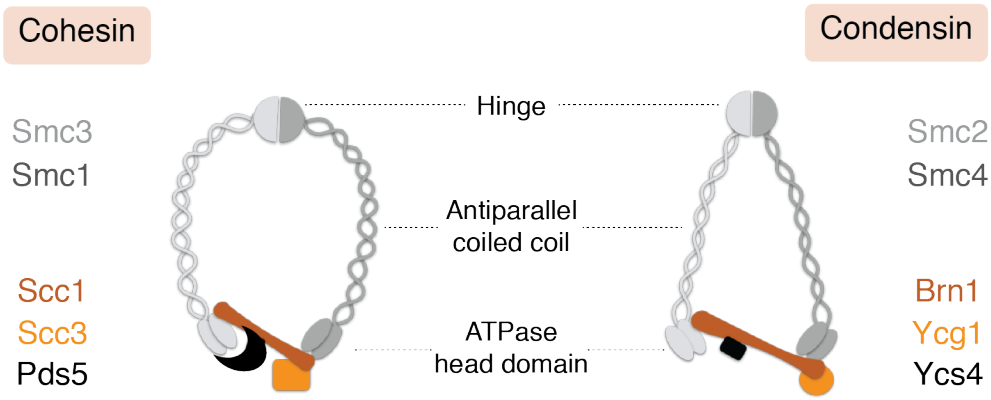

Figure 1.2.1.1.1 - Structure of cohesin and condensin in budding yeast - Two SMC complexes heterodimerise via their hinge domains.The kleisin subunit (Scc1 for cohesin, Brn1 for condensin) makes asymmetric contacts with the globular ATPase head domain of SMCs to form a tripartite ring. Both complexes have additional associated subunits but their arrangement within the complex is not well defined.

In addition to the SMC proteins and the kleisin subunit, the cohesin complex contains two accessory subunits that modulate cohesin's interaction with

regulatory proteins: Scc3 (Tóth et al., 1999) and Pds5 (Hartman et al., 2000). Although Scc3 and Pds5 are not part of the structural tripartite ring, they associate with Scc1 and are essential for sister chromatid cohesion in budding yeast. Unlike budding yeast, higher eukaryotes have two Scc3 homologs (SA1 and SA2) as well as two Pds5 homologs (Pds5A and Pds5B) which can form different cohesin complexes with the members of the tripartite ring (Losada et al., 2000; Sumara et al., 2000). Vertebrate cohesin complexes containing the different Scc3 isoforms show distinct distribution along chromosomes, suggestive of functional differences between the two complexes (Canudas and Smith, 2009; Kojic et al., 2018).

1.2.1.2 Topological linkage and ring opening

As Smc1, Smc3 and Scc1 form a tripartite ring it has been proposed that cohesin hold sister chromatids together by a topological embrace (Haering et al., 2002; Gruber et al., 2003). First, it was shown using circular minichromosomes in yeast, that the cohesin-DNA interaction can be disrupted either by proteolytic cleavage or DNA linearization, indicating that the cohesin ring can trap DNA (Ivanov and Nasmyth, 2005). Later, it was shown that when the cohesin ring is covalently closed through chemical crosslinking, dimeric DNA-protein complexes can be purified that persist even in denaturing conditions (Haering et al., 2008). Dimeric DNA molecules could be converted to monomers by the proteolytic cleavage of the closed cohesin ring, demonstrating that a cohesin ring can trap two DNA molecules. This was also confirmed to be true *in vivo* (Gligoris et al., 2014), suggesting that cohesin indeed holds sister chromatids together by topologically encircling them. Interestingly, it appears that the entrapment of both single and sister DNA molecules happens in the small (K) compartment within the cohesin ring, that forms between the SMC heads and the kleisin subunit (Figure 1.2.1.2.1). However, while single DNA molecules can be entrapped of K compartments of both E and J heads, sister DNA molecules are entrapped in J-K compartments, suggesting that sister DNA entrapment in J-K might be the feature of sister chromatid cohesion (Chapard et al., 2019).

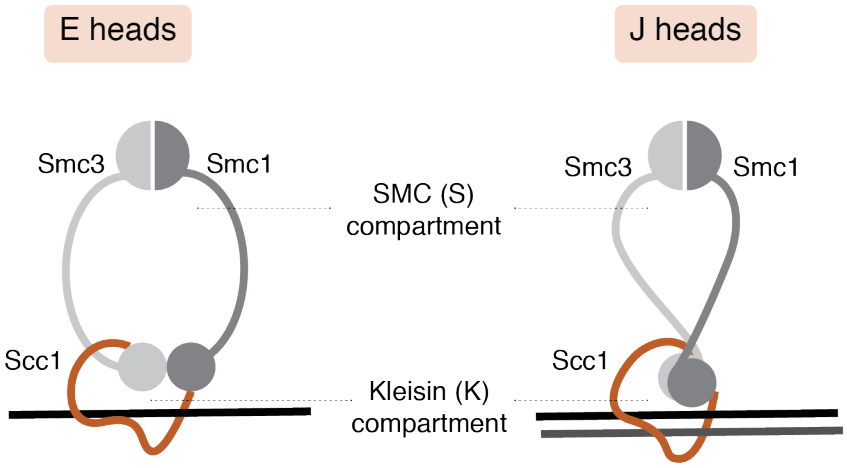

Figure 1.2.1.2.1 - SMC head configurations in the cohesin complex - In the presence of ATP, SMC heads adopt an engaged (E heads) configuration. In the absence of ATP, the SMC heads rotate into a juxtaposed (J heads) state. Single DNA molecules can be entrapped in the K compartment of both E and J heads, while sister DNA entrapment happens in K compartment associated with J heads.

How do DNA strands get inside the cohesin ring? The embrace model postulates a ring-opening mechanism for the cohesin complex. Although cohesin association with chromosomes is known to require ATP hydrolysis at the Smc1/Smc3 head domains (Arumugam et al., 2006), it still debated whether the entry of DNA into the cohesin ring happens at the head interface (Murayama and Uhlmann, 2015; Marcos-Alcalde et al., 2017) or at the Smc1-Smc3 hinge interface (Gruber et al., 2006). Most recent evidence suggests that the opening of cohesin ring upon its association with DNA might happen through ATP-hydrolysis in the head domain, that in turn induces conformational changes in the hinge domain (Srinivasan et al., 2018).

1.2.1.3 Cohesin loading onto chromosomes

Cohesin association with chromosomes depends on the cohesin loading complex comprising Scc2 and Scc4 (Ciosk et al., 2000). The interaction between the cohesin complex with its loader requires the presence of the Scc3 subunit (Hu et al., 2011) and the assembly of the full cohesin ring (Fernius et al., 2013). In mammalian cells, cohesin loading onto chromosomes begins during telophase of the previous cell cycle, in manner that is dependent on the

Scc2/4 orthologs, Nipbl/Mau2 (Darwiche et al., 1999; Krantz et al., 2004; Tonkin et al., 2004; Gerlich et al., 2006). In contrast, in budding yeast, Scc1 production is limited to G1 which restricts cohesin loading to after its synthesis. Once made, Scc1 binds to Scc2, which mediates the interaction of the cohesin complex with DNA (Onn and Koshland, 2011; Murayama and Uhlmann, 2014), and stimulates cohesin's ATPase activity (Hu et al., 2015). As a consequence, cohesin is loaded onto chromosomes through ATP hydrolysis by the Smc1 and Smc3 head domain (Arumugam et al., 2003), leading to the opening of the Smc1/Smc3 hinge interface (Gruber et al., 2006; Srinivasan et al., 2018). After the loading reaction is complete, the loader dissociates from chromosomes while cohesin remains bound, as suggested by the rapid turnover of Scc2 on chromosomes (Hu et al., 2011). Concomitantly, Pds5 associates with Scc1, replacing Scc2 (Petela et al., 2018).

Besides mediating cohesin loading onto chromosomes, Scc2/4 also determines the chromosomal sites for cohesin loading. Interestingly, cohesin's loading and distribution on chromosomes is not dictated by specific DNA sequences (Onn and Koshland, 2011; Murayama and Uhlmann, 2014). Instead, it appears that in budding yeast the chromatin factor that determines the sites of Scc2/4 recruitment and cohesin loading, is the chromatin remodeller complex RSC (Lopez-Serra et al., 2014). According to recent evidence, RSC has a dual role in loading cohesin onto chromosome arms: first, it acts as chromatin receptor for the cohesin loader by directly interacting with Scc2/4, second, it provides nucleosome-free DNA which serves as a substrate for cohesin loading (Muñoz et al., 2019).

1.2.1.4 Cohesin translocation on chromosomes

Cohesin is not uniformly distributed along chromosomes. Instead, cohesin is enriched in short (1-4kb) cohesin associated regions which are AT rich (Laloraya et al., 2000; Filipski and Mucha, 2002; Glynn et al., 2004) and tend to coincide with intergenic regions between convergent genes (Blat and Kleckner, 1999; Laloraya et al., 2000; Lengronne et al., 2004; Glynn et al., 2004). Notably, cohesin is also enriched over a ~30kb region flanking

centromeres (Blat and Kleckner, 1999; Megee et al., 1999; Tanaka et al., 1999; Glynn et al., 2004; Weber et al., 2004).

Crucially, the linear distribution of cohesin is different from that of the loading complex (Ciosk et al., 2000). Genome-wide mapping of Scc2/4 localization demonstrated that differently to cohesin, the loading complex associates with core centromeres as well as highly transcribed genes (Lengronne et al., 2004; Hu et al., 2011; Petela et al., 2018). This suggests that following its loading, cohesin might translocate along chromosomes. Indeed, analysis of *scc2-4* mutants revealed that cohesin initially co-localizes with its loader (Lengronne et al., 2004). Following loading, cohesin translocates on chromosomes in a manner that is dependent on cohesin's ATPase activity (Hu et al., 2011) as mutations in Smc1 and Smc3 that prevent ATP hydrolysis increase colocalization of cohesin with Scc2/4 at core centromeres and at highly transcribed genes. Besides cohesin's ATPase activity, transcription was also found to play an important role in re-distributing cohesin on chromosomes. First, cohesin enrichment sites on chromosome arms correlate with intergenic regions between convergent genes (Lengronne et al., 2004). Second, transcriptional activation was found to lead to the re-distribution of cohesin to the 3' end of genes (Lengronne et al., 2004; Ocampo-Hafalla et al., 2016). Importantly, cohesin enrichment sites were found to coincide with convergent gene sites not only in budding yeast but also in *S. pombe* (Lengronne et al., 2004) and mammalian cells (Busslinger et al., 2017). Furthermore, single molecule studies demonstrated that cohesin can diffuse along DNA and while it is able to bypass some DNA-bound proteins, transcription restricts cohesin translocation (Davidson et al., 2016). This indicates that transcription might indeed position cohesin across the genome either by moving it along DNA or by preventing its further movement on chromosomes.

1.2.1.5 Establishment of sister chromatid cohesion

Cohesin has to be loaded onto chromosomes before S-phase in order to provide sister chromatid cohesion (Skibbens et al., 1999; Tóth et al., 1999; Ivanov et al., 2002; Ben-Shahar et al., 2008; Unal et al., 2008; Rowland et al.,

2009). This suggests that following its association with chromosomes, a DNA replication-coupled process converts cohesin into functional cohesion. This was found to depend on the acetyltransferase Eco1, that is thought to travel with the replication fork (Lengronne et al., 2006; Lopez-Serra et al., 2013) and acetylates Smc3 at positions K112, K113 (Skibbens et al., 1999; Tóth et al., 1999; Ivanov et al., 2002; Ben-Shahar et al., 2008; Unal et al., 2008; Rowland et al., 2009). Prior to DNA replication, cohesin shows rapid turnover on chromosomes (Gerlich et al., 2006). This is dependent on the interaction of $Rad61^{Wapl}$ (Kueng et al., 2006) with Pds5 (Sutani et al., 2009), which destabilises the Smc3-Scc1 interaction (Murayama and Uhlmann, 2015; Beckouët et al., 2016), leading to ring opening and release of cohesin from chromosomes. Eco1-mediated cohesin acetylation blocks the disengagement of Scc1 from Smc3 head domain, thus preventing Rad61-mediated cohesin release from chromosomes (Beckouët et al., 2016). Biochemically, acetylated Smc3 is more frequently associated with the J configuration of SMC heads that is capable of mediating sister DNA entrapment *in vitro* (Chapard et al., 2019). As *RAD61* deletion bypasses the lethality of *ECO1* deletion (Ben-Shahar et al., 2008; Unal et al., 2008; Rowland et al., 2009), it is currently thought that the primary function of Eco1 in cohesion establishment is to counteract Rad61 activity. However, it was found that *eco1Δ rad61Δ* does not lead to complete rescue of sister chromatid cohesion, so the exact function of Eco1-mediated cohesin acetylation is still debated (Guacci and Koshland, 2012; Guacci et al., 2015).

In contrast to budding yeast where Smc3 acetylation is sufficient for sister chromatid cohesion, in mammalian cells Smc3 acetylation recruits the cohesin-associated protein sororin. Sororin binds to Pds5, displacing Wapl and preventing the opening of the Smc3-Scc1 interface (Rankin et al., 2005; Nishiyama et al., 2010; Ladurner et al., 2016). Accordingly, sororin becomes dispensable for cohesion in the absence of Wapl, indicating that its main function is to antagonise Wapl activity (Nishiyama et al., 2010).

1.2.1.6 Proteolytic cleavage of cohesin

Sister chromatid cohesion is established in S-phase and persists until anaphase (Irniger et al., 1995). When chromosomes are ready to be segregated, sister chromatid cohesion is removed which requires the activity of the APC/C (Figure 1.2.1.6.1). The APC/C is a multisubunit E3 ubiquitin ligase that polyubiquitinates proteins, targeting them for proteasome-mediated degradation (reviewed in Primorac and Musacchio, 2013). The APC/C is activated at the metaphase-to-anaphase transition and triggers anaphase onset by targeting the anaphase inhibitor Pds1 (securin) for degradation (Cohen-Fix et al., 1996; Ciosk et al., 1998). Pds1 degradation releases the protease Esp1 (separase) from inhibition which leads to the proteolytic cleavage of Scc1 (Ciosk et al., 1998). Opening the cohesin ring through Scc1 cleavage is both necessary and sufficient for anaphase onset and thus chromosome segregation (Uhlmann et al., 1999; Uhlmann et al., 2000).

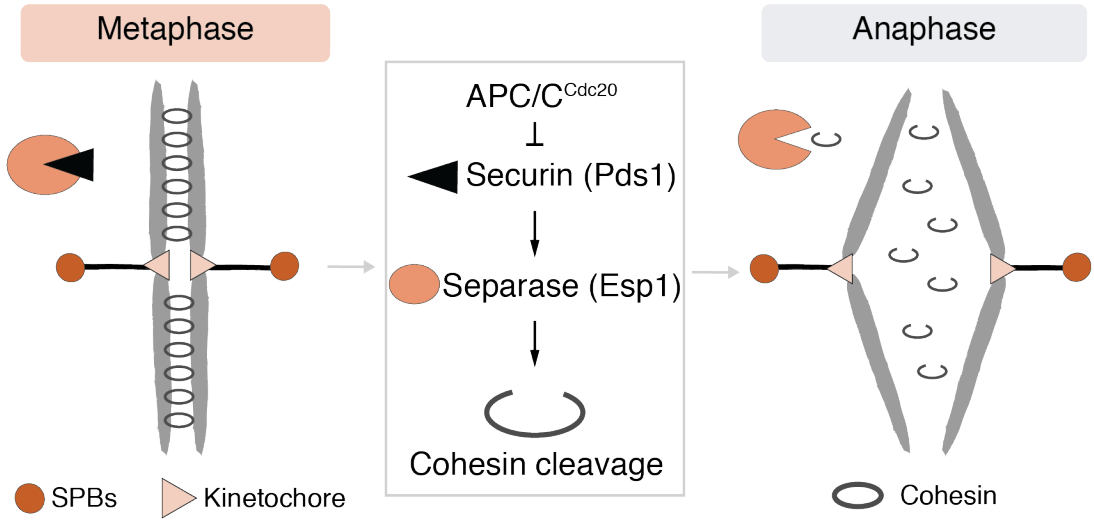

Figure 1.2.1.6.1 - The proteolytic cleavage of cohesin - When chromosomes are ready to be segregated the APC/C becomes activated and triggers anaphase onset by targeting the anaphase inhibitor Pds1 (securin) for degradation. Pds1 degradation releases the protease Esp1 (separase) from inhibition which leads to the proteolytic cleavage of Scc1. The opening of th cohesin ring leads to the segregation of sister chromatids.

1.2.2 Cohesin as a genome organiser

1.2.2.1 The 3D organisation of genomes

Genetic material in the eukaryotic nucleus exists as a conserved structural and functional complex of DNA and proteins, called chromatin. The fundamental repeating units of chromatin are nucleosomes that consist of 146bp DNA wrapped around a core of histone proteins. Histones H2A, H2B, H3 and H4 are each present in two copies in a nucleosome forming an octameric protein complex that binds and compacts DNA. Chromatin is further organised spatially into 3-dimensional structures which govern genomic processes such as DNA replication and repair, gene expression and chromosome transmission. In interphase, proper chromosome architecture is required to support functional interactions between distant loci. In mitosis, through chromosome compaction and individualisation, changes in genome organisation are required to establish chromosomal structures that are competent for segregation.

Although genome folding shows surprising variability between organisms, the organisational principles remain largely similar (reviewed in Szabo et al., 2019). At the most local level, chromosomes are structured through chromatin loops that form when two loci come to be in closer physical proximity to each other than to their intervening sequences. Through looping interactions domains form: called topologically associating domains (TADs) in higher eukaryotes, self-interacting domains (SIDs) in yeast, and chromosomal interaction domain (CIDs) in bacteria, comprise DNA sequences that preferentially interact with themselves rather than other sequences in the genome. In higher eukaryotes, TADs associate into further higher order structures, referred to as compartments. Finally, the largest 3-dimensional units of organisation are the chromosomes themselves, that occupy separate chromosome territories. In addition to genomic contacts that occur between sequences that are on the same chromosome (*cis*-contacts), interactions happen between different chromosomes as well (*trans*-contacts), although much less frequently.

Proper 3D genome organisation has been extensively implicated in cellular processes, functioning through the spatial restriction of interactions that are involved in gene expression regulation (reviewed in Zheng and Xie, 2019). Accordingly, for example, changes in gene expression can be accompanied by dynamic changes in local chromatin structure. Moreover, alterations in the 3D genome are associated with developmental disorders and human diseases, indicating that genome structure and function are inherently linked. Crucially however, it is still a matter of debate to what extent the 3D organisation of genomes has regulatory roles, and to what extent it is a consequence of genome function.

1.2.2.2 The role of cohesin in structuring genomes

The spatial organisation of genomes requires architectural proteins that mediate chromatin *cis*-looping. Besides its canonical role in holding sister chromatids together, cohesin also has a major function as a genome organiser and mediates long-range intrachromosomal interactions (reviewed in Nishiyama, 2019). Cohesin-dependent *cis*-looping is important for chromosome compartmentalisation during interphase, as well as for mitotic chromosome compaction. As opposed to the topological entrapment of sister chromatids required for cohesion, cohesin-mediated chromosomal *cis*-interactions happen through non-topological linkages.

In mammalian cells cohesin defines interphase loops: most loop bases and TAD boundaries coincide with cohesin enrichment sites, together with convergently arranged binding sites for the architectural protein CTCF (CCCTC-binding factor) (Wendt et al., 2008; Dixon et al., 2012; Rao et al., 2014). Similarly, in fission yeast self-interacting domains (or globules) form in a cohesin-dependent manner (Mizuguchi et al., 2014), and in budding yeast cohesin loading and accumulation sites appear to act as weak boundaries for local interaction domains (Hsieh et al., 2015; Hsieh et al., 2016). Strikingly, in budding yeast cohesin has a prominent role in the mitotic compaction of chromosome arms through the formation of intra-arm *cis*-loops (Schalbetter et

al., 2017) that form between adjacent cohesin peaks (Garcia-Luis et al., 2019), a role independent from its function in sister chromatid cohesion.

1.2.2.3 The role of condensin in genome organisation

Besides cohesin, eukaryotic SMC complexes also include additional, structurally similar but functionally diverse, protein complexes: condensin and the Smc5/6 complex (reviewed in Uhlmann, 2016). While Smc5/6 has a primary role in DNA repair and recombination, condensin has a prominent function in genome organisation. Similar to cohesin, condensin comprises two SMC subunits, Smc2 and Smc4, which heterodimerize through their hinge domain (Figure 1.2.1.1.1). Smc2 and Smc4 are connected at the head domains by the kleisin subunit Brn1, closing the condensin ring. Two more *bona fide* subunits, Ycg1 and Ycs4, associate with Brn1 to form the complete condensin complex (Strunnikov et al., 1995; Freeman et al., 2000). Additionally, in higher eukaryotes Smc2 and Smc4 can associate with a different set of regulatory subunits, and give rise to the condensin II complex (reviewed in Hirano, 2012). Like cohesin, condensin is capable of the topological entrapment of DNA (Cuylen et al., 2011), however, in contrast to cohesin, condensin does not require a loading factor to associate with DNA. Moreover, condensin hydrolyses ATP at a much faster rate than cohesin (Hirano and Hirano, 2006; Arumugam et al., 2006), and exhibits more dynamic association with DNA (Gerlich et al., 2006). Therefore, although the subunit organisation of cohesin and condensin shares many similarities, the complexes differ in regulatory mechanisms which leads to differences in their cellular functions.

As opposed to cohesin, the canonical role of condensin is the mitotic compaction of chromosomes. In higher eukaryotes condensin I and II act sequentially to establish mitotic chromosome structures (Ono et al., 2003). Similarly, in fission yeast overall chromosome condensation requires condensin (Sutani et al., 1999; Kakui et al., 2017). Interestingly, in budding yeast condensin has a less universal role and is mainly involved in structuring the rDNA (Strunnikov et al., 1995; Lavoie et al., 2000; Freeman et al., 2000;

Schalbetter et al., 2017). Despite some differences between organisms, condensin is nevertheless universally required for the establishment of mitotic chromosomal structures that allow accurate chromosome packaging and segregation (reviewed in Hirano, 2012, 2016).

1.2.2.4 Mechanisms of loop formation by SMC complexes

Much effort has been spent deciphering the mechanism by which cohesin and condensin structure interphase and mitotic chromosomes. The default model of compaction by SMC complexes suggested that chromatin loops are formed through the stochastic stabilisation of chromosomal interactions. This model attributes a mere crosslinker role for cohesin and condensin. However, multiple lines of evidence suggest that this simplistic model cannot explain the formation of mitotic chromosome structures. First, chromatin loops tend to be mostly intrachromosomal and their formation leads to chromosome individualisation. Second, loops are non-overlapping and linearly arranged along a longitudinal chromosome axis (Ono et al., 2003; Naumova et al., 2013). Both of these observations argue against the stochastic crosslinking model which predicts increase in *trans* interactions and the formation of overlapping loops upon chromosome condensation. Accordingly, polymer simulations indicated that stochastic crosslinking would produce spherical globules upon chromosome compaction (Marko and Siggia, 1997) as opposed to elongated structures as observed in living cells.

An alternative hypothesis, dating from 2001 (Nasmyth, 2001) but gaining much attention recently, attributes an active role to cohesin and condensin in chromosome folding. According to this model, cohesin and condensin mediate non-topological interactions via the processive extrusion of chromatin loops: the SMC complex binds two adjacent DNA sites, then using its enzymatic activity, it reels the DNA inside the SMC ring, moving one or both contact points away from the other. This leads to the bridging of more distant sites and the enlargement of the chromatin loop (Figure 1.2.2.4.1). The loop extrusion process is thought to be dependent on ATP hydrolysis, which is supported by the observation that condensin-dependent DNA compaction requires ATP

hydrolysis while DNA binding does not (Strick et al., 2004). Initial evidence came from *in silico* models that indicated that loop extrusion can indeed explain key aspects of loop and domain formation (Alipour and Marko, 2012; Sanborn et al., 2015; Goloborodko et al., 2016). Crucially, recent work provides experimental support for the loop extrusion model: condensin was observed to extrude naked DNA loops *in vitro* (Ganji et al., 2018). The process was force-dependent, required ATP hydrolysis, and occurred in an asymmetric way with condensin anchoring to DNA and reeling it in at only one side. This work provides unambiguous evidence for the loop extrusion mechanism and a tempting speculation that it could be the unifying principle of genome organisation by SMC complexes. Indeed, loop extrusion activity for the human cohesin complex was very recently demonstrated *in vitro* (Davidson et al., 2019). Although loop extrusion between cohesin and condensin were similar in terms of rate and requirement for ATP, significant differences were found which likely contribute to the different physiological roles of the two complexes. Loop extrusion by cohesin happened symmetrically and required the NIPBL-MAU2 cohesin-loader complex. Interestingly, loop extrusion did not require the opening of the cohesin ring, indicating that the complex interacts with DNA non-topologically to organise interphase genomes (Davidson et al., 2019).

However, at present there is no direct evidence for the loop extrusion process *in vivo*. Also, is currently unclear how chromatin-related factors such as nucleosomes, or DNA processes such as transcription could be accommodated by loop extruding factors. While these key questions remain unanswered, a plethora of biochemical and cell biological observations strongly support the hypothesis that genome structuring by SMC complexes might indeed happen via loop extrusion *in vivo* (reviewed in van Ruiten and Rowland, 2018; Baxter et al., 2019; Sedeño Cacciatore and Rowland, 2019).

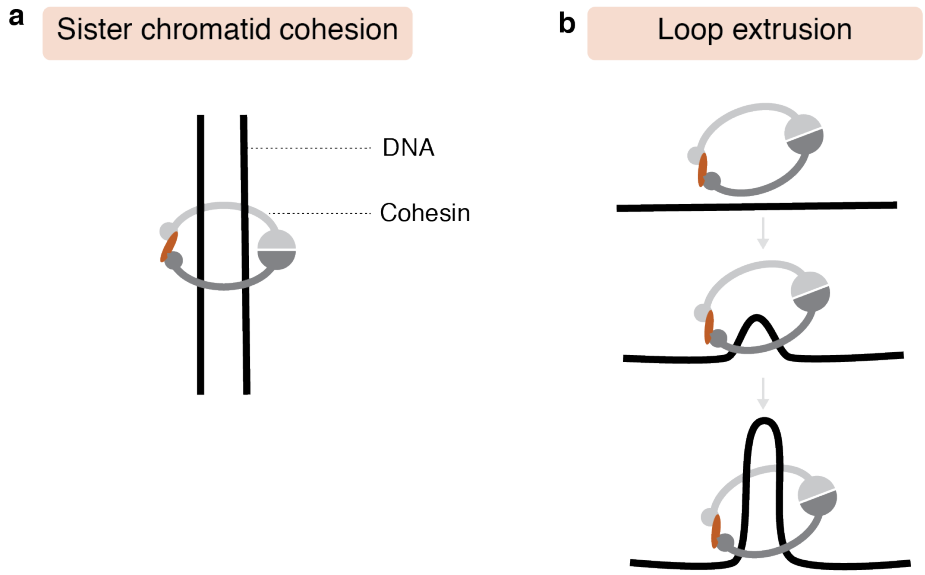

Figure 1.2.2.4.1 - Interaction models between cohesin and DNA - **a**, Topological embrace or co-entrapment of two DNA molecules generates sister chromatid cohesion. **b**, The process of loop extrusion - progressive enlargement of DNA loops by cohesin - organises interphase chromatin.

1.2.3 Other roles of the cohesin complex

1.2.3.1 Transcriptional regulation

Although it is yet unclear how much it is mechanistically related to cohesin's ability to structure genomes, cohesin is also known to play a prominent role in the regulation of gene expression in metazoans as suggested by multiple observations (reviewed in Dorsett and Ström, 2012). First, cohesin can increase enhancer-promoter communication, potentially by mediating chromatin looping and bringing distal regulatory elements into physical proximity. Second, cohesin on chromosomes binds close to paused RNA polymerase II, where it is thought to modulate the transition of RNA polymerase II from the paused to the elongation state (reviewed in Dorsett and Merkenschlager, 2013). Third, in vertebrates cohesin together with CTCF regulates transcriptional repression and activation, and can both mediate and disrupt enhancer-promoter interactions (reviewed in Merkenschlager and

Nora, 2016). Accordingly, cohesin depletion results in global changes in gene expression. Cohesin's prominent role in transcriptional regulation is further exemplified by the severe phenotype of Cornelia de Lange syndrome (CdLS). CdLS is a rare genetic disease that is cause by the disruption of cohesin function, either by mutations in the cohesin complex, or in its regulators (reviewed in Liu and Krantz, 2008). CdLS patients typically suffer from congenital anomalies, developmental delay and intellectual disability which are thought to be caused by global transcriptional deregulation, possibly through the disruption of interphase genome organisation.

1.2.3.2 Cohesin in DNA repair

Under genotoxic stress conditions cohesin is also required for an adequate DNA damage response and repair (Sjögren and Nasmyth, 2001; Ström et al., 2004). When DNA double strand breaks occur, cohesin is recruited to the break site in manner that is dependent on the Scc2/4 cohesin-loader complex. Broadly, cohesin supports genome stability by inhibiting DNA synthesis in response to damage, by promoting the use of the sister chromatid as a repair template and by preventing chromosome rearrangement by inhibiting the joining of two distinct double strand breaks (reviewed in Litwin, Pilarczyk and Wysocki, 2018). Accordingly, cohesin mutants are sensitive to DNA damaging agents, such as γ irradiation, as a consequence of defective DNA repair function (Birkenbihl and Subramani, 1992).

1.3 Chromosome biorientation in metaphase

The segregation of sister chromatids is an irreversible event that must be tightly controlled, as any errors can be deleterious to the progeny. Cohesin-dependent events such as establishment of sister chromatid cohesion during DNA replication, chromosome compaction and timely cohesin removal at the metaphase-to-anaphase transition are key to ensuring accurate chromosome segregation. However, besides cohesin, successful cell division requires additional fundamental processes that monitor the correct attachment of chromosomes to the mitotic spindle apparatus: the mitotic spindle moves chromosomes inside the cell by attaching to kinetochores, large protein complexes that assemble on chromosomes. The pre-requisite of the metaphase-to-anaphase transition is the establishment of proper microtubule-kinetochore interactions that is sensed by the cell and only then cell cycle progression is permitted.

1.3.1 The spindle assembly checkpoint

Premature chromosome segregation is prevented by the spindle assembly checkpoint (SAC) that blocks the metaphase-to-anaphase transition (reviewed in London and Biggins, 2014). The SAC relies on the inhibition of APC/C in the presence of improperly attached kinetochores. Although the primary function of kinetochores is to provide the chromosomal attachment sites for spindle microtubules, they also serve as important signalling hubs for chromosome segregation processes. As for the SAC, improperly attached kinetochores are the source of an inhibitory signal that induces a robust but reversible cell cycle arrest in metaphase, preventing premature progression into anaphase (Li and Nicklas, 1995; Rieder et al., 1995).

When the SAC is activated in the absence of proper microtubule-kinetochore attachments, a signalling cascade is initiated at kinetochores (reviewed in London and Biggins, 2014). SAC signalling leads to the hierarchical recruitment of checkpoint proteins to the KMN network, the core microtubule binding site on kinetochores. The signalling cascade is initiated by the Mps1

kinase, that phosphorylates the Spc105 (Knl1 in higher eukaryotes) subunit of the kinetochore. Spc105 phosphorylation leads to the recruitment of checkpoint proteins Bub1 and Bub3 (London et al., 2012), which in turn are required for the kinetochore localisation of Mad1 and Mad2 (Gillett et al., 2004). Kinetochore-bound Mad2 activates unbound Mad2 through a conformational change which leads to the assembly of the mitotic checkpoint complex (MCC), a diffusible inhibitor of the APC/C (De Antoni et al., 2005). The MCC is composed of the checkpoint proteins Mad2 (in the active conformation), Mad3, Bub3, and the APC/C co-activator Cdc20 (Hardwick et al., 2000; Sudakin et al., 2001). The MCC inhibits APC/C by sequestering Cdc20, as well as by acting as a pseudo-substrate to APC/C (Burton and Solomon, 2007). As anaphase onset is triggered by the APC/C^{Cdc20}-dependent degradation of securin, which in turn leads to separase-dependent cohesin cleavage (Cohen-Fix et al., 1996; Ciosk et al., 1998), APC/C inactivation efficiently blocks the metaphase-to-anaphase transition. Thus, the SAC is able to prevent premature chromosome segregation by delaying progression to anaphase until all kinetochores are properly attached to the mitotic spindle.

Once correct attachments are made, SAC signalling must be turned off in order to allow progression to anaphase (reviewed in Bokros and Wang, 2016). Broadly, checkpoint silencing involves the reversal of Mps1-dependent phosphorylation of Spc105 by protein phosphatase 1 (PP1), the disassembly of MCC by Cdc20 autoubiquitination, and the degradation of Mps1.

1.3.2 Chromosome biorientation at metaphase

Spindle pole bodies (SPBs) constitute the microtubule organising centres in yeast (centrosomes in higher eukaryotes), from where the majority of microtubules are nucleated. Like chromosomes, SPBs are present in a single copy in interphase, undergo duplication in S-phase after which they migrate away from each other. Separation of SPBs is crucial for the assembly of the bipolar spindle, the apparatus that segregates chromosomes to daughter cells. The onset of chromosome segregation requires appropriate contacts between

sister chromatids and the bipolar spindle: sister kinetochores must attach to microtubules emanating from opposite spindle poles. This attachment state, called biorientation, ensures that when chromosome segregation is triggered, sister chromatids are pulled apart from each other and thus get equally partitioned into the nascent daughter cells.

Generally, kinetochore capture by microtubules initially occurs via lateral contacts between one sister kinetochore and a microtubule from one SPB (reviewed in Tanaka, 2010). This is followed by the poleward transport of cohered sister chromatids which converts the lateral attachment to end-on attachment. Finally, the capture of the other sister kinetochore occurs in a similar way. If the second kinetochore is captured by microtubules that emanate from the opposite spindle pole, biorientation is established and the resulting amphitelic microtubule attachments exert pulling forces on chromosomes. However, cohesin resists the pulling force which creates tension at kinetochores. This tension is crucial, first because tension itself stabilises microtubule-kinetochore interactions (Nicklas and Koch, 1969; Akiyoshi et al., 2010) which leads to the selective stabilisation of correct attachments. Second, this microtubule-based tension is the signal of proper microtubule-kinetochore attachments, allowing sister chromatid segregation to take place. Accordingly, in addition to unattached kinetochores (Rieder et al., 1995), microtubule contacts that do not generate tension activate the SAC indirectly (Li and Nicklas, 1995) and prevent progression into anaphase.

1.3.3 Tension sensing

An elegant screen identified the budding yeast Shugoshin (Sgo1) as a protein required for tension sensing (Indjeian et al., 2005). Shugoshins are a family of centromeric adapter proteins that were first discovered as factors required for chromosome segregation fidelity during meiosis, the reductional cell division that produces gametes (Kerrebrock et al., 1992). During mitosis, Sgo1 localises to pericentromeres from where it is removed in response to tension (Lee et al., 2008; Liu et al., 2013; Nerusheva et al., 2014; Eshleman and

Morgan, 2014). Sgo1 recruitment to the pericentromere requires phosphorylation of histone H2A on Ser121 by the SAC protein Bub1 (Fernius and Hardwick, 2007; Kawashima et al., 2010). Once recruited, Sgo1 acts as a platform to localise key effector proteins to the pericentromere that modulate the interaction of chromosomes, kinetochores and microtubules. Following sister chromatid biorientation, Sgo1 is removed from chromosomes in a tension-dependent and chromosome-autonomous manner. Tension-induced Sgo1 re-localisation also removes effector proteins from pericentromeres when biorientation is achieved (Indjeian and Murray, 2007). How tension is translated to a molecular signal that removes Sgo1 from chromosomes is yet to be understood.

1.3.4 Error correction

Although sister chromatids have an inherent bias to biorient on the mitotic spindle (Indjeian and Murray, 2007) incorrect attachment can be made: syntelic attachments form when sister kinetochores attach to the same pole, and the attachment of one kinetochore to both poles leads to merotelic attachments. The latter does not affect budding yeast, as budding yeast kinetochores have a single microtubule binding site (Winey et al., 1995). If established though, aberrant microtubule-kinetochore interactions have to be removed (Figure 1.3.4.1).

As opposed to correct tension-generating microtubule-kinetochore interactions, incorrect attachments lead to the destabilisation of microtubule-kinetochore contacts. This destabilisation process is dependent on the error correction pathway that is governed by the chromosome passenger complex (CPC). The CPC consists of INCENP (Sli15), Borealin (Bir1), Suvivin (Nbl1) and Aurora B (Ipl1) (reviewed in Carmena et al., 2012), and it localises to kinetochores that lack tension. Although not required for the initial localisation of CPC to kinetochores, Sgo1 is required for both the maintenance of CPC localisation, and tension-dependent removal of CPC once kinetochores come

under tension (Peplowska et al., 2014; Verzijlbergen et al., 2014; Nerusheva et al., 2014).

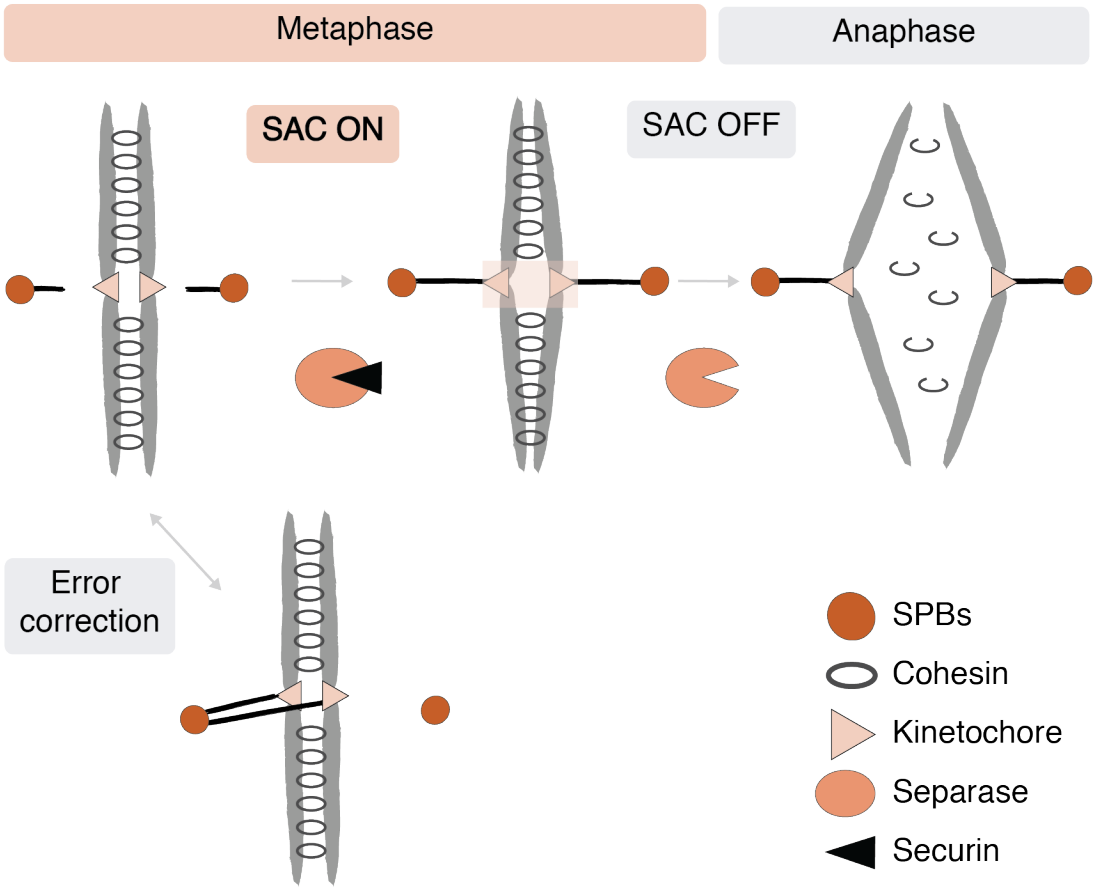

Figure 1.3.4.1 - Model of chromosome segregation in metaphase - Replicated copies of chromosomes are held together by cohesin until they biorient on the mitotic spindle. Metaphase arrest imposed by the spindle assembly checkpoint (SAC) blocks cell cycle progression while incorrect attachments are removed by the error correction machinery. When biorientation is achieved, tension generated at kinetochores signals proper microtubule-kinetochore contacts which turns SAC singalling off. This results in securin degragation which in turn releases active separase that triggers anaphase onset by the proteolytic cleavage of cohesin.

The kinase constituent of CPC, Ipl1 is central to the error correction pathway: when Ipl1 is defective, kinetochores can attach to microtubules but biorientation is impaired (Biggins and Murray, 2001; Tanaka et al., 2002). When at the kinetochore, Ipl1 phosphorylates kinetochore components that weakens their interactions with microtubules, thus facilitating the turnover of

incorrect attachments and keeping SAC signalling active. In contrast, when biorientation is achieved and kinetochores get stretched (Maresca and Salmon, 2009; Uchida et al., 2009) Ipl1 substrates get dephosphorylated by PP1, preventing the destabilisation of tension-generating contacts (Liu et al., 2010; Welburn et al., 2010).

1.3.5 Chromosome segregation errors and aneuploidy

Chromosome segregation is a complex process and even though a plethora of mechanisms ensure its accuracy, errors occur nevertheless. Defects in chromosome condensation, sister chromatid cohesion, spindle abnormalities and errors in cell cycle regulation can all lead to chromosome mis-segregation. Unequal chromosome segregation leads to aneuploidy, a condition in which the number of chromosomes in a cell is not the exact multiple of the haploid set. Importantly, aneuploidy leads to changes in the dosage of genes on the mis-segregated chromosome, or through changing the expression of transcription factors it can lead to the mis-regulation of genes on correctly segregated chromosomes.

Altered gene dosage is detrimental to cellular fitness and health. Accordingly, aneuploidy is associated with a range of human conditions, and over >80% of human cancers show aneuploidy. In cancer, chromosome segregation errors are thought to contribute to tumorigenesis. Subsequently, chromosome mis-segregation leads to karyotypic and clonal diversity which provides the driving force for tumour evolution towards invasiveness and drug resistance (reviewed in Ricke and Van Deursen, 2013; Potapova and Gorbsky, 2017).

If chromosome segregation errors occur during the production of germ cells, aneuploidy will affect the whole organism. In humans, aneuploidies are extremely poorly tolerated during embryonic development, and in most cases are embryonic lethal. Accordingly, meiotic aneuploidy is a major cause of infertility and miscarriages in humans. Only a few aneuploid conditions, such as trisomy 13, 18 and 23 are viable, but cause severe congenital diseases

such as Patau, Edwards and Down syndrome, respectively (reviewed in Potapova and Gorbsky, 2017).

Irrespective of whether through mitotic or meiotic divisions, chromosome segregation errors that lead to abrupt changes in gene dosage are almost always detrimental to multicellular organisms, giving rise to abnormal embryos and malignant cells. Interestingly, in contrast to metazoans, chromosome mis-segregation can be an important source of adaptive evolution for unicellular organisms: in budding yeast, aneuploidy has been shown to play a role in adaptation to certain sub-optimal conditions (Dunham et al., 2002; Voordeckers et al., 2015). This highlights fundamental differences between multicellular and unicellular organisms. In the former, proliferative competition between cells leads to disease and compromise the viability of the entire organism, stressing the requirement for elaborate regulation of all cell division events. On the other hand, chromosome missegregation may enable a unicellular organism to exploit new environmental conditions as karyotypic diversity is only limited by fitness cost.

1.4 Pericentromeres in cell division

Accurate chromosome segregation requires each chromosome to build a single kinetochore, a complex macromolecular assembly which mediates the interaction between the chromosome and the mitotic spindle. The kinetochore assembles at a specialised chromosomal locus on each chromosome, called the centromere. Accordingly, the primary purpose of centromeres is to direct the assembly of kinetochores. Despite their conserved function, centromeres show divergence in sequence as well as chromatin state between different organisms.

Centromeres are generally surrounded by specialised chromosomal domains, called pericentromeres. Like centromeres, pericentromeres are also diverse in nature but invariable in function, facilitating chromosome biorientation and segregation. Broadly, pericentromeres can be characterised as centromere-flanking regions enriched in cohesin that are often heterochromatic (Tomonaga et al., 2000; Warren et al., 2000; Laloraya et al., 2000; Sonoda et al., 2001). The specialised chromatin environment of pericentromeres facilitates processes such as suppression of centromere-proximal recombination, recruitment of cohesin and shugoshin to the vicinity of centromeres and the establishment of a preferred higher-order structure or kinetochore geometry for biorientation.

1.4.1 Regional centromeres vs point centromeres

In most eukaryotes, kinetochores assemble on long arrays of repetitive DNA associated with so-called regional centromeres (Figure 1.4.1.1). Instead of DNA sequence *per se*, regional centromeres are specified and inherited epigenetically: this involves non-DNA sequence based factors that are able to propagate information through cell divisions. The epigenetic mark that defines centromeres is the presence of the centromere-specific histone H3 variant, CENP-A. In centromeric chromatin, histone H3 is replaced by CENP-A in histone octamers, and CENP-A nucleosomes are interspersed with clusters of canonical H3 nucleosomes (reviewed in Allshire and Karpen, 2008). CENP-A

chromatin is embedded in a heterochromatin environment that is marked by H3K9 di- and trimethylation. Although usually devoid of genes, centromeric and pericentromeric sequences are often transcribed, and resulting non-coding RNAs have functional importance in processes such as heterochromatin establishment, centromeric chromatin stabilisation and protein recruitment. For example in fission yeast, transcription of the outer repeats that flank the central domain of centromeres dictates the establishment of heterochromatin through the RNA interference pathway (reviewed in Smurova and De Wulf, 2018). The establishment and maintenance of heterochromatin is in turn essential for stabilising centromeres and actively recruiting cohesin.

In contrast to most eukaryotes, budding yeast has point centromeres where the entire kinetochore assembly is governed by a short ~125 bp DNA sequence (Clarke and Carbon, 1980). This contrasts with regional centromeres that range from ~40 kb (fission yeast) to megabases (human) in size. In budding yeast, the centromeric DNA sequence is composed of CDEI, CDEII and CDEIII, where factors that associate with CDEI and CDEIII direct the incorporation of a single CENP-A (Cse4) nucleosome to CDEII (Stoler et al., 1995; Meluh et al., 1998). Subsequently, the rest of the kinetochore is built on the CENP-A nucleosome through a cooperative multi-step assembly mechanism (Hornung et al., 2014). Although CENP-A is present at the centromere, budding yeast pericentromeres are devoid of other centromere-specific epigenetic marks. Moreover, pericentromeres lack heterochromatin and contain actively transcribed genes. However, like pericentromeres associated with regional centromeres, they accumulate high levels of cohesin that is important for biorientation (Eckert et al., 2007; Ng et al., 2009).

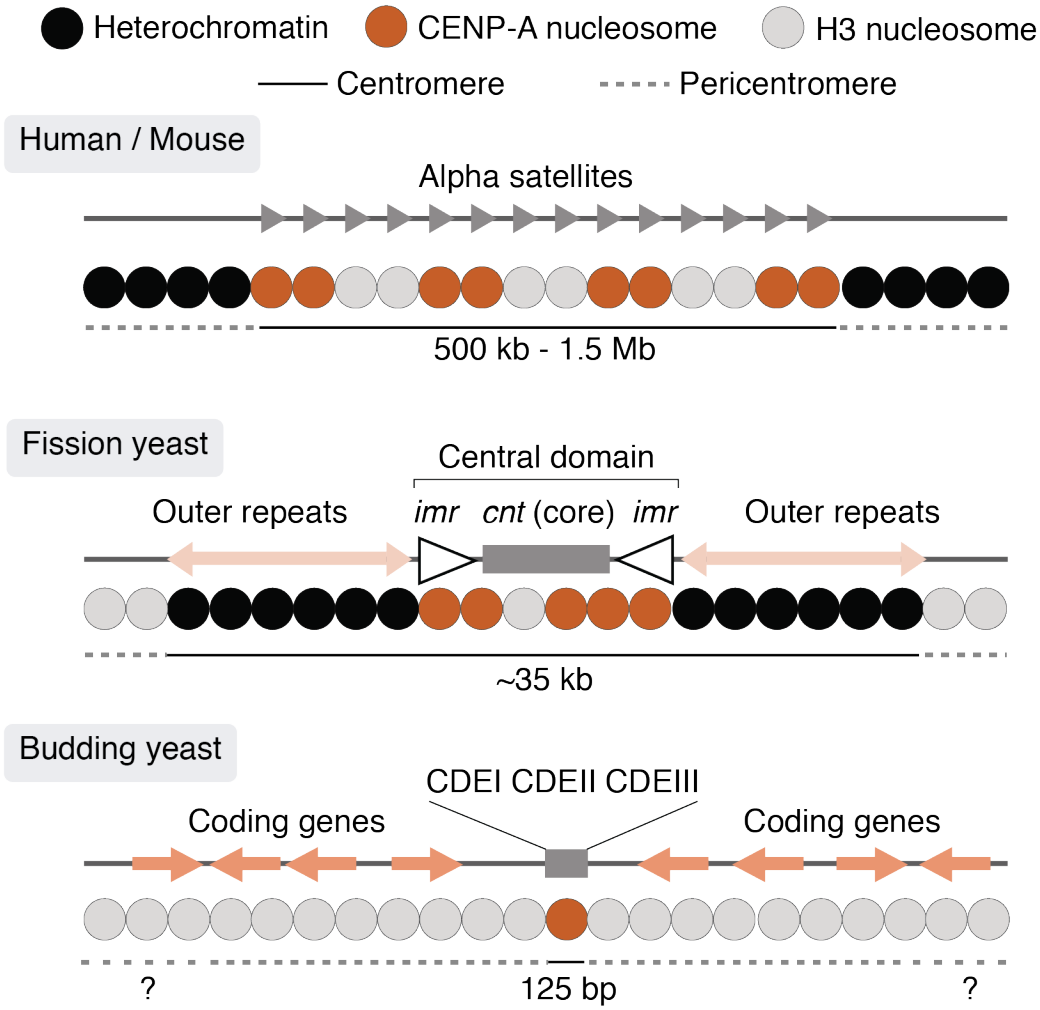

Figure 1.4.1.1 - Centromere organisation in mammals, fission yeast and budding yeast - Regional centromeres of mammals and fission yeast are complex and large, and reside embedded in the heterochromatic environment of the pericentromere. In contrast, budding yeast point centromeres are short, contain a single CENP-A (Cse4) nucleosome, and the pericentromere is euchromatic with actively transcribed genes. The precise extent of pericentromeres in budding yeast is not known.

1.4.2 Pericentromeric cohesin

A shared feature of all pericentromeres is the presence of high cohesin density. In fission yeast and in metazoans, cohesin is recruited to the pericentromere through a heterochromatin-directed pathway. HP1 (Swi6 in fission yeast) localises to heterochromatin though binding the H3K9me2/3 mark on histones, where it contributes to the maintenance and propagation of heterochromatin. In fission yeast, HP1 directly interacts with the cohesin

subunits Scc1 (Rad21) (Bernard et al., 2001), Scc3 (Psc3) (Nonaka et al., 2002) and the Dbf4-dependent kinase (DDK) (Natsume et al., 2013). In mammals the cohesin-HP1 interaction is indirect, and requires the protein kinase Haspin (Yi et al., 2018) that binds both HP1 and the accessory cohesin subunit Pds5B (Liang et al., 2018). Thus, this heterochromatin-directed pathway is responsible for the high density of cohesin over the pericentromeres of regional centromeres.

1.4.2.1 Kinetochore-driven cohesin loading

As budding yeast pericentromeres are devoid of heterochromatin, pericentromeric cohesin enrichment is achieved through targeted cohesin loading at centromeres. This depends on the recruitment of the Scc2/4 cohesin-loader complex to the centromere, via the Ctf19 kinetochore sub-complex (Eckert et al., 2007; Fernius and Marston, 2009; Ng et al., 2009; Hinshaw et al., 2015; Hinshaw et al., 2017). In early G1, the cell-cycle regulated Dbf4-dependent kinase DDK is recruited to the kinetochore by Ctf3, where it phosphorylates the N-terminal tail of Ctf19 (Hinshaw et al., 2017). In late G1 when Scc1 is synthesised, the cohesin ring associates with the loading complex and localises to the kinetochore. This happens through an interaction between the phosphorylated Ctf19 tail and a conserved surface patch on Scc4, the localisation module of the loading complex (Hinshaw et al., 2017). Importantly, as DDK plays an essential role in controlling replication initiation (Sheu and Stillman, 2010; Natsume et al., 2013), this mechanism provides temporal connection between the establishment of sister chromatid cohesion and DNA replication.

Following loading at centromeres, cohesin is thought to translocate bidirectionally on chromosomes and accumulate in the pericentromere. This is supported by multiple observations. First, Scc2/4 shows a much narrower localisation around centromeres than cohesin (Lengronne et al., 2004; Hu et al., 2011; Fernius et al., 2013). Second, the disruption of centromeric cohesin loading results in reduction of cohesin levels throughout the pericentromere (Fernius and Marston, 2009; Ng et al., 2009; Hinshaw et al., 2015; Hinshaw et

al., 2017). Third, cohesin mutants that are defective in translocation on chromosomes accumulate high levels of cohesin at core centromeres but not in pericentromeres, in a localisation pattern reminiscent to that of Scc2/4 (Hu et al., 2011; Hu et al., 2015). However, in the absence of *cis*-acting chromosomal factors, it is not understood how the region of cohesin accumulation and thus the pericentromere is delimited in budding yeast.

1.4.2.2 Pericentromeric cohesin and kinetochore geometry

Pericentromeric cohesin is important to signal amphitelic microtubule-kinetochore attachments as it generates tension which allows cell cycle to process to anaphase. However, it has been observed that sister chromatids have an intrinsic bias to biorient on the mitotic spindle (Indjeian and Murray, 2007) which led to the proposal that in addition to its tension-based role (Dewar et al., 2004), pericentromeric cohesin might establish a preferred kinetochore geometry for capture by microtubules from opposite poles: a back to back geometry would allow sister kinetochores to protrude in opposite directions. Indeed, cells that lack pericentromeric cohesin enrichment are slow to achieve biorientation and rely more on the error correction machinery (Eckert et al., 2007; Fernius and Marston, 2009; Ng et al., 2009). Additionally, in fission yeast, the artificial tethering of the outer repeats rescues the biorientation defect that cells exhibit in the absence of heterochromatin-directed cohesin recruitment (Sakuno et al., 2009). Altogether these observations argue for a role of kinetochore geometry in biorientation.

1.4.3 Shugoshin, the pericentromeric adaptor protein

Besides cohesin, pericentromeres are enriched in other proteins that play crucial roles ensuring accurate chromosome segregation. A key factor is the pericentromeric adaptor protein Sgo1. In addition to its role in error correction, Sgo1 localisation to the pericentromere is crucial for cohesion protection in meiosis and mammalian mitosis, as well as for the recruitment of condensin to the pericentromere.

1.4.3.1 Pericentromeric cohesin protection

In budding yeast mitosis, cohesin removal from chromosomes occurs in one step, by the separase-dependent proteolytic cleavage of Scc1 at the metaphase-to-anaphase transition. In metazoans, as well as generally in meiosis cohesin is removed from chromosomes in a step-wise manner, first from chromosome arms, then from centromere-proximal regions. In metazoans, a mechanism termed the prophase pathway allows the destabilisation of cohesin from chromosome arms, leading to arm resolution prior to cohesin cleavage (reviewed in Haarhuis et al., 2014). During meiotic divisions chromosomes segregate twice: homologous chromosome segregate in meiosis I which is accompanied by separase-dependent cohesin removal from chromosome arms. Pericentromeric cohesion persists beyond meiosis I in order to ensure the accurate segregation of sister chromatids in meiosis II (reviewed in Duro and Marston, 2015).

Although in case of the prophase pathway, cohesin removal from chromosome arms depends on the Wapl-mediated ring opening at the Smc3-Scc1 interphase prior to metaphase, while in meiosis I it involves cohesin cleavage by separase, in both cases cohesin protection in centromere-proximal regions requires shugoshin (reviewed in Marston, 2015). The protective function of shugoshin depends on the recruitment of its interaction partner PP2A. PP2A counteracts phosphorylation of cohesin at sites that make it susceptible to binding to Wapl and cleavage by separase, in metazoan mitosis and in meiosis, respectively. Thus shugoshin-mediated PP2A recruitment prevents cohesin removal from the pericentromere, ensuring accurate chromosome segregation is meiosis II and in metazoan mitosis.

1.4.3.2 Condensin recruitment to the pericentromere

In budding yeast mitosis, Sgo1 recruits the chromosome organiser condensin to the pericentromere. Condensin at the pericentromere is thought aid the sensing of tensionless attachments and bias chromosomes for biorientation, possibly through modulating the conformation of pericentromeric chromatin (Peplowska et al., 2014; Verzijlbergen et al., 2014). This role of Sgo1 is

independent from its roles in recruiting the CPC and Rts1-PP2A to the pericentromere. In higher eukaryotes it is unclear if shugoshin has a similar role in recruiting condensin to the pericentromere. Nevertheless, condensin I localises to mammalian centromeres where it is thought to stabilise chromosome structure (Oliveira et al., 2005; Gerlich, Hirota, et al., 2006; Ribeiro et al., 2009).

1.4.4 The centromere paradox

1.4.4.1 Pre-anaphase separation of centromeres

Despite high cohesin density over pericentromeric regions in budding yeast, it has been observed that centromere-proximal regions of sister chromatids separate prior to anaphase (Goshima and Yanagida, 2000; He et al., 2000; Tanaka et al., 2000). This is the result of biorientation, when microtubules emanating from opposite spindle poles exert tension on sister kinetochores. The tension – that also signals proper microtubule-kinetochore contacts – separates sister chromatids in the vicinity of centromeres, that broadly coincides with the region of pericentromeric cohesin enrichment (Stephens et al., 2011). Meanwhile, cohesin on chromosome arms resists the pulling forces of microtubules, keeping chromosome arms tightly cohered until cohesin is cleaved. The separation of centromeres is transient and is rapidly followed by re-association of sisters. This indicates that centromere-proximal chromatin exhibits spring-like behaviour, and the elasticity required for it was found to be conferred by of cohesin and condensin (Stephens et al., 2011). However, this observation poses a conundrum: how can sister chromatids separate in the region of highest cohesin density? Although the stretched cohesin ring can span up to 50 nm (Haering et al., 2002), the distance between sister centromeres can be as much as 1 μm (Goshima and Yanagida, 2000), suggesting that sister chromatid cohesion at centromeres is incompatible with this phenomenon.

1.4.4.2 Pericentromeric cohesin is sensitive to tension

Interestingly, microtubule-based tension appears to reduce cohesin association with chromosomes in the vicinity of centromeres (Eckert et al., 2007; Ocampo-Hafalla et al., 2007; Fernius and Marston, 2009; Nerusheva et al., 2014). The removal is partial as microscopy of metaphase cells indicates that a substantial amount of cohesin remains associated with chromosomes in the proximity of centromeres (Yeh et al., 2008; Hu et al., 2011). When tension is abrogated, cohesin can re-accumulate at pericentromeres in a manner that does not require the cohesin loader Scc2/4 (Ocampo-Hafalla et al., 2007). How cohesin removal occurs is unclear: the separation of sister centromeres occurs in the absence of cohesin proteolysis, the only known cohesin removal pathway in budding yeast mitosis. Nevertheless, tension-dependent removal of cohesin from pericentromeres could explain how sister centromeres transiently separate upon biorientation.

1.4.4.3 Cruciform chromosome conformation at pericentromeres

When biorientation is established, spindle forces move sister centromeres apart prior to anaphase onset (Goshima and Yanagida, 2000; He et al., 2000; Tanaka et al., 2000). This observation is paradoxical as the distance between sister centromeres (~1 μm) (Goshima and Yanagida, 2000) greatly exceeds the diameter of the stretched cohesin ring (50nm) (Haering et al., 2002). This suggests that the function of pericentromeric cohesin might not be related to its canonical function of holding sister chromatids together. In order to explain this paradox, it was proposed that cohesin at pericentromeres forms intra-sister linkages that tether the left and right chromosome arms together, resulting in a cruciform chromosome conformation (Yeh et al., 2008). This would allow sister kinetochores to protrude in opposite directions and adopt a back-to-back geometry (Figure 1.4.4.3.1). In turn, the back-to-back geometry of the cruciform would facilitate the capture of the protruding kinetochores by microtubules emanating from opposite poles (Ng et al., 2009), explaining why kinetochores have intrinsic bias to biorient on the spindle (Indjeian and Murray, 2007).

In support of this idea, the pericentromere of chromosome III in budding yeast was found to form an intramolecular loop: chromosomal regions on the left and right chromosome arms, as far 23 kb away from the centromere, are in physical proximity in metaphase (Yeh et al., 2008). The formation of this intramolecular pericentromeric loop depends on the presence of a kinetochore, but not on microtubule-kinetochore attachments (Anderson et al., 2009). This suggest that pericentromeric cohesin might not be functional in sister chromatid cohesion, but might instead establish intra-sister linkages. Indeed, later it has been demonstrated in a different context that not all contacts made by cohesin hold sister chromatids together: cohesin also establishes intra-sister linkages in budding yeast that result in the mitotic compaction of chromosome arms (Schalbetter et al., 2017). Additionally, the juxtaposition of chromosome arms by SMC complexes has also been observed. In *Bacillus subtilis* condensins have been found to topologically encircle DNA flanking their loading site, tethering the left and right chromosome arms together, and generating loops as they move from the replication origin to the terminus (Wang et al., 2017). Although the pericentromeric cruciform is an attractive idea to reconcile the pre-anaphase separation of sisters in the presence of high pericentromeric cohesin density, as well as to explain how kinetochore geometry facilitates biorientation, it does not account for the tension-dependent displacement of cohesin from pericentromeres.

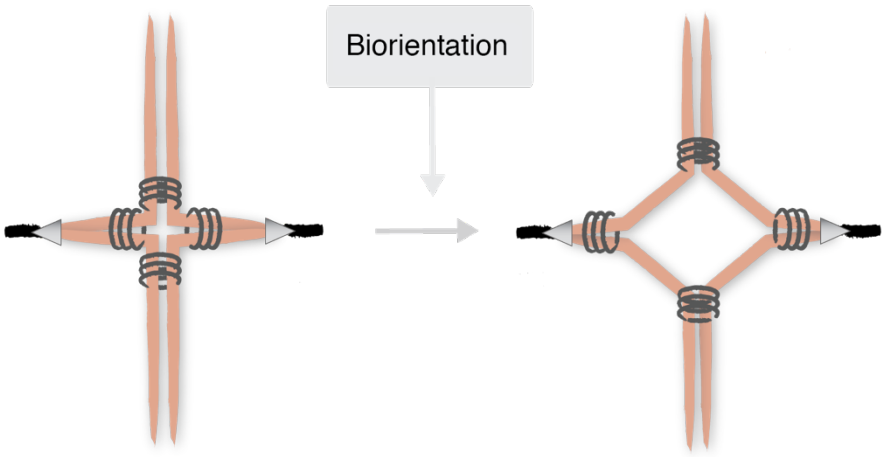

Figure 1.4.4.3.1 - Cruciform chromosome conformation at the pericentromere - Cohesin tethers the left and right sides of pericentromre together to establish intra-sister linkages. The model was proposed by Yeh *et al*. (2008) in order to explain the pre-anaphase separation of sister centromeres and the simultaneous rentention of cohesin.

1.5 Aims of this study

Cohesin plays a central role in several distinct mechanisms that are crucial for faithful chromosome segregation. In addition to its canonical role in holding replicated chromosomes together until their segregation in anaphase, cohesin is required for mitotic chromosome condensation, it facilitates biorientation through the establishment of a preferred kinetochore geometry, and it resists the pulling forces of microtubules once biorientation is achieved. Several lines of evidence provide support for the notion that cohesin at pericentromeres has specialized properties: unlike chromosome arms, sister chromatids in centromere-proximal regions separate in response to spindle tension prior to anaphase and this is accompanied by decrease in cohesin density specifically in the pericentromere.

The nature and function of cohesin in centromere-proximal regions has been the interest of many investigations, especially in the years following the discovery of the cohesin complex. These studies were crucial to appreciate the central role of cohesin in mitosis as well as the importance of pericentromeric cohesin domains for chromosome biorientation. However, technical developments that utilize high throughput sequencing now provide new tools for studying chromatin-related processes. By making use of these technological advancements and combining them with classical cell biology, this project aims to re-visit fundamental questions concerning mitotic chromosome segregation fidelity. To do this, I will use the widely studied model organism budding yeast that provides an excellent model system, as the lack of repetitive sequences in centromere-proximal regions makes sequencing-based approaches readily feasible.

Aim 1: What *cis*-acting features confine cohesin enrichment to pericentromeres?

In fission yeast and higher eukaryotes, pericentromeres are defined epigenetically, by the presence of heterochromatin. Cohesin recruitment to the pericentromere happens directly through heterochromatin-associated factors

which thus limit cohesin enrichment to the pericentromere. On the contrary, in budding yeast, cohesin that gets loaded at core centromeres translocates on chromosomes and accumulates in the pericentromere. In the absence of heterochromatin in budding yeast, the chromosomal features that confine cohesin enrichment to pericentromeres remain ambiguous. Therefore, first I aimed to precisely map pericentromeric cohesin enrichment domains in order to identify chromosomal features that are able to restrict cohesin to centromere-proximal regions, and thus define the limits of pericentromeres.

Aim 2: What is the structure of pericentromeres?

Cohesin enrichment at pericentromeres facilitates biorientation. Several lines of evidence suggest that this function might not depend on the canonical role of cohesin in holding sister chromatids together. Instead, it has been suggested that pericentromeres adopt a specialized chromosome conformation that promotes biorientation through cohesin-mediated intra-sister linkages in the vicinity of centromeres. To understand how pericentromere structure promotes biorientation, I set out determine chromosome conformation at the pericentromere in metaphase, and how it changes in response to microtubule-based tension. In addition, I investigate how chromosome organizers, cohesin and condensin, contribute to pericentromere structure.

Aim 3: What are the implications of pericentromere integrity for chromosome segregation?

If pericentromere structure set by cohesin is important for chromosome segregation, then its disruption should lead to phenotypic consequences. Therefore, in the final part of this project, through the manipulation of chromosomal determinants that delimit cohesin enrichment, I aim to disrupt the integrity of the pericentromere and study its consequences on pericentromere structure, chromosome biorientation and cellular fitness.

Chapter 2 Materials and Methods

2.1 General information

2.1.1 Supplier information

Growth media reagents were supplied by Difco, Formedium and Sigma. Chemicals and reagents were supplied by various companies including Abcam, Thermo Scientific, Fisher, Biorad, Gibco BRL, Beckman, Scientific Laboratory Supplies, Merck, Melford, Illumina, New England Biolabs, Promega, Qiagen, Invitrogen, Bioo Scientific, unless stated otherwise.

2.1.2 Sterilisation

Growth media was sterilised by autoclaving (15 min, 120°C, 15 pounds/inch^2) and glassware was sterilised by baking (16 hours, 250°C). Media was sterilised using 0.22µm filters, either in syringe (Millipore) or bottle top format (Nalgene).

2.2 DNA methods

2.2.1 Polymerase chain reaction (PCR)

2.2.1.1 ExTaq

To amplify DNA for yeast transformations, the high-sensitivity and high-efficiency ExTaq (TaKaRa RR001) PCR reaction was used according to manufacturer's instructions, using the supplied buffer and dNTP mix. In general, all PCR primers were designed to have annealing temperatures ~55°C. PRC composition and cycling conditions are specified in Table 2.2.1.1.1, 2.2.1.1.2.

2.2.1.2 Q5

For molecular cloning using Gibson assembly and homology template amplification for CRISPR, DNA fragments were amplified using Q5 (NEB M0491) PCR reaction, according to manufacturer's instructions. In general, all

PCR primers were designed to have annealing temperatures ~55°C. PRC composition and cycling conditions are specified in Table 2.2.1.2.1, 2.2.1.2.

Table 2.2.1.1.1 – ExTaq PCR composition

Reagent	Volume
ExTaq	1 µl
10x ExTaq Buffer	20 µl
ExTaq dNTPs	16 µl
20 µM forward primer	10 µl
20 µM reverse primer	10 µl
Template DNA (~200-500 ng/µl)	2 µl
dH_20	141 µl

Table 2.2.1.1.2 – ExTaq PCR cycling conditions

Step	Temperature (°C)	Time (min)
1	95	5:00
2	95	0:30
3	55	0:30
4	72	1 min/kb
Repeat steps 2-4 29 times		
5	72	3:00
6	10	forever

Table 2.2.1.2.1 – Q5 PCR composition

Reagent	Volume
Q5	1 µl
5x Q5 Buffer	20 µl
2.5 mM dNTPs	8 µl
20 µM forward primer	2.5 µl
20 µM reverse primer	2.5 µl
Template DNA (~200-500 ng/µl)	2 µl
dH_20	64 µl

Table 2.2.1.2.2 – Q5 PCR cycling conditions

Step	Temperature (°C)	Time (min)
1	98	0:30
2	98	0:10
3	55	0:30
4	72	1 min/kb
Repeat steps 2-4 29 times		
5	72	3:00
6	10	forever

2.2.1.3 Colony PCR

To verify yeast genotypes by colony PCR, in-house-purified Taq polymerase was used with 2.5 mM dNTPs and 10x PCR buffer (500 mM KCl, 20 mM MgCl2, 100 mM Tris-HCl pH 8.3, 0.1 % gelatin). For template DNA, a small amount of yeast was directly added to the chilled PCR reaction, which was

transferred to a pre-heated PCR block. In general, all PCR primers were designed to have annealing temperatures ~55°C. PRC composition and cycling conditions are specified in Table 2.2.1.3.1, 2.2.1.3.2.

Table 2.2.1.3.1 – Colony PCR composition

Reagent	Volume
Taq	0.4 µl
10x PCR Buffer	2 µl
2.5mM dNTPs	1.6 µl
20 µM forward primer	2 µl
20 µM reverse primer	2 µl
dH_20	14 µl

Table 2.2.1.3.2 – Colony PCR cycling conditions

Step	Temperature (°C)	Time (min)
1	95	10:00
2	95	0:30
3	55	0:30
4	72	1 min/kb
Repeat steps 2-4 29 times		
5	72	5:00
6	10	forever

2.2.1.4 Phusion High-Fidelity DNA Polymerase (NEB M0530)

To amplify NGS libraries Phusion High-Fidelity DNA Polymerase was used with NextFlex primers (Bioo Scientific). PRC composition and cycling conditions are specified in Table 2.2.1.4.1, 2.2.1.4.2.

Table 2.2.1.4.1 – Phusion PCR composition

Reagent	Volume
NGS library	1/3 of total
Phusion	0.5 µl
5x Phusion Buffer	10 µl
2.5mM dNTPs	4 µl
12.5 mM PCR primer mix	2 µl
DMSO	1.5 µl
dH_20	up to 50 µl

Table 2.2.1.4.2 – Phusion PCR cycling conditions

Step	Temperature (°C)	Time (min)
1	98	0:30
2	98	0:10
3	65	0:30
4	72	0:30
Repeat steps 2-4 12 times		
5	72	5:00
6	10	forever

2.2.2 Purification of DNA

2.2.2.1 Short fragments

Short DNA fragments were purified using commercially available PCR purification kits according to manufacturer's specifications. PCR and restriction digest fragments were purified using Qiagen PCR purification kit (28104), while ChIP-seq DNA fragments were purified using Promega Wizard SV PCR purification kit (A9281).

2.2.2.2 Large fragments, plasmids

Larger DNA fragments (>10kb) and plasmids were purified by ethanol (EtOH) precipitation. DNA was incubated at -20°C for at least 30 minutes with 2.5x volume of 100% EtOH and 1/10th volume of 3 M NaOAc, then it was pelleted for 10 minutes at 13000 rpm at 4°C. DNA was cleared from salt by washing with cold 70% EtOH and centrifugation at 13000 rpm for 5 minutes at 4°C. Following, the DNA was air-dried and finally resuspended in 10-50 µl dH_20.

2.2.3 Agarose gel electrophoresis

To visualise products of PCR reactions, cloning reactions, restriction enzyme digests and fragment size distributions, DNA was analysed on agarose gels stained with 0.5 µg/ml ethidium bromide (EtBr). 0.6% w/v (for fragments >10 kb), 1% w/v (for fragments 300 bp – 10 kb) or 2% w/v (for fragments <500bp) were made by heating agarose in TAE buffer (40 mM Tris, 1 mM EDTA, 0.1 % v/v acetic acid). Once cooled, the gel was poured into a gel cast (Thermo Scientific) and EtBr and combs were added. Once set, the gel was submerged in a TAE-filled gel tank and was loaded with DNA mixed with Orange G loading dye (10 % glycerol, 1 mM EDTA pH 8.0, 0.1 % w/v Orange G), in 6:1 ratio. For size comparison, NEB DNA ladders were used: 1 kb (N3232), 100 bp (N3231) or Low Molecular Weight (N3233), depending on the expected size of DNA fragments. DNA fragments were then separated by constant voltage of 90V-120V for 35-50 minutes, and finally visualized in a UV transilluminator.

2.2.4 Plasmid cloning

Plasmids generated in this study are detailed in Appendix I.

2.2.4.1 Restriction-enzyme based cloning

Plasmids containing 224x *tetO* repeats and a genomic targeting sequence were made by restriction enzyme-based cloning. 5-10 µl of AMp327 (*pRS306(tetOx224)*) backbone was digested with HindIII-HF (R3104) and XbaI (R0145) according to manufacturer's instructions, for 2 hours at 37°C, and resulting linear DNA fragments were purified by EtOH precipitation. Targeting sequences to be integrated to the backbone were amplified from yeast genomic DNA (wild type W303 strain AMy1176 - *MATa, ade2-1, leu2-3, ura3, trp1-1, his3-11,15, can1-100, GAL, psi+*), with PCR primers containing restriction enzyme cut sites: forward primer with XbaI site, reverse primers with HindIII site. The PCR fragments were checked by gel electrophoresis, purified using Qiagen PCR purification columns and digested with HindIII and XbaI according to manufacturer's instructions, for 2 hours at 37°C. DNA concentration for backbone and insert were checked on a Nanodrop device, and a 20 µl T4 (M0202) ligation reaction was set up with a 1:5 backbone:insert molar ratio. The ligation was carried out overnight at 18°C, following which the products were EtOH precipitated in the presence of 5 µl of brewer's yeast tRNA (Sigma-Aldrich R5636). Ligation products were taken up in 10 µl dH_2O which transformed into electrocompetent DH5α cells.

Plasmids cloned with this method are AMp1411, AMp1412, AMp1413, AMp1433, AMp1436, AMp1437, AMp1538, AMp1539, AMp1562, AMp1669, AMp1670, AMp1676, AMp1677, AMp1678, AMp1776, AMp1792.

2.2.4.2 Gibson assembly

All Gibson assembly primers were designed so that following PCR, 40 bp homology between adjacent fragments would be generated. Fragments were prepared either by Q5 PCR reaction, or by linearization (AMp58, empty YIplac211) using EcoRV (R3195). Following PCR, 8 µl product was subjected to treatment with 1 µl DpnI (R0176) in 1x CutSmart buffer for to degrade

plasmid template: a 30-minute incubation at 37°C after which DpnI was inactivated for 20 minutes at 80°C. Fragment concentrations were measured on a Nanodrop device, and Gibson assembly was set up in a 1:2 vector:insert molar ratio, using ~0.5 pmol vector DNA. The DNA mixture was added to 30 µl Gibson assembly master mix (Table 2.2.4.2.1), and incubated for 1 hour at 50°C. 2 µl Gibson assembly product was transformed into chemically competent DH5α cells.

Plasmids cloned using Gibson assembly were AMp1781, AMp1796.

Table 2.2.4.2.1 – Composition of Gibson assembly reactions

Solution	Reagent	Concentration
5x ISO Buffer	Tris-HCl, pH 7.5 MgCl2 dGTP (N0446) dTTP (N0446) dATP (N0446) dCTP (N0446) DTT PEG-8000 NAD	0.5 M 50 mM 1 mM 1 mM 1 mM 1 mM 50 mM 1% (w/v) 5 mM
Gibson assembly master mix	ISO buffer T5 Exonuclease (M0363) Phusion Polymerase (F0530) Taq Ligase (M0208)	1x 0.08 units/reaction 0.5 units/reaction 80 units/reaction

2.2.4.3 Golden Gate cloning

For CRISPR/Cas9-mediated genome editing, gRNA expression vectors were created by Golden Gate cloning. 20 bp gRNA sequence was designed using Benchling's gRNA Design Tool. Complementary single stranded oligos were ordered with appropriate overhangs that were annealed to one another by progressive cooling to generate double stranded gRNA. The resulting overhangs allowed the cloning of the double stranded gRNA into a gRNA expression vector (AMp1278, pWSP082) using Golden Gate cloning. Golden gate reaction compositions and cycling conditions are detailed in Tables 2.2.4.3.1, 2.2.4.3.2.

Table 2.2.4.3.1 – Golden Gate reaction composition

Solution	Reagent	Volume / Concentration
Golden Gate Mix	T4 ligase (M0202) T4 ligase buffer (B0202) BSA 10 mg/ml Esp3I (R0734)	1 µl 1 µl 0.1 µl 0.5 µl
Golden Gate Reaction	GG mix gRNA oligos entry vector (AMp1278) water	2.6 µl 10 nM 3 ng/µl up to 10 µl

Table 2.2.4.3.2 – Golden Gate reaction cycling conditions

Step	Temperature (°C)	Time (min)
1	37	5:00
2	16	5:00
Repeat steps 1-2 30 times		
3	50	2:30
4	80	2:00
5	10	forever

2.2.5 Verification of cloning products

2.2.5.1 Diagnostic digest

Generally, ~20 miniprep plasmids per cloning reaction were screened for correct assembly using a combination restriction of enzymes, and the digests were ran on 1% agarose gels. For *tetO* plasmids, the presence of insert and appropriate backbone size were verified by digestion with HindIII and XbaI, and electrophoresis on 0.6% v/w agarose gel.

2.2.5.2 Sanger sequencing

To sequence plasmids or genomic DNA purified from yeast the Big Dye Terminator Kit 3.1 (Applied Biosystems) reaction was used. Primers were designed to be place ~500 bp away from one another, as well as to sequence over cloning junctions. Sequencing reactions were set up on ice and placed in

a pre-warmed PCR block. Following, reactions were sent to Edinburgh Genomics where they were analysed on an ABI3730 DNA Analyzer (Applied Biosystems). The resulting FASTA sequences were inspected in Benchling. Sequencing reaction composition and cycling conditions are detailed in Tables 2.2.5.2.1, 2.2.5.2.2.

Table 2.2.5.2.1 – Big Dye reaction composition

Reagent	Volume
BigDye	2 µl
BigDye 5x Buffer	2 µl
Template DNA (200-500 ng/µl)	1 µl
5 µM sequencing primer	0.5 µl
dH_20	4.5 µl

Table 2.2.5.2.2 – Big Dye reaction cycling conditions

Step	Temperature (°C)	Time (min)
1	95	5:00
2	95	0:30
3	55	0:15
4	60	1:00
Repeat steps 2-4 25 times		
5	10	forever

2.2.6 Plasmid preps from *E. coli*

Composition of solutions used for plasmid preps are detailed in Table 2.2.6.1.

Table 2.2.6.1. Solutions used in minipreps and midipreps

Solution	Reagent	Concentration
TE buffer	Tris-HCl pH 7.5 EDTA pH 8	10 mM 1 mM
GTE	Glucose Tris-HCl pH 7.5 EDTA pH 7.5	50 mM 25 mM 10 mM
High Salt Buffer	CH_3CO_2K (potassium acetate) acetic acid	2.5 M to pH 4.8
Alkaline SDS (made fresh each time)	NaOH SDS	200 mM 1% v/v

2.2.6.1 Minipreps

For small-scale plasmid preps, 1.5 ml overnight culture of plasmid-containing *E. coli* grown in selective media was pelleted at 3000 rpm for 10 minutes. The pellet was resuspended in 100 µl GTE to which first 150 µl alkaline SDS, then

150 µl high salt buffer was added. Following a 15-minute incubation on ice, the mixture was pelleted at 13000 rpm for 5 minutes at 4°C and the supernatant was transferred to a fresh tube containing 900 µl 100% EtOH. Following centrifugation at 13000 rpm for 5 minutes at 4°C, the supernatant was aspirated and the DNA pellet was washed with 500 µl 70% EtOH and centrifuged again under similar condition. The DNA pellet was finally air-dried and resuspended in 50 µl 1x TE.

2.2.6.2 Midipreps

For larger-scale plasmid preps, 50 ml overnight culture of plasmid-containing *E. coli* grown in selective media was pelleted at 3600 rpm for 15 minutes. The pellet was resuspended in 2.5 ml GTE to which first 5 ml alkaline SDS, then 2.5 ml µl high salt buffer was added. The mixture was vortexed and pelleted at 3600 rpm for 5 minutes following which the supernatant was transferred to a fresh tube by pouring through a Kimwipe. 10 ml isopropanol was added and the mixture was centrifuges at 3600 rpm for 5 minutes. The pellet was resuspended in 750 µl TE, to which 1 ml 5 M LiCl was added to precipitate RNA. Following a 20-minute incubation on ice, the mixture was centrifuged at 3600 rpm for 5 minutes and the supernatant was transferred to a fresh tube containing 3.5 ml 100% EtOH. The solution was placed at -20°C for 15 minutes before the DNA was pelleted at 3600 rpm for 5 minutes. The supernatant was discarded, the DNA pellet was resuspended in 200 µl TE, transferred to a fresh 1.5 ml tube and mixed with 500 µl 100% EtOH and 20 µl 3M NaOAc. Following a 15-minute incubation at -20°C, DNA was pelleted at 13000 rpm for 5 minutes at 4°C, washed with 500 µl 70% EtOH and centrifuged again under similar condition. The DNA pellet was finally air-dried and resuspended in 200 µl 1x TE.

2.2.7 Isolation of genomic DNA from yeast

A small patch of budding yeast cells were taken from a plate and resuspended in 200 µl DNA breakage buffer (10 mM Tris-HCl pH 8.0, 1 mM EDTA pH 8.0, 100 mM NaCl, 2 % v/v Triton X-100, 1 % v/v SDS) to which a scoop of 0.5 mm silica beads (Biospec Products) were added. This was mixed with 200 µl

phenol:chloroform:isoamyl alcohol (PCI) and vortexed on a multi-vortexed for 4 minutes. The mixture was then centrifuged for 5 minutes at 13000 rpm, following which the aqueous layer was transferred to a fresh tube containing 1 ml 100% EtOH. The DNA was then pelleted for 5 minutes at 13000 rpm at 4°C. The supernatant was discarded, the DNA was air-dried and resuspended in 50 µl TE.

2.3 *E. coli* methods

2.3.1 General information

Escherichia coli strains were used in this study for plasmid amplification. Compositions of *E. coli* growth media are detailed in Table 2.3.1.1. All plasmids contained ampicillin resistance cassette for the selection of positive clones. For selection of positive clones LB media (liquid and agar) were supplemented with 100 µg/ml ampicillin. In between usage, *E. coli* were stored at 4°C on LB plates containing ampicillin. *E. coli* strains are listed in Table 2.3.1.2.

Table 2.3.1.1 – *E. coli* growth media used in this study

Media	Component	Concentration
LB media	Bacto-tryptone Bacto-yeast extract NaCl NaOH	1% w/v 0.5% w/v 0.5% w/v to pH 7.2
LB agar plate	Bacto-tryptone Bacto-yeast extract NaCl NaOH Agarose	% w/v 0.5% w/v 0.5% w/v to pH 7.2 2% w/v
SOC media	Bacto-tryptone Bacto-yeast extract NaCl MgCl2 MgSO4 KCl Glucose	2% w/v 0.5% w/v 20 mM 20 mM 10 mM 10 mM 20 mM

Table 2.3.1.2 - *E. coli* strains used in this study

Strain	Genotype	Application
DH5α chemically competent	F⁻ φ80*lac*ZΔM15 Δ(*lac*ZYA *arg*F)U169 *rec*A1 *end*A1 *hsd*R17(r_K^-, m_K^+) *pho*A *sup*E44 λ⁻ *thi* 1 *gyr*A96 *rel*A1	Gibson assembly, Golden Gate cloning
DH5α electrocompetent	F⁻ φ80*lac*ZΔM15 Δ(*lac*ZYA-*arg*F)U169 *rec*A1 *end*A1 *hsd*R17(r_K^-, m_K^+) *gal*⁻ *pho*A *sup*E44 λ⁻ *thi*1 *gyr*A96 *rel*A1	Cloning of *tetO* plasmids
SURE competent cells	e14-(McrA-) Δ(*mcrCB-hsdSMR-mrr)171 endA1 gyrA96 thi-1 supE44 relA1 lac recB recJ sbcC umuC::*Tn5 (Kanr) *uvrC* [F´ *proAB lacIqZΔM15* Tn10 (Tetr)]	Amplification of *tetO* plasmids

2.3.2 Growth conditions

E. coli were propagated at 37°C, either on LB plates or in liquid LB cultures shaken at 200-250 rpm. Bacteria containing *tetO* plasmids were grown similarly but at 30°C to minimise recombination.

2.3.3 Bacterial transformations

2.3.3.1 Transformation by electroporation

For the amplification of *tetO* plasmids electrocompetent DH5α cells were used. Cells were thawed on ice, 40 µl of cell suspension was transferred to a pre-chilled electroporation cuvette (Cell Project) and mixed with ~1 µg of plasmid DNA. Cuvettes were dried and pulsed in a BioRad Gene Pulser II at 2.5V (200 Ω, 2.5 µF). Cells were immediately resuspended in 1 ml SOC, transferred to a fresh tube, and let to recover at 30°C for 2 hours, at ~250 rpm. Following the recovery period, cell were concentrated by centrifugation at 3000 rpm for 3 minutes, plated on LB plates containing 100 µg/ml ampicillin and grow at 30°C for at least two days.

2.3.3.2 Transformation of chemically competent *E. coli*

For the amplification of plasmids other than those containing *tetO* repeat sequences, chemically competent DH5α cells were used. To that end, 100 µl of cell suspension was thawed on ice, mixed with 5-10 µl cloning product and incubated on ice for a further 30 minutes, before cells were heat-shocked in a 42°C water bath for 45 seconds. Cells were immediately put on ice for 2 minutes after which 1 ml SOC was added to the transformation mixture. Recovery was carried out at 37°C for 1 hour, and finally cells were spread on pre-warmed selective plates (LB with 100 µg/ml ampicillin) and grown at 37°C overnight.

2.3.3.3 Transformation of SURE cells

To further amplify correct *tetO* plasmids SURE competent cells were used that are deficient in recombination. This helped to preserve the number of *tetO* repeats in the array. A 14-ml BD Falcon polypropylene round-bottom tube was pre-chilled on ice, SOC medium was pre-heated to 42°C. SURE cells were thawed on ice and 100 µl cell suspension was added to each tube, along with 1.7 µl β-mercaptoethanol provided with the kit. Following a 10-minute incubation on ice (swirling the tube every 2 minutes), ~50 ng DNA was added to each tube, and mixture was incubated for a further 30 minutes on ice. Following, cells were heat-shocked in a 42°C water bath for 45 seconds, put back on ice for 2 minutes, and let to recover with 1 ml SOC media at 30°C, ~200-250 rpm. Cells were then spread on LB plates containing 100 µg/ml ampicillin and grown at 30°C for at least 24 hours.

2.4 Yeast methods

2.4.1 General information

For long-term storage, live yeast from plates following a <24 hour growth period were resuspended in 20% glycerol and frozen at -80°C in cryo-vials. For short-term storage yeast plates were kept at 4°C. Yeast were either grown in YPDA media at 30°C or at room temperature. Strains containing the *MET-CDC20* construct were grown in synthetic media lacking methionine (referred

to as -met), at 30°C or at room temperature, *ipl1-321* strains were grown at 25°C or at room temperature. Composition of growth media is detailed in Table 2.4.1.1, drug concentrations for selective growth are detailed in Table 2.4.1.2.

Table 2.4.1.1 – Composition of growth media used in this study

Media	Component	Concentration
YPDA media	2 % w/v Bacto-peptone 1 % w/v Bacto-yeast extract 4 % w/v Glucose Adenine	2% w/v 1% w/v 4% w/v 0.3 mM
YPDA agar plates	2 % w/v Bacto-peptone 1 % w/v Bacto-yeast extract 4 % w/v Glucose Adenine Agar	2% w/v 1% w/v 4% w/v 0.3 mM 2% w/v
Amino acid dropout media (supplemented with appropriate amino acids)	Synthetic yeast nitrogen base Formedium SC Glucose Adenine	1 % w/v 1x 2 % w/v 0.3 mM
Amino acid agar plates (supplemented with appropriate amino acids)	Synthetic yeast nitrogen base Formedium SC Glucose Adenine Agar	1 % w/v 1x 2 % w/v 0.3 mM 2 % w/v

Table 2.4.1.2 – Drug concentrations used for selective growth

Marker gene	Drug	Concentration
KANMX6	G418 (Life Technologies, 11811031)	300 µg/ml
HPHMX6	Hygromycin B (Merck, 400052)	300 µg/ml
NATMX6	Nourseothricin (Werner, 2202200)	100 µg/ml

2.4.2 Generation of yeast strains

2.4.2.1 High efficiency yeast transformation

To integrate *tetO* arrays at desired loci, rescue constructs with model genes to chromosome IV, to delete Rad61 and to remove 6HA tag from *MCD1* using CRISPR, exogenous DNA was introduced to cells using high efficiency yeast

transformation (solutions in Table 2.4.2.1.1). For this, yeast were grown overnight at room temperature in 10 ml media (YPDA or -met for *MET-CDC20* strains). In the morning, cultures diluted to OD_{600}=0.2 in 20 ml media, let to grow for 4-5 hours until the culture reached OD_{600}=0.5-0.8, and harvested by centrifugation at 3000 rpm for 3 minutes. Pelleted cells were washed first with 10 ml dH_2O, then 1 ml dH_2O and 1ml LiTE solution, before being resuspended in 100 µl LiTE. 50 µl of cell suspension was then mixed with the transforming DNA (200 µl ExTaq PCR product or 10 µl plasmid (linearized for *tetO*)), 10 µl 10mg/ml sonicated salmon sperm DNA, and 300 µl 40% PEG-4000. The yeasts were incubated at 30°C, 250 rpm for 30 minutes, after which they were heat-shocked on a 42°C heat block for 15 minutes. Yeasts were spun down at 3000 rpm for 3 minutes, the supernatant was removed, the cell pellet was resuspended in 200 µl TE and spread onto selective plates (for drug markers transformants were first grown for 16 hours on non-selective plates, then transferred onto drug plates). Transformants were grown for 2 days at 30°C after which colonies were streaked to singles on selective plates. Transformants were verified by colony PCR and microscopy (*tetO* strains).

Table 2.4.2.1.1 – Solutions used for high-efficiency yeast transformations

Solution	Composition	Concentration
LiTE	LiAc pH 7.5 Tris-HCl pH 7.5 EDTA pH 8	100 mM 10 mM 1 mM
40% PEG-4000	LiAc pH 7.5 Tris-HCl pH 7.5 EDTA pH 8 PEG-4000	100 mM 10 mM 1 mM 50% v/w

2.4.2.2 Yeast crosses

In order to generate new combinations of existing genotypes yeast strains were crossed. To make diploid cells, yeast from opposite mating types were mixed on plates for at least 8 hours at 30°C, after which they were streaked to single colonies on plates containing 10 µg/ml alpha-factor and a selection marker absent from the *MATα* strain, but present in the *MATa* strain, to restrict

growth to diploid cells only. Diploids were patched onto YPDA media, grown for a day, and transferred to sporulation plates (1% w/v potassium acetate, 1x synthetic complete amino acids, 2 % w/v agar) for at least 2 days at 30°C.

2.4.2.3 Tetrad dissection

Following the 2-day sporulation period, tetrads were digested 20 µl 1 mg/ml zymolyase (100T, AMS Biotechnology) in 2 M sorbitol for 8 min. The reaction was stopped by the addition of 1 ml dH_2O and 20 µl suspension was spread in the middle of a YPDA or -met plate. Individual spores in a tetrad were separated using a Nikon Eclipse 50i microscope equipped with a micromanipulator, and grown for at least 2 days at 30°C. Following, yeast were patched on non-selective plates before genotypes were verified by replica-plating onto selective plates, and by colony PCR.

2.4.3 Yeast growth conditions

Amino acid, mating pheromone and microtubule drug concentrations to synchronize cells in in various cell cycle stages and conditions are detailed in Table 2.4.3.1.

2.4.3.1 Cycling cells

Asynchronous mitotic cultures in the exponential phase were created by diluting overnight cultures to OD_{600}=0.2 in the morning, and letting them grow during the day, for 4-5 hours at room temperature.

Table 2.4.3.1 – Reagents used for cell cycle arrests

Arrest type	Reagent	Initial Concentration	Re-add Concentration
G1	alpha-factor	10 µg/ml	5 µg/ml
Metaphase No Tension	Benomyl (Sigma-Aldrich 45339)	30 µg/ml	-
Metaphase No Tension	Nocodazole (Sigma-Aldrich M1404)	15 µg/ml	7.5 µg/ml
Metaphase Tension/No Tension	L-Methionine (Foremedium DOC0169)	8 mM	4 mM

2.4.3.2 Metaphase arrest – Tension

Strains containing Cdc20 under a methionine-repressible promoter (*MET-CDC20*) were synchronized in metaphase in the following way. In -met media, overnight cultures were grown and diluted to OD_{600}=0.2 in the morning. Following a 1-1.5 hour-long pre-growth, cultures were diluted back to OD_{600}=0.2 and alpha-factor was added. Alpha-factor was re-added after 90 minutes, and after a total to 3 hours cells were checked for G1 cell morphology (shmoo) on a light microscope. To release cells from G1, alpha-factor was washed out from the culture using a Kontes filtration system: yeasts were transferred to Whatman membrane filters (pore size 0.45 µm) and washed 10 times with 1x volume fo YPDA media lacking glucose and adenine. After, yeast were transferred to flasks containing YPDA with 8mM methionine to shut down Cdc20 expression. Methionine was re-added after 60 minutes, and after a total of 2 hours, cells were checked for metaphase cell morphology (dumbbell) on a light microscope and cells were harvested. All was carried out at either room temperature (microscopy assays) or at 25°C (ChIP-seq and Hi-C).

2.4.3.3 Metaphase arrest – No tension

MET-CDC20 strains were synchronized in metaphase in the absence of microtubules similarly to as described in 2.4.3.2 Metaphase arrest – Tension with the following modification. Following G1 arrest, the release YPDA media (in addition to 8 mM methionine) also contained microtubule drugs benomyl and nocodazole. Nocodazole (along with methionine) was re-added to cultures after 60 minutes, and after 2 hours cells were checked for metaphase cell morphology (dumbbell) on a light microscope, and cells were harvested. All was carried out at either room temperature (microscopy assays) or at 25°C (ChIP-seq and Hi-C).

2.4.3.4 Nocodazole washout

First, with strains carrying *MET-CDC20* a no-tension metaphase arrest was carried out as described in 2.4.3.3. Subsequently, cells were filtered again 10 times with YPDA lacking glucose and adenine (Kontes filtering system,

Whatman membrane filters) in order to wash out microtubule drugs. Cells were then released into YPDA media with 8 mM methionine, and samples were taken at 20-minute intervals for 2 hours. All was carried out at room temperature.

2.4.3.5 G1 release

For the G1 release experiment, cells lacking *MET-CDC20* were synchronised in G1 at room temperature using alpha-factor as described in 2.4.3.2, except that cells were grown in YPDA rather than -met media. After filtering, cells were released into YPDA media pre-warmed to 32°C and grown for 2 hours at 32°C when samples were taken. At 40 minutes, alpha factor was added to cultures to prevent entry to the next cell cycle.

2.4.3.6 Plating assay

For viability assays, cells lacking *MET-CDC20* were grown at room temperature overnight in YPDA media. In the morning, cultures were diluted to OD_{600}=0.2 in YPDA, grown for 3 hours and diluted again to OD_{600}=0.2. Next, 500 µl of culture was taken, diluted serially 1:2000 in dH_2O, and 150 µl of the final dilution was plated per plate, to a total of 6 plates per condition (estimated ~200 cells per plate). Following, nocodazole was added to the cultures, and the plating was repeated 2 hours and 4 hours after nocodazole treatment. Nocodazole was re-added every 90 minutes. Plates were then grown for 2 days at 25°C, after which the number of colonies per plate were counted.

2.4.3.7 *S. pombe* growth conditions

In order to calibrate ChIP-seq experiments experimental budding yeast cell were combined with calibrating fission yeast cells (AM635 h- ade6-210 leu1-32 ura4-D18 his3-D1 arg3-D4 rad21::rad21-6HA:KANMX6, or AM1863 h- ade6-216 leu1-32 ura4-D18 rad21::rad21-6HIS-3FLAG::NatMX6). To grow fission yeast for ChIP-seq calibration, overnight cultures were grown at 30°C in YES (0.5% (w/v) bacto-yeast extract, 3% (w/v) glucose, 0.02% (w/v) Adenine, 0.02% (w/v) Histidine, 0.02% (w/v) Leucine, 0.02% (w/v) Uracil, 0.02% (w/v) Lysine), diluted to OD_{600}=0.1 in the morning, and grown at room temperature until they reached OD_{600}=~0.25. *S. pombe* cells were grown in

large batches (~5 litres), and harvested in 100 ml aliquots. Fixing and freezing conditions were kept similar to budding yeast.

2.4.4 Fixing conditions

2.4.4.1 GFP dot samples

For microscopical analysis of *tetO*/TetR-GFP markers, 900 µl of metaphase-arrested cells (tension) were fixed in 3.7% formaldehyde (Sigma-Aldrich 252549) at room temperature for 8 minutes. Cells were pelleted at 13000 rpm for 1 minute, quickly washed with 1 ml 80% EtOH and resuspended in 20 µl of 1 µg/ml DAPI (4',6-diamidino-2-phenylindole) in PBS. Samples were stored at 4°C and analysed within 48 hours.

2.4.4.2 ChIP-seq samples

100 ml of cells were fixed with 10 ml of 11% formaldehyde (final concentration ~1%) in dilulent (143 mM NaCl, 1.43 mM EDTA, 71.43 mM Hepes-KOH pH 7.5), for 30 minutes at room temperature with slow shaking at 90 rpm. Cells were then pelleted at 3000 rpm for 3 minutes at 4°C, washed twice with 10 ml TBS (20 mM Tris-HCl pH 7.5, 150 mM NaCl) and once with 10 ml FA buffer + 0.1% SDS lacking protease inhibitors (Table 2.5.1.1). Cell pellets were transferred to Fastprep tubes (MP Biomedicals), frozen in liquid nitrogen and stored at -80°C until further use.

2.4.4.3 Hi-C samples

200 ml of cells were fixed with 17.6 ml 37% formaldehyde (final concentration 3%) for 20 minutes at 250 rpm at 25°C, and the fixing reaction was quenched with 35.2 ml 2.5M glycine for 5 minutes at 250 rpm at 25°C. Cells were pelleted at 3600rpm for 5min in 5x 50ml Falcon tubes, washed with 20ml cold water each. Next, samples were pooled and resuspended in 5ml 1x NEB2 (B7002S), drop-frozen in liquid nitrogen and stored at -80C until further use.

2.4.4.4 Immunofluorescence

To verify the efficiency of metaphase arrest, samples for tubulin immunofluorescence were taken. 1 ml of culture was pelleted at 13000 rpm for 1 minute, and fixed in 500 µl 3.7% formaldehyde diluted in 0.1 M KPi buffer pH

6.4 (27.8 ml of 1 M K_2HPO_4, 72.2 ml of 1 M KH_2PO_4, 900 ml dH_2O), overnight at 4°C. Pellets were then washed 3 times with 1 ml 0.1 M KPi, once in 1.2 M sorbitol citrate (1.2 M sorbitol, 0.1 M K_2HPO_4, 36 mM citric acid) and stored at -20°C in 1 ml 1.2 M sorbitol citrate until further use.

2.5 Molecular biology methods

2.5.1 Chromatin immunoprecipitation (ChIP) for ChIP-seq

Table 2.5.1.1 – Composition of ChIP solutions

Solution	Composition	Concentration
1x FA lysis buffer	Hepes-KOH pH 7.5 NaCl EDTA Triton X-100 Na-Deoxycholate PMSF Roche EDTA-free protease inhibitors	100 mM 300 mM 2 mM 2% v/v 0.2% v/v 1 mM 1x
ChIP wash buffer 1	FA lysis buffer NaCl SDS	1x 275 mM 0.1% v/v
ChIP wash buffer 2	FA lysis buffer NaCl SDS	1x 500 mM 0.1% v/v
ChIP wash buffer 3	Tris-HCl pH 8 LiCl EDTA NP-40 Na Deoxycholate	10 mM 250 mM 1 mM 0.5% v/v 0.5% v/v
ChIP wash buffer 4	Tris-HCl pH 8 EDTA	10 mM 1 mM
TES buffer	Tris-HCl pH 7.5 EDTA SDS	50 mM 10 mM 1%

Solutions used for ChIP-seq are detailed in Table 2.4.5.1. For each condition, 2 aliquots of budding yeast cells (each pelleted from 100 ml culture) and two aliquots of fission yeast cells (each pelleted from 100 ml culture) were thawed on ice. Fission yeast aliquots were resuspended in 400 µl 1x FA buffer + 0.5%

SDS, and this was added to the budding yeast cells pellets, along with a scoop of silica beads (0.5mM, Biospec Products). Cells were lysed by shaking on a Fastprep Bio-Pulveriser (FP120) at 6.5 speed for 3 times 30 seconds, with 10 minutes on ice between them. The bottom of the tube was then pierced using a hot needle, and this was placed inside a 15 ml Falcon tube containing a fresh Fastprep tube. The cell lysate was transferred to the fresh tube be centrifuging the assembly at 3000 rpm for 3 minutes (4°C). Following, chromatin was pelleted at 13000 rpm for 15 minutes (4°C) and the supernatant was aspirated. Chromatin pellet was washed with 1 ml 1x FA buffer + 0.1% SDS, pelleted again and finally resuspended in 300 µl 1x FA buffer + 0.1% SDS. The samples were sonicated for 2x 20 cycles of 30 seconds on/off at high setting, in a Diagenode Bioruptor sonicator, with a 20-minute resting period on ice in between. Next, cell debris was pelleted at 13000 rpm for 15 minutes (4°C) and the solubilised chromatin (supernatant) was transferred to a fresh tube containing 1 ml 1x FA buffer + 0.1% SDS. Samples were spun again at 13000 rpm for 15 minutes (4°C), and the two aliquots of the same sample were pooled in a 15 ml Falcon tube. For each condition, 10 µl input sample frozen at -20°C, and a further 100 µl sample was incubated in 1 mg/ml Proteinase K (Life Technologies 25530015) overnight at 65°C to check sonication efficiency. The remaining sample was split to 2x 1 ml aliquots that were each incubated with 15 µl of protein G Dynabeads (Invitrogen, 20 mg/ml) (washed 4 times in 1x FA buffer + 0.1% SDS), and either 7.5 µl of 0.4 mg/ml anti-HA 12CA5 (Roche 11666606001) or 5 µl of 1 mg/ml anti-FLAG M2 (Sigma F1804) for IP. IPs were incubated overnight at 4°C on a rotating wheel.

The following day, beads were collected on a magnet and washed sequentially with 1 ml of ChIP was buffer 1, 2, 3, and 4, with a 5-minute rotation in each buffer. After the final wash, the two aliquots of the same sample were pooled in 200 µl TES buffer and boiled for 20 minutes at 65°C (with a brief vortexing half-way) to elute DNA. Beads were spun down for 3 minutes at 13000 rpm, the supernatant was transferred to a fresh tube and beads were washed with 200 µl TE for 15 minutes with rotation. Beads were pelleted again and the supernatant was combined with the previous one (200 µl TES). Meanwhile,

input samples were thawed and their volume was brought up to 400 µl with TE. Both inputs and IPs were incubated at 65°C overnight in 1 mg/ml proteinase K for decrosslinking. Additionally, decrosslinked samples from the day before were cleaned up using Qiagen PCR purification kit and run on a 2% agarose gel with a 100 bp ladder to check for the level of DNA sheering.

The following day, input and IP samples were cleaned up using Promega Wizard SV Purification kit, and DNA was eluted in 35 µl Hyclone water (GE Lifesciences). Finally, 3 µl of sample was used to measure DNA concentration on a Qubit 3.0 Fluorometer high-sensitivity DNA assay (Thermo Fisher Scientifc), according to manufacturer's instructions.

2.5.2 Sequencing library preparation

Ideally 2 ng, but at least 0.5 ng input and IP DNA was subjected to blunting and phosphorylation using NEB Blunt Enzyme Mix (E1201), at room temperature for 45 minutes (Table 2.5.2.1) in DNA LoBind tubes (Eppendorf 0030108051). Ampure XP (Beckman) beads equilibrated to room temperature were used in a 1.6:1 ratio to samples (80 µl of beads mixed to 50 µl of sample), to purify fragments >100 bp onto beads. According to the standard Ampure XP protocol, beads were incubated with samples for 10 minutes, collected on a magnet for 5 minutes, washed twice with 250 µl of 70% EtOH and dried for 3-4 minutes. DNA was eluted from beads by resuspending beads in 30 µl Hyclone water (GE Lifesciences) for 5 minutes, beads were collected on a magnet for 3 minutes and the supernatant was transferred to a fresh tube.

Table 2.5.2.1 – Blunting reaction

Reagent	Volume
DNA	0.5-2 ng
10x Blunting buffer	5 µl
1 mM dNTPs	5 µl
Blunt Enzyme Mix	1 µl
dH_2O	up to 50 µl

Table 2.5.2.2 – dA-tailing reaction

Reagent	Volume
DNA	27.7 µl
NEB2	3.3 µl
10mM dATP	1 µl
Klenow (exo-)	1 µl

Table 2.5.2.3 – Adapter ligation reaction

Reagent	Volume
DNA	33 µl
2x Quick ligase buffer	35 µl
0.5 µM adapters	1 µl
Quick ligase	1 µl
dH_2O	to 70 µl

Next, a dA-tailing reaction was carried out using Klenow (exo-) (NEB M0212) at 37°C for 30 minutes (Table 2.5.2.2). The enzyme was heat-inactivated for 5 minutes at 75°C and the reaction was cooled on ice for 5 minutes. Using the dA overhangs, NextFlex (Perkin Elmer NOVA-514102) Barcoded adapters were ligated to the fragments, using Quick Ligase (M2200) for 25 minutes at room temperature (Table 2.5.2.3). Excess adapters were cleared by two sequential rounds of 1:1 Ampure XP purification (as detailed above) first with 70 µl beads, then with 50 µl. DNA was eluted in 30 µl water, and 10 µl was taken out by Phusion PCR amplification (detailed in 2.2.1.4). Following PCR, first large DNA fragments were cleared by a 0.65x purification (32.85 µl of Ampure XP beads added to 50 µl sample), a ratio that binds >300 bp fragments on beads. Following the binding, beads were collected and the supernatant containing the fragments of interest (<300 bp) was transferred to a fresh tube. The 80 µl supernatant was mixed with 55 µl of beads, resulting in 1:1.6 purification that binds fragments >100 bp onto beads. Beads were eluted in 50 µl water and subjected to a final 1:1 Ampure XP purification. Finally, amplified libraries were eluted in 30 µl water. To quantify libraries, 1 µl sample was loaded on a Qubit 3.0 Fluorometer high-sensitivity DNA assay (Thermo Fisher Scientific), according to manufacturer's instructions. To determine size distribution, 1 µl sample was analyzed on a 2100 Bioanalyzer High Sensitivity DNA chip (Agilent), according to manufacturer's instructions.

2.5.3 Hi-C

Lysates were prepared by grinding the frozen cell pellet in a chilled mortar with a pestle for 15 minutes, with 4 addition of liquid nitrogen. 1/10th of the initial pellet weight (~0.5 g) was taken in a 2 ml Eppendorf tube, washed with 1 ml 1x NEB3.1 (B7203) and resuspended in 1.1 ml 1x NEB3.1. Chromatin was solubilized by adding 110 µl of 1% SDS to the sample and incubating it at 65°C, after which the tube was place on ice. 127 µl 10% Triton-X100 was added to the reaction to quench SDS. Finally, to digest chromatin, the sample was incubated with 57.6 µl 50 U/µl DpnII enzyme (R0543M), at ~250 rpm at 37°C overnight.

The next morning, a fill-in reaction (Table 2.5.3.1) was set up to mark restriction sites with biotin-14-dCTP (Thermo Fisher Scientific 19518018) and to generate blunt ends. The tube was placed back at 37°C ~250 rpm for a further 2 hours, after which it was incubated with 276.5 µl of 10% SDS, at 65°C for 20 minutes. Following, a dilute ligation reaction was set up in a 50 ml Falcon (Table 2.5.3.2), to which samples were added. Samples were aliquoted into 13x 2 ml Eppendorf tubes and incubated at 16°C for 8 hours. Tubes were inverted every 1-2 hours. After the 8-hour incubation period, samples were pooled in a 50 ml Falcon tube and treated with 270 µl 5 mM EDTA (pH 8). To each sample 172.8 µl 10 mg/ml proteinase K was added, and decrosslinking was carried out in a 65°C overnight.

The following day, 172.8 µl 10 mg/ml proteinase K was re-added to tubes which were incubate at 65°C for a further 2 hours. After, the samples were split to two 50 ml Falcons, and to each falcon 20 ml Phenol:Chloroform:Isoamyl alcohol (PCI) was added. Samples were vortexed for 1 minute, transferred to and spun in 2x 50 ml MaXtract tubes (Qiagen 129073) for 10 minutes, at 1500 g at 4°C. The aqueous phase was then split to 3x 10 ml aliquots in JA-20 centrifuge tubes (Beckman), and to each tube 1ml 3M NaOAc and 25 ml 100% EtOH was added to precipitate DNA at -20°C for 1 hour. Samples were spun at 18000 rpm for 20 minutes at 4°C (Beckman JA-20 rotor), washed with 10 ml 70% EtOH, incubated at -20°C for 1 hour and finally spun again 18000 rpm for

20 minutes at 4°C (Beckman JA-20 rotor). The supernatant was disposed of, the DNA pellet was dried in the fume hood for 30 minutes and the DNA was resuspended in 7.5ml 1x TE on the bench for 1-2 hours. Next, samples were concentrated to ~250 µl of volume using Amicon-15 30 kDa columns (Millipore UFC903024), the column was rinsed with 200 µl TE which was combined with the sample. DNA was extracted using 500 µl PCI and 1.5 ml MaXtract tubes (Qiagen 129046) with centrifugation at 12000rpm for 10 minutes at room temperature. The aqueous phase was transferred to a fresh tube containing 45 µl 3 M NaOAc and 1 ml 100% EtOH, and DNA was precipitated at -20°C for 1 hour. DNA was pelleted at 14000 rpm for 20 minutes at 4°C, washed with 500 µl 70% EtOH and pelleted again. The DNA pellet was air-dried for 30 minutes before resuspension in 20 µl 1x TE on ice for 1 hours. Following, the samples were treated with 4 µl 10 mg/ml RNase A for 1 hour at 37°C, in order to degrade RNA. Next, DNA was quantified on a Qubit 3.1 Flourometer (load 1 µl of Hi-C DNA in 1:10 dilution) and biotin was removed from unligated end (Table 2.5.3.3) using T4 DNA polymerase (NEB M0203). The reaction was incubated at 20°C for 4 hours, after which it was inactivated for 20 minutes at 75°C. Sample volume was then brought up to 130 µl (2 µl of sample was removed to a separate tube for running it on a gel later), and the samples were sonicated on a Bioruptor device (Diagenode), 2x 30 cycles of 30 second on/off at high setting. DNA was then purified using Qiagen MinElute columns (28004) and eluted with 32 µl of EB (Qiagen) pre-heated to 65°C (2 µl of sample was removed to a separate tube for running it on a gel later). Following, DNA ends were repaired (Table 2.5.3.4) for 30 minutes at 20°C using T4 DNA polymerase (M0203), T4 Polynucleotide kinase (M0201) and DNA polymerase Klenow fragment (M0210), and DNA was purified again on MinElute columns (Qiagen), this time eluting in 22 µl of EB (Qiagen) pre-heated to 65°C. Finally, to prepare fragments for adapter ligation, dA-tailing was carried out using Klenow (exo-) (M0212) for 30 minutes at 37°C (Table 2.5.3.5).

Next, the Hi-C library was fractionated using Ampure XP beads. Reaction volume was brought up to 500 µl to with 450 µl Ampure XP beads were added (0.9X), incubated for 10 minutes at room temperature following which beads

were collected on a magnet for 5 minutes. The supernatant containing fragments <300bp was transferred to a new tube containing 500 µl beads harvested and resuspended in 100 µl Ampure XP mix (1.1X). The reaction was incubated for 10 minutes, beads were collected for 5 minutes and following washing and drying, DNA (200-300 bp) was eluted from beads for 10 minutes with 85 µl EB pre-heated to 65°C.

To isolated biotinylated DNA fragments, 80 µl of the 1.1X fraction was mixed with 10 µl of MyOne Streptavidin C1 beads (Invitrogen 65001) (pre-washed twice with 400 µl TWB) resuspended in 80 µl 2x BB. The reaction was incubated at room temperature with rotation for 1 hour. The following 3-minute washes were performed with rotation after: 200 µl 1x BB, 50 µl 1x Quick ligase buffer. Beads were resuspended in 10 µl water, and a Quick Ligase reaction was set up for 15 minutes at room temperature, to ligate NextFlex sequencing adapters (Table 2.5.3.6). Afterwards, the following 3-minute washes were performed with rotation after: 200 µl 1x TWB, 200 µl 1x TWB, 100 µl 1x BB, 100 µl 1x TE and 25 µl 1x TE. After each was the sample was transferred to a fresh tube. Finally, beads were resuspended in 9 µl water, and they were added to 3x 50 µl Phusion PCR reaction (2.2.1.4). Following PCR, sample volume was brought up to 200 µl, and samples were subjected to two rounds of 1.1X Ampure XP purification, using 220 µl beads. Finally, the amplified Hi-C library was eluted from beads using 32 µl of TLE buffer pre-heated to 65°C. 1 µl of sample was diluted 1:10, and 1-1 µl was analyzed on Qubit 3.0 for quantity and 2100 Bioanalyzer for purity and size distribution. Compositions of Hi-C solutions are detailed in Table 2.5.3.7.

Table 2.5.3.1 – Fill-in reaction

Fill-in mix	Per Hi-C sample (µl)
10x NEBuffer 2	15.4
100 mM dATP	0.43
100 mM dGTP	0.43
100 mM dTTP	0.43
0.4 mM biotin-14-dCTP	108
5 U/ul Klenow (DpolI)	28.8
Total	153.49

Table 2.5.3.2 – Ligation reaction

Ligation mix	Per Hi-C sample (µl)
10% Triton X-100	2400
10x Ligation Buffer	2400
10 mg/ml BSA	259.2
100mM ATP	259.2
Water	19248
T4 DNA ligase 1 U/ul	648
Total	25214.4

Table 2.5.3.3 – Biotin removal

Reagent	1x reaction (µl
Hi-C library	1ug
10 mg/ml BSA	0.1
10x NEB2	1
1.25 mM each dNTP (5 mM total)	0.1
T4 DNA polymerase	1
Water	To 10
Total	10 ul

Table 2.5.3.4 – End repair

Component	Per Hi-C sample (µl)
10x NEB ligation buffer	14
25 mM dNTPs each (100 mM total)	1.4
T4 DNA Polymerase	5
T4 Polynucleotide kinase	5
Klenow fragment DpolI	1
Water	13.6
Total	40

Table 2.5.3.5. – dA-tailing

Composition	Volume (µl)
10X NEBuffer 2	3
10 mM dATP	0.75
Klenow (exo-)	2.25
Water	4
Total	10

Table 2.5.3.6 – Adapter ligation

Composition	Volume (µl)
2X NEB Quick Ligation Buffer	13
Quick Ligase	1
NextFlex Adapeters 1:5	2
Total	16

Table 2.5.3.7 – Hi-C solutions

Solution	Composition	Concentration
1x TE	Tris-HCl pH 8 EDTA pH 8.0	10 mM 1 mM
10x Ligation buffer	Tris-HCl pH 7.5 $MgCl_2$ DTT	500 mM 100 mM 100 mM
2x BB	Tris-HCl pH 8.0 EDTA pH 8.0 NaCl	10 mM 1 mM 2 M
1x TWB	Tris-HCl pH 8.0 EDTA pH 8.0 NaCl Tween-20	5 mM 0.5 mM 1 M 0.05% v/v%
TLE buffer	Tris-HCl pH 8.0 EDTA pH 8.0	10 mM 0.1 mM

2.5.4 MiniSeq sequencing conditions

The molarity of ChIP-seq NGS libraries was calculated from the Qubit v3.0 concentration measurements and the average fragment size from the 2100 Bioanalyzer results. Following, all libraries were diluted to 1 nM in Qiage EB, and samples sequenced on the same sequencing cartridge were pooled together in a 15% to 85% input:IP ratio, in ~50 µl volume. 5 µl of pooled library was denatured with 5 µl 0.1 N NaOH at room temperature for 5 minutes, after which the reaction was stopped by the addition of 5 µl Tris-HCl pH 7.0. The libraries were diluted with 985 µl hybridisation buffer (supplied with the MinSeq sequencing cartridge), and 150 µl of the pooled libraries was further diluted by

350 µl hybridisation buffer. The resulting 500 µl 1.5 pM library was loaded on a thawed sequencing cartridge (Illumina FC-420-1002) and sequenced in an Illumina MiniSeq instrument in a paired-end manner, with read 1 and read 2 each being 76 bp long.

2.6 Microscopy methods

2.6.1 Immunofluorescence

Multi-well glass slides were treated with 0.1% polylysine for 5 minutes, after which they were rinsed and dried. Meanwhile, fixed and washed cells were digested at 30°C for ~45 minutes in 222 µl digestions solution until cells became dark-phase with jagged edges. Digested cells were gently washed with 1 ml 1.2 M sorbitol citrate, pelleted at 3000 rpm for 3 minutes and resuspended in 30 µl 1.2 M sorbitol citrate. 5 µl of cell suspension was placed in each well of the glass slide for 10 minutes, after which cells were fixed on slides by 3 minutes in 100% methanol followed by 10 seconds in 100% acetone. To each well 5 µl primary antibody was added (1 mg/ml rat α-tubulin, 1:50 dilution in PBS-BSA, Bio-Rad AbD Serotec) and the slides were incubated in a wet chamber at room temperature for 2 hours. Subsequently, wells were washed 5 times with 10 µl PBS-BSA, and incubated with secondary antibody (1.25 mg/ml donkey anti-rat-FITC, 1:100 dilution in PBS-BSA, JacksonImmuno Research) in a similar fashion. Wells were washed again 5 times with 10 µl PBS-BSA, and sealed with a cover slip using nail varnish, in 3 µl DAPI mount. Immersion oil (Zeiss) was placed on slides which then were analysed on Zeiss Axioplan 2 fluorescence microscope with a 100 x Plan ApoChromat NA 1.45 lens. 200 cells were categorised as “interphase”, “metaphase” or “anaphase”, based on spindle morphology. Solution compositions are detailed in Table 2.6.1.1.

Table 2.6.1.1 – Solutions used for immunofluorescence

Solution	Composition	Concentration /Amount
1.2 M sorbitol citrate	sorbitol citric acid K_2HPO_4	1.2 M 36 mM 0.1 M
Digestion solution	1.2 M sorbitol-citrate Glusulase (Perkin-Elmer) 10 mg/ml zymolyase (T100, AMS Biotechnology)	200 µl 20 µl 2 µl
PBS-BSA	BSA NaCl K_2HPO_4 KH_2PO_4 NaN_3	1% w/v 150 mM 40 mM 10 mM 0.1%
DAPI mount	P-phenylenediamine K_2HPO_4 KH_2PO_4 NaCl NaN3 DAPI glycerol	1 mg/ml 40 mM 10 mM 150 mM 0.1% 0.05 µg/ml 90%

2.6.2 GFP dot assays

To look at separation of *tetO*/TetR-GFP markers at different loci, biorientation assays, and G1 release experiments, 5 µl of fixed cells were placed on a glass slide and pressed down with a coverslip. Immersion oil (Zeiss) was placed on slides which then were analysed on Zeiss Axioplan 2 fluorescence microscope with a 100 x Plan ApoChromat NA 1.45 lens. 200 cells were counted for the number of GFP foci, and 100 cells were counted for the number of SBPs.

2.6.3 Distance measurements

For distance measurements slides were prepares in a similar fashion as in 2.6.2. Following, images were taken on Zeiss Axioplan 2 fluorescence microscope with a 100 x Plan ApoChromat NA 1.45 lens, Photometrics Evolve EMCCD camera (Photometrics, Tucson, USA) controlled using MicroManager

1.4 acquisition software (US National Institutes of Health). 5 Z-stack were taken 0.5 µm apart, in GFP channel (35 ms exposure) and in dsRed channel (50 ms exposure). Distance between GFP dots was measured in Image J, using a custom plugin that can be found at the github repository https://github.com/dkelly604/CellClicker_.

2.6.4 Live cell imaging

For live-cell imaging, a no-tension metaphase arrest was carried out as described in 2.4.3.3, with the following modifications: cells were arrested in synthetic complete media with 8mM methionine to which no benomyl was added. 200 µl of culture was placed in a pre-washed CellASIC ONIX microfluidics plate (purged and loaded according to manufacturer's instructions) and kept in nocodazole until imaging was set up on a Zeiss Axio Observer Z1 (Zeiss UK, Cambridge) equipped with a Hamamatsu Flash 4 sCMOS 327 camera, Prior motorized stage and Zen 2.3 acquisition software. Nocodazole was washed out after the first images were taken, then cells were imaged at 15-minute intervals at 25°C, for 3 hours. Images were then analysed in Image J.

2.7 Bioinformatics

2.7.1 ChIP-seq data analysis

ChIP-seq data was analysed by Daniel Robertson (Bioinformatics Core Facility, WCCB). Briefly, for strains where gene orientation was reversed, reference genomes were assembled *in silico*, for all other strains the sacCer 3 assembly was used as reference. Occupancy ratio for calibrated ChIP-seq was calculated as in (Hu et al., 2015) At each position, he number of reads were normalized to the total number of reads, multiplied by the occupancy ratio and visualised in IGV (Integrated Genome Viewer, Broad Institute). ChIP-seq pile-ups were generated using SeqPlots (Stempor and Ahringer, 2016), mean (+/- 3 kb plots) or median (+/- 25 kb and 100 kb plots) number of calibrated reads

was determined per 50bp window and its $\log_2$ value was graphed. For +/- 3 kb plots, dark shading indicates standard error, light shading marks 95% confidence interval. Scripts used to generate ChIP-seq plots can be found at the github repository https://github.com/AlastairKerr?tab=repositories.

2.7.2 Hi-C data analysis

Hi-C data was analysed by Daniel Robertson (Bioinformatics Core Facility, WCCB), using HiC-Pro v2.11.1 (Servant et al., 2015) and bowtie2 v2.3.4.1. After the removal of singletons, duplicated reads, multi-hits, and invalid pairs, valid interaction pairs were converted to .cool format, binned at 1 kb resolution, and uploaded to a local HiGlass (Kerpedjiev et al., 2018) server for visualization. Cooltools library was used to generate pile-ups, with duplicating contacts around center point in forward and reverse orientations in order to generate maps with mirror symmetry. For ration pile-ups, the $\log_2$ difference was plotted. All scripts used to generate Hi-C plots are deposited at https://github.com/danrobertson87/Paldi_2019.

Chapter 3 Cohesin enrichment sites between convergent genes mark pericentromere borders

3.1 Introduction

Pericentromeres are specialised chromosomal domains that flank centromeres. Although the function of centromeres – to specify sites for kinetochore assembly, and pericentromeres – to facilitate sister chromatid biorientation, is conserved through all domains of eukaryotic life, the DNA sequences that govern these functions are not. Centromeres can be divided into two main types: large regional centromeres that are often repetitive in nature, and small point centromeres (reviewed in Allshire and Karpen, 2008; Bloom and Costanzo, 2017). Accordingly, their associated pericentromeres are also different in nature: pericentromeres flanking regional centromeres are large and heterochromatic, while pericentromeres associated with point centromeres are shorter and euchromatic.

Despite diverse pericentromeric DNA sequences and chromatin states, pericentromeres universally contain high cohesin density. In fission yeast, an organism with regional centromeres, epigenetic factors such as Swi6/HP1 direct cohesin recruitment to pericentromeric heterochromatin (Bernard et al., 2001; Nonaka et al., 2002). In contrast, in budding yeast that has point centromeres, pericentromeric cohesin enrichment is a result of kinetochore-driven cohesin loading (Fernius and Marston, 2009; Ng et al., 2009; Hinshaw et al., 2015; Hinshaw et al., 2017) and the pericentromere remains euchromatic with actively transcribed genes.

In the absence of specific epigenetic marks at budding yeast pericentromeres it is unclear what the *cis*-acting features are that set the limits to cohesin enrichment. Work in this chapter seeks to determine the patterns of

pericentromeric cohesin enrichment, as well as how it is established and limited to centromere-proximal chromosomal regions.

3.2 Protocol Optimisation

3.2.1 Calibrated ChIP-seq

In the past, chromatin immunoprecipitation (ChIP) has been widely used to study *in vivo* DNA-cohesin interactions over the pericentromere as well as genome-wide (Megee et al., 1999; Lengronne et al., 2004; Glynn et al., 2004; Weber et al., 2004; Ocampo-Hafalla et al., 2007; Fernius and Marston, 2009). Broadly, ChIP relies on the covalent stabilisation of DNA-protein complexes using formaldehyde, the immunoprecipitation of a protein of interest, and the subsequent analysis of DNA fragments associated with the specific protein (Solomon et al., 1988; Dedon et al., 1991). DNA analysis can involve the detection of purified DNA using PCR (Orlando et al., 1997) or quantitative PCR (ChIP-qPCR) (Nishida et al., 2005) to determine protein occupancy at specific genomic loci. Alternatively, to determine the genome-wide binding of a protein, ChIP can be coupled with DNA microarrays (ChIP-chip) (Blat and Kleckner, 1999; Ren et al., 2000; Iyer et al., 2001) or the purified DNA can be further processed for the generation of Next Generation Sequencing (NGS) libraries (ChIP-seq) (Johnson et al., 2007; Robertson et al., 2007).

Although these techniques provide accurate measures for protein distribution within genomes, they cannot be used to measure changes in protein occupancy between different samples, as the difference between outputs can be equally due to changes in protein occupancy and changes in loading throughout the genome. This limitation was overcome by the development of calibrated ChIP-seq (Hu et al., 2015) which simultaneously measures changes in protein distribution within and between samples. To calibrate ChIP-seq, prior to cell lysis experimental cells are combined with an invariable number of calibration cells that: 1) can be fixed and lysed under the same conditions, 2) express the same epitope as the experimental cells, and 3) can be

distinguished from the experimental cells by sequencing. The spike-in of calibrating cells provides an internal standard for the measurement of variation between samples that arise from differences in cell lysis, chromatin sheering, immunoprecipitation, decrosslinking and DNA purification efficiency.

In order to calibrate ChIP-seq experiments, here the original protocol (Hu et al., 2015) was modified and instead of *Candida glabrata*, a defined number of *Schizosaccaromyces pombe* cells were mixed to the experimental *Saccharomyces cerevisiae* cells prior to cells lysis. Fixing conditions were identical between the experimental and calibrating cells, and the fission yeast strain was expressing the kleisin subunit (Scc1/Mcd1/Rad21) of the cohesin complex tagged with a 6HA epitope.

At the start of this project, ChIP-seq experiments suffered from low DNA yield. Previously, this has been compensated for by increasing the number of biological repeats that were pooled together prior to sequencing library preparation. As this made sample preparation lengthy, I optimised the calibrated ChIP-seq protocol to improve DNA yield. Decreasing sonication time and switching to the Wizard SV PCR purification kit (Promega) resulted in sufficient increase in DNA recovery for my applications (Figure 3.2.1.1).

3.2.2 Sequencing library preparation

In the past, purified ChIP and input samples were sent for NGS library preparation and sequencing to the EMBL Core Genomics facility (Heidelberg, Germany). Following the purchase of an Illumina MiniSeq NGS sequencing platform in 2017, we had the opportunity to sequence ChIP-seq libraries locally, virtually eliminating waiting time. This however, also required the establishment of a library preparation and sequencing workflow for calibrated ChIP-seq. A standard library preparation protocol was adapted from (Shukla et al., 2018) which allowed the generation of high quality and high purity NGS libraries (Figure 3.2.2.1) in a cost-efficient manner (for protocol details refer to 2.5.2).

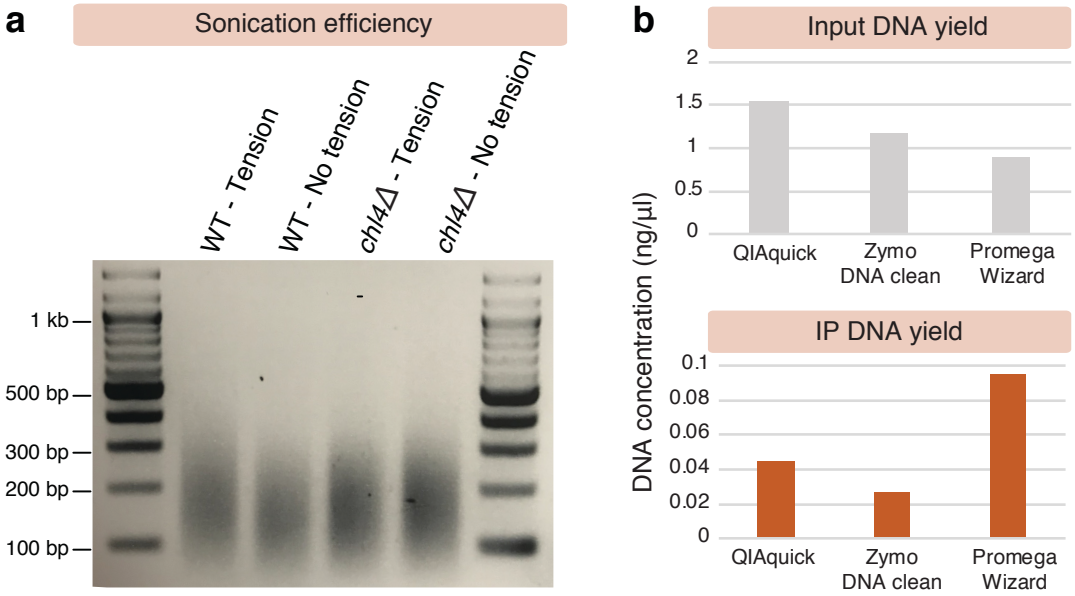

Figure 3.2.1.1. - Calibrated ChIP-seq protocol optimisation - **a**, Decrosslinked and purified DNA separated on 2% agarose gel shows sufficient level of chromatin sheering by 2x 30 cycles of 30 seconds ON/OFF sonication on a Bioruptor (Diagenode) device at 'High' setting. **b**, Testing DNA yield using different DNA purification columns: QIAquick PCR purification kit (Qiagen), DNA clean and concentrator-25 (Zymo Research) and Wizard SV Gel and PCR Clean-Up System (Promega).

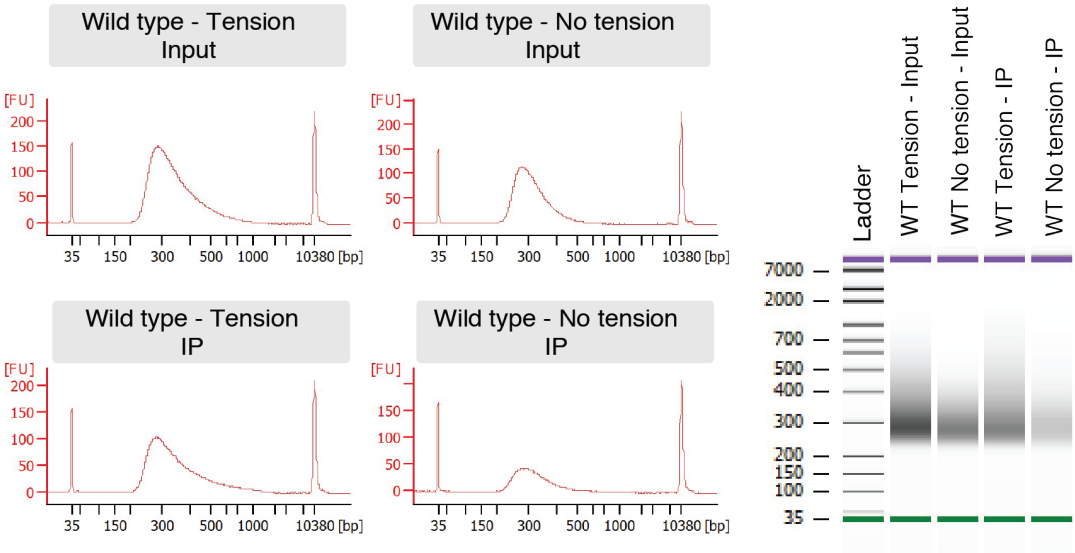

Figure 3.2.2.1. - ChIP-seq library sizing, quantitation and purity assessment - Agilent 2100 Bioanalyzer profiles of ChIP-seq sequencing libraries shows suitable DNA fragment distribution, purity and concentration for sequencing library preparation.

3.2.3 Next Generation Sequencing

Finally, sequencing conditions had to be optimised (Table 3.2.3.1). Based on the experimental (12.1 Mb) and calibrating genome sizes (14.1 Mb), sequencing depth (25 M reads per run), sequencing length (75 bp on either end) and the coverage required for ChIP-seq (~100x), it was determined that ideally 4 but up to 8 calibrated sequencing libraries can be multiplexed in a single sequencing run. Inputs and IPs were combined 15% versus 85% ratio to increase coverage over IPs. The recommended pooled and denatured 1.8 pM library loading concentration was lowered to 1.5 pM to avoid flow cell over-clustering. Post-sequencing quality control indicated that the above parameters generate high-quality and high-complexity sequencing datasets (Figure 3.2.3.2).

MiniSeq kit	MiniSeq High Output Reagent Kit (150-cycles)
Library concentration	1.5 pM
Paried/Single End	Paired end
R1 length	76 bp
R2 length	76 bp
Indexing reads	6 bp

Figure 3.2.3.1. - MiniSeq settings - Table summarizing MiniSeq run settings used in this study.

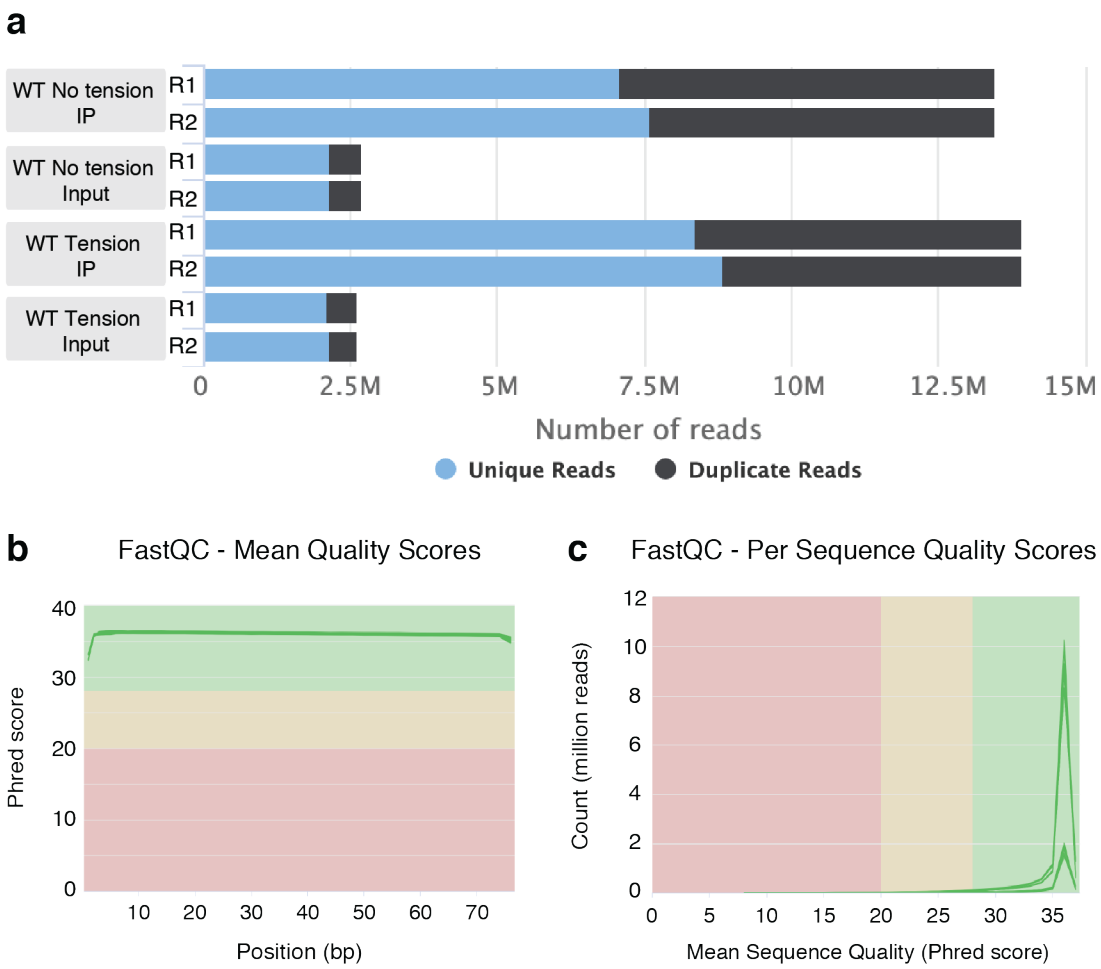

Figure 3.2.3.2. - MultiQC quality control plots - a, Unique and duplicated sequence counts for each sample. **b**, Sequence quality histogram showing the mean quality value across each base position in the read. **c**, The number of reads with average quality scores. Quality control analyses and plots were produced by Daniel Robertson (WCCB Bioinformatics Core Facility).

3.3 Results

3.3.1 The pericentromere is enriched in cohesin during an undisturbed mitotic cell cycle

In order to map genome-wide cohesin occupancy during an undisturbed mitotic cell cycle, cohesin ChIP-seq was performed in an exponentially growing asynchronous cell population (Figure 3.3.1.1). Cohesin distribution on chromosomes was similar to that previously found in metaphase-arrested cells: while cohesin associates with chromosome arm sites, it is highly enriched over pericentromeric regions (Megee et al., 1999; Glynn et al., 2004; Weber et al., 2004; Eckert et al., 2007). This experiment therefore rules out the possibility that pericentromeric cohesin enrichment is an artefact of the genetic or nocodazole-induced metaphase arrest (explained in 3.3.2) that will be used throughout this study.

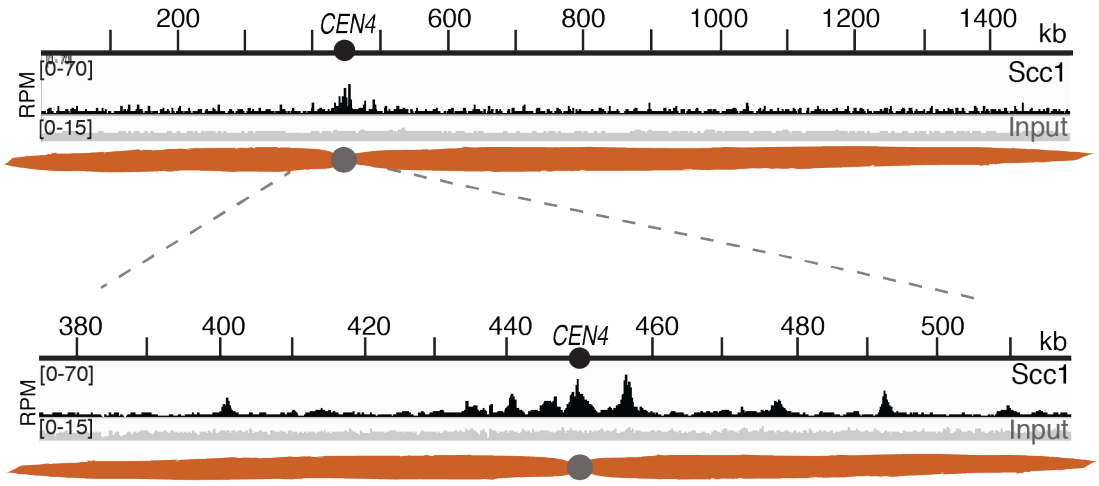

Figure 3.3.1.1. - The pericentromere is enriched in cohesin - Cohesin (Scc1) enrichment on chromosome IV (top panel) and in the pericentromeric region of chromosome IV (bottom panel) in cycling wild type cells.

3.3.2 Tension-sensitive pericentromeric cohesin is flanked by tension-insensitive cohesin peaks between convergent genes

It has been previously reported that unlike chromosome arms, pericentromeric cohesin ChIP signal in metaphase is sensitive to microtubule-based tension (Eckert et al., 2007; Ocampo-Hafalla et al., 2007; Fernius and Marston, 2009; Nerusheva et al., 2014). To precisely map the extent of pericentromeres we made use of this observation and mapped the region occupied by tension-sensitive cohesin. Cells expressing Scc1-6HA were pre-arrested in G1 using α-factor and released into metaphase-arrest induced by the depletion of Cdc20 (see 2.4.3.2, 2.4.3.3). Release from G1 was carried out either in the presence (no tension) or in the absence (tension) of microtubule depolymerising drugs (benomyl and nocodazole) and calibrated cohesin ChIP-seq was performed.

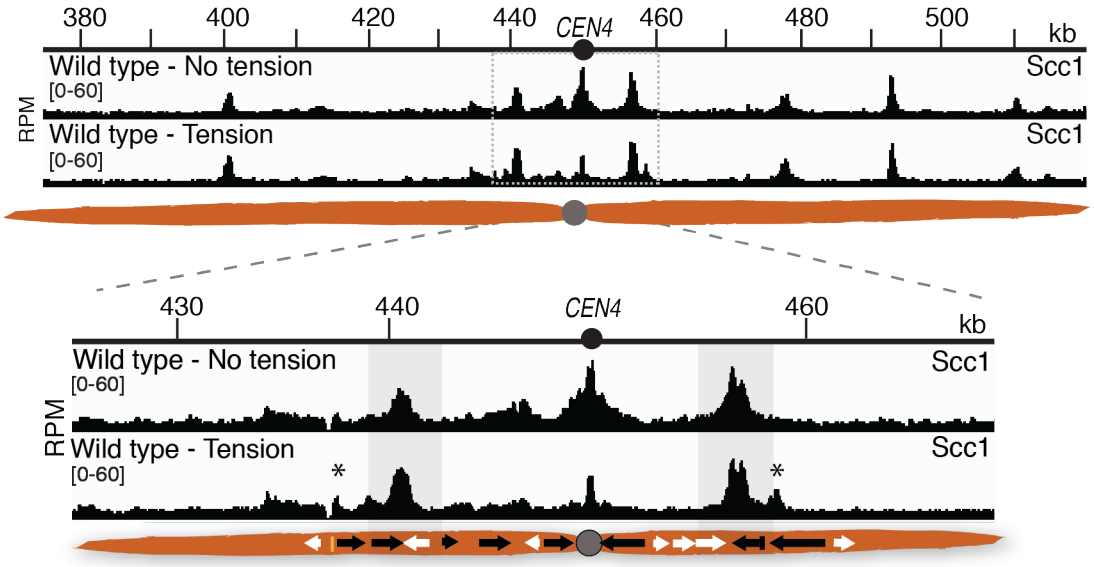

Figure 3.3.2.1. - Tension-sensitive pericentromeric cohesin is flanked by prominent tension-insensitive cohesin peaks - Cohesin (Scc1) enrichment in the pericentromeric region of chromosome IV in wild type cells arrested in metaphase either in the presence (no tension) or absence (tension) of nocodazole and benomyl. Pericentromere border regions are shaded in grey. Black and white arrows indicate genes transcribed towards and away from the centromere, respectively. Asterisk indicates additional cohesin peak under tension.

Indeed, in the presence of microtubule-based tension pericentromeric cohesin enrichment was reduced over a ~15-25kb region surrounding centromeres, while cohesin at chromosome arms remained unchanged (Figure 3.3.2.1). Interestingly, flanking the tension-sensitive cohesin domain, prominent cohesin peaks persisted in the presence of tension. Hereafter, these centromere-flanking regions that retain high levels of cohesin in the presence of spindle tension will be referred to as the borders of the pericentromere. Additionally, under tension, the appearance of smaller cohesin peaks were observed on the centromere-distal side of the tension-insensitive pericentromere border peaks (Figure 3.3.2.1, asterisks).

Closer inspection revealed that on all 16 chromosomes cohesin peaks at pericentromere borders form between convergent genes (Figure 3.3.2.1, 3.3.2.2), which are known sites for cohesin accumulation (Lengronne et al., 2004; Glynn et al., 2004). Accumulation of high levels of cohesin and thus border formation did not always occur at the most centromere-proximal convergent gene site, and border convergent genes were frequently associated with a second gene transcribed towards the centromere, on the telomere side of the border. Pericentromere borders were found to be mostly symmetrically arranged around centromeres (Figure 3.3.2.2) defining pericentromeres ranging from 9.5 kb to 29.8 kb, and with an average size of 16.5 kb. Although it was an intriguing possibility, no correlation between chromosome size and pericentromere size was found (Figure 3.3.2.3).

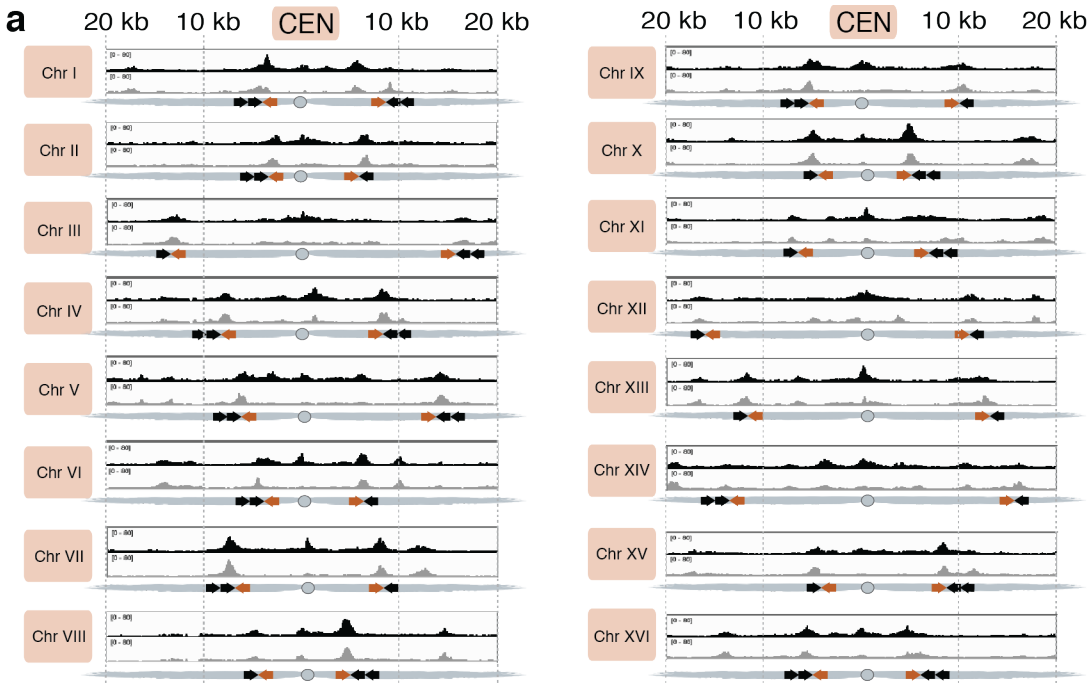

b

Chr.	Left border			Right border		
I	*EFB1 (YAL003w)*	*VPS8 (YAL002w)*	*TFC3 (YAL001c)*	*SEN34 (YAR008w)*	*YAR009c*	*YAR010c*
II	*YBL005w-B*	*UPT20 (YBL004w)*	*HTA2 (YBL003c)*	*COQ1 (YBR003w)*	*GPI18 (YBR004c)*	-
III	-	*BUD3 (YCL014w)*	*YCL012c*	*SAT4 (YCR008w)*	*RVS161 (YCR009c)*	*ADY2 (YRC010c)*
IV	*RPT2 (YDL007w)*	*PTC1 (YDL006w)*	*MED2 (YDL005c)*	*RAD57 (YDR004w)*	*MAF1 (YDR005c)*	*SOK1 (YDR006c)*
V	*MIT1 (YEL007w)*	*YEA6 (YEL006w)*	*VAB2 (YEL005c)*	*PAC2 (YER007w)*	*TMA20 (YER007c-A)*	*SEC3 (YER008c)*
VI	-	*YFL002w-A*	*SPB4 (YFL002c)*	*RPN11 (YFR004w)*	*SAD1 (YFR005c)*	-
VII	*YGL006w-A*	*PMC1 (YGL006w)*	*COG7 (YGL005c)*	*PEX31 (YGR004w)*	*TFG2 (YGR005c)*	-
VIII	-	*MRP4 (YHL004w)*	*LAG1 (YHL003c)*	*LEU5 (YHR002w)*	*TCD1 (YHR003c)*	*NEM1 (YHR004c)*
IX	*CFD1 (YIL003-w)*	*YIL002w-A*	*INP51 (YIL002c)*	*IST3 (YIR005w)*	*PAN1 (YIR006c)*	-
X	-	*CYR1 (YJL005w)*	*SYS1 (YJL004c)*	*MPP10 (YJR002w)*	*MRX12 (YJR003c)*	*SAG1 (YJR004c)*
XI		*RPL14A (YKL006w)*	*BYE1 (YKL005c)*	*OSH6 (YKR003w)*	*ECM9 (YKR004c)*	*YKR005c*
XII	-	*DRS1 (YLL008w)*	*LMO1 (YLL007c)*	*SSL1 (YLR005w)*	*SSK1 (YLR006c)*	-
XIII	-	*YAP1 (YML007w)*	*GIS4 (YML006c)*	*YMR007W*	*PLB1 (YMR008c)*	-
XIV	*YNL010w*	*IDP3 (YNL009w)*	*ASI3 (YNL008c)*	*CSE2 (YNR010w)*	*PRP2 (YNR011c)*	-
XV	-	*SIN3 (YOL004w)*	*PFA4 (YOL003c)*	*UTP23 (YOR004w)*	*DNL4 (YOR005c)*	*TSR3 (YPR006c)*
XVI	*NCR1 (YPL006w)*	*AEP3 (YPL005w)*	*LSP1 (YPL004c)*	*PDH1 (YPR002w)*	*YPR003c*	*YPR004c*

Figure 3.3.2.2. - Tension-sensitive pericentromeric cohesin is flanked by prominent tension-insensitive cohesin peaks - **a**, Scc1 cohesin ChIP-seq signal and the absence (black) and presence (grey) of tension at all 16 pericentromeres. Schematic shows the positions of convergent gene pairs flanking the centromere. Borders were defined as the innermost cohesin peak near the centromere that persisted in the presence of tension. Grey ovals represent centromeres, convergent gene pairs at the borders are indicated by arrows. Frequently, border convergent genes are associated with an additional gene on the chromosome arm side, that is transcribed towards the centromere. **b**, Table of convergent genes identified at pericentromere borders for each chromosome.

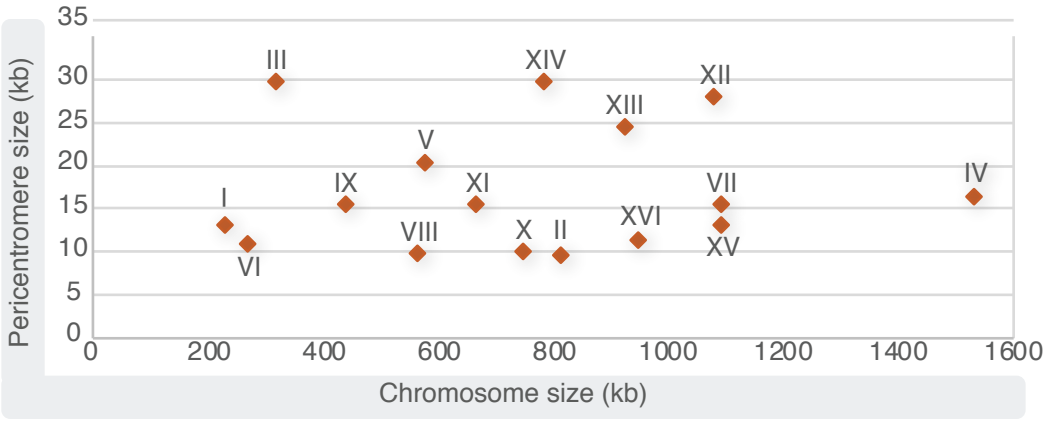

Figure 3.4.1.5. - Pericentrome size does not correlate with chromosome size - Pericentromere size determined in Table 3.4.1.3 plotted against chromosome size.

Next, the mean cohesin ChIP signal across the 16 centromeres and 32 borders as well as the adjacent chromosome arms sites was plotted. This analysis confirmed that while cohesin at centromeres diminishes under tension, cohesin at pericentromere borders and at chromosome arm peaks does not (Figure 3.3.2.4).

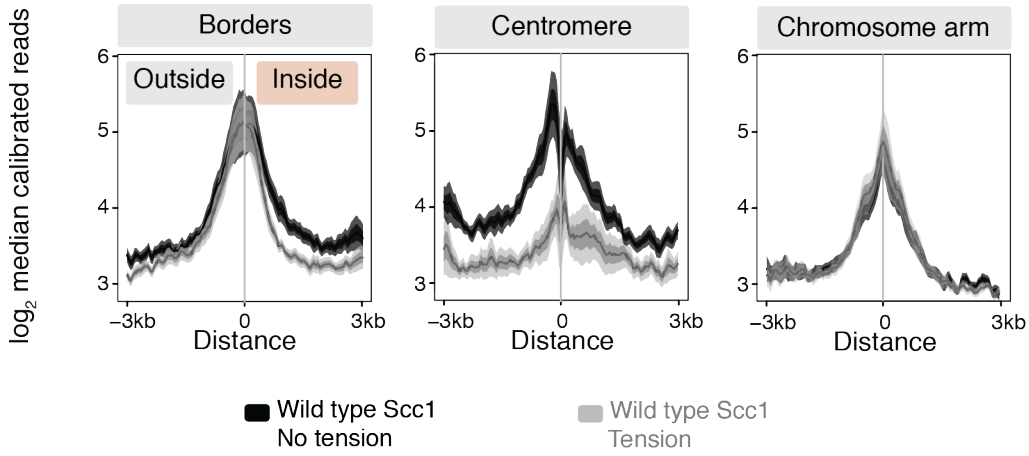

Figure 3.3.2.4 - Cohesin occupancy at borders remains unchanged under tension - SeqPlots show mean calibrated ChIP reads (solid line), standard error (dark shading) and 95% confidence interval (light shading) at borders and centromeres of all chromosomes for wild type cells, either in the presence or absence of tension. To represent chromsome arms, similar plots for the next convergent gene site on each chromosome arm are shown.

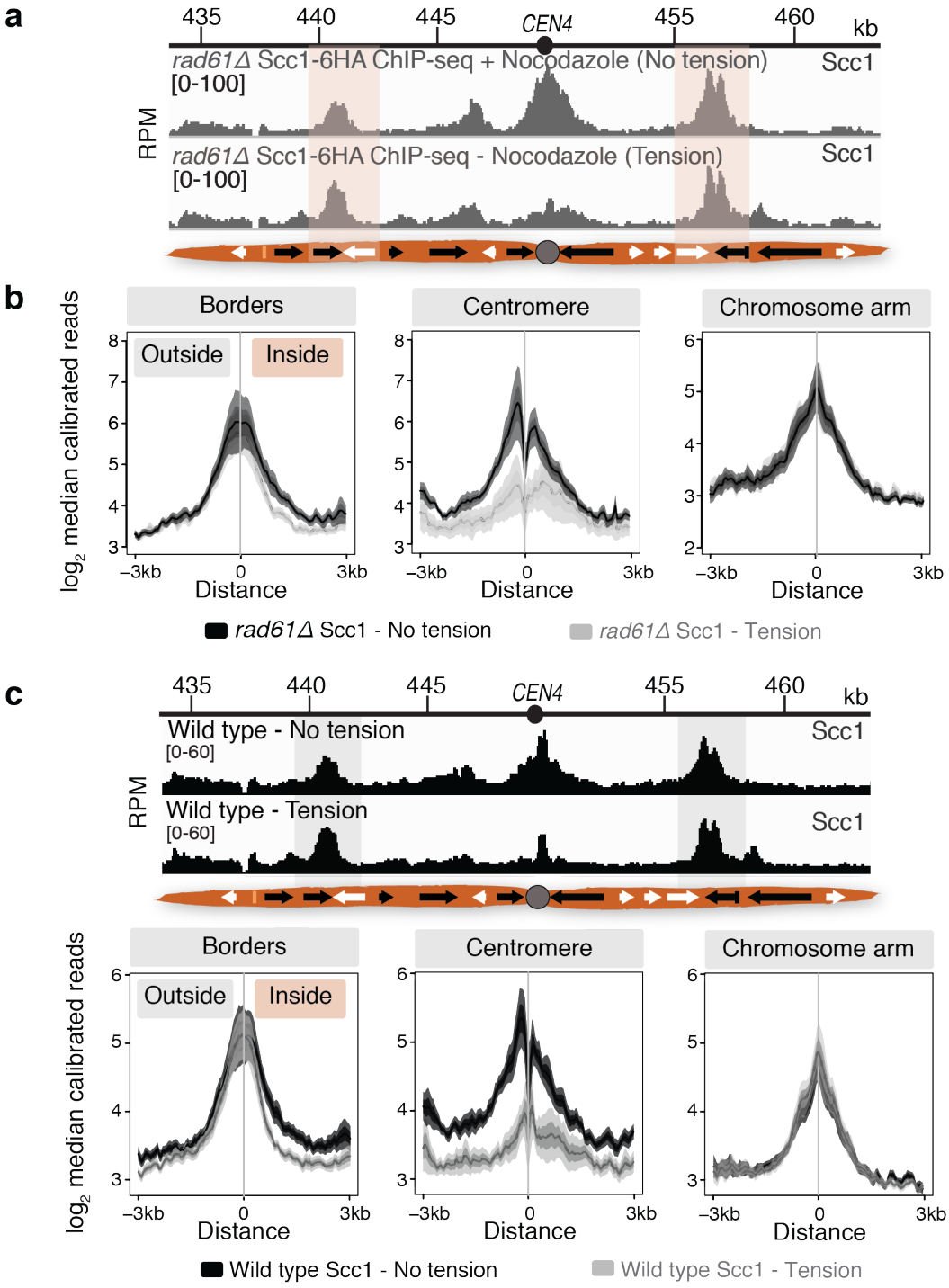

Figure 3.3.3.1. - Wpl1/Rad61 is not required for the tension-dependent removal of cohesin at metaphase - a. Scc1-6HA calibrated ChIP-seq profiles for the pericentromeric region of chromosome IV in *rad61Δ* cells in the absence and presence of spindle tension. **b**. SeqPlots show mean calibrated ChIP reads (solid line), standard error (dark shading) and 95% confidence interval (light shading) at borders and centromeres and arms of all chromosomes in *rad61Δ* cells, either in the presence or absence of tension. **c**. Similar plots for wild type are shown for comparison (reproduced from Figures 3.3.2.1, and 3.3.2.4).

3.3.3 Decrease in pericentromeric cohesin occupancy under tension occurs independently of Rad61/Wapl

The cohesin associated factor Rad61/Wpl1 promotes cohesin turnover on chromosomes in early mitosis (Kueng et al., 2006; Lopez-Serra et al., 2013). To investigate if Rad61/Wpl1 was required for the tension-dependent removal of cohesin from the pericentromere, *rad61Δ* cells expressing Scc1-6HA were arrested in metaphase by Cdc20 depletion, with or without microtubule tension. As tension-induced decrease in pericentromeric cohesin signal occurred to a similar extent to that in wild type cells, this phenomenon proved to be independent of Rad61/Wapl (Figure 3.3.3.1), suggesting that the removal occurs passively.

3.3.4 Cohesin enrichment at pericentromere borders partially depends on kinetochore-driven cohesin loading

The Ctf19 kinetochore subcomplex enhances cohesin association with the pericentromere through directly interacting with the Scc2/Scc4 cohesin loader (Fernius and Marston, 2009; Ng et al., 2009; Hinshaw et al., 2015; Hinshaw et al., 2017). This targeted cohesin loading results in high levels of cohesin throughout the pericentromere. As cohesin accumulation sites are different from its loading sites (Ciosk et al., 2000; Lengronne et al., 2004), current models posit that cohesin can translocate on chromosomes (Lengronne et al., 2004; Ocampo-Hafalla et al., 2016) in a manner that is dependent on its ATPase activity (Hu et al., 2011). To determine if cohesin loaded at the centromere accumulates in pericentromere border regions, the kinetochore-driven cohesin loading pathway was abolished by the deletion of the Chl4 subunit of the Ctf19 complex, and calibrated cohesin ChIP-seq was performed on metaphase-arrested cells (Figure 3.3.4.1).

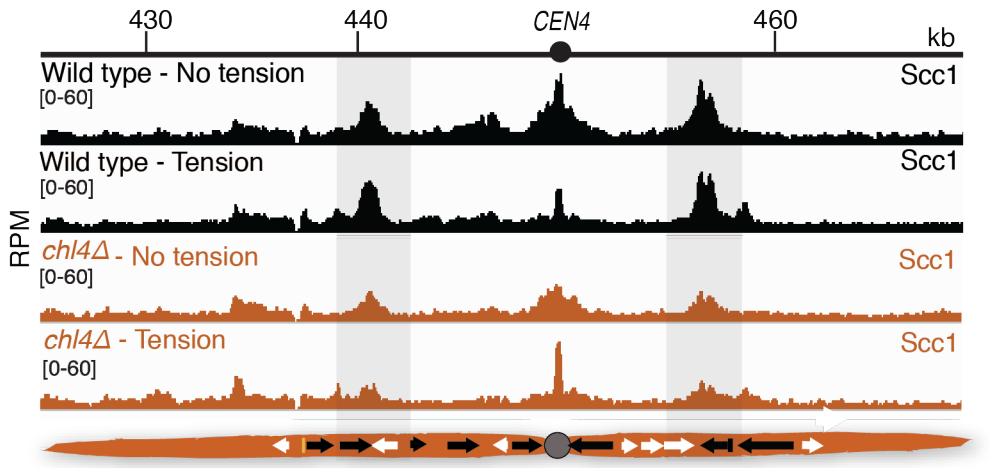

Figure 3.3.4.1. - Cohesin enrichment at pericentromere borders is partially dependent on centromeric cohesin loading - Cohesin (Scc1) enrichment in the pericentromeric region of chromosome IV in wild type (top panels) and *chl4Δ* (bottom panels) cells arrested in metaphase either in the presence (no tension) or absence (tension) of nocodazole and benomyl. Pericentromere border regions are shaded in grey. Black and white arrows indicate genes transcribed towards and away from the centromere, respectively.

Cohesin was reduced, but not completely absent, both throughout the pericentromere and at pericentromere borders. This was confirmed by plotting the mean cohesin ChIP signal at centromeres, pericentromere borders and the adjacent chromosome arm sites (Figure 3.3.4.2). This analysis revealed that Chl4 promotes cohesin association with centromeres and pericentromere borders, but not chromosome arms.

We noted the presence of residual cohesin at centromeres and at borders in *chl4Δ*, which can be explained two ways. First, even in the absence of *CHL4* there is residual cohesin loading at the centromeres (Fernius and Marston, 2009; Hinshaw et al., 2017) Second, in *chl4Δ* cohesin is still loaded onto chromosomes at arm loading sites, therefore cohesin might migrate from chromosome arms to pericentromere borders. Altogether, these observations indicate that some cohesin that is loaded at the centromere collects in pericentromere border regions, and cohesin at pericentromere borders might

consist of cohesin that was loaded at centromeres and cohesin coming from chromosome arms.

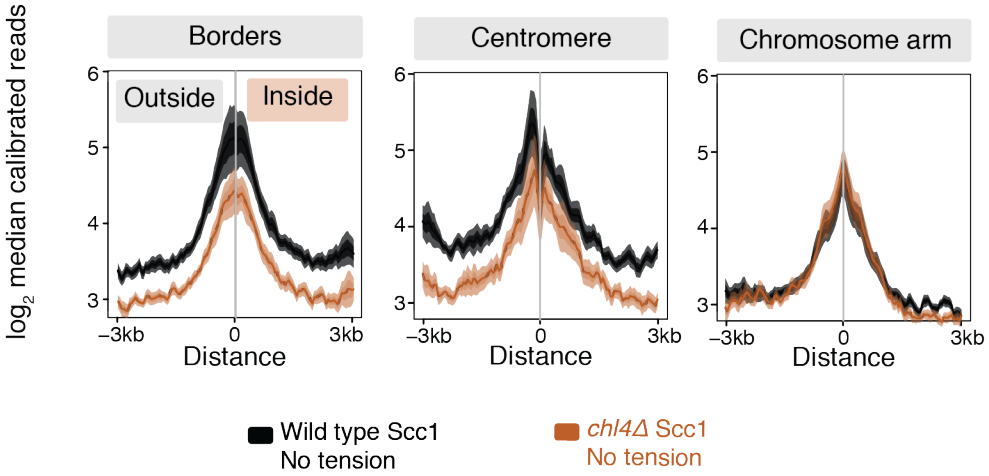

Figure 3.3.4.2. - Cohesin occupancy at borders decreases in the absence of centromere-driven cohesin loading - SeqPlots show mean calibrated ChIP reads (solid line), standard error (dark shading) and 95% confidence interval (light shading) at borders and centromeres of all chromosomes for wild type and *chl4Δ*, in the absence of tension.For comparison, similar plots for the next convergent gene site on each chromosome arm are shown.

3.3.5 Pericentromeres and borders are enriched in shugoshin and condensin

Besides cohesin, pericentromeres are enriched in the pericentromeric adaptor protein Shugoshin (Sgo1) and its interaction partner, condensin (Peplowska et al., 2014; Verzijlbergen et al., 2014). Shugoshin associates with pericentromeres in the absence of spindle tension and it is removed from chromosomes once biorientation is achieved (Nerusheva et al., 2014). Condensin is recruited to and removed from pericentromeres in a similar fashion, in a shugoshin-dependent manner. This shugoshin-dependent pericentromeric condensin recruitment promotes biorientation and accurate chromosome segregation during mitosis (Peplowska et al., 2014; Verzijlbergen et al., 2014). To investigate if shugoshin and condensin localisation extends to pericentromere borders, Sgo1-6HA (shugoshin) and Brn1-6HA (kleisin subunit

of condensin) ChIP-seq was performed on metaphase-arrested cells treated with microtubule drugs (Figure 3.3.5.1). This, along with plots for mean cohesin, shugoshin and condensin signals (Figure 3.3.5.2), showed that centromeres and pericentromere borders, but not the adjacent chromosome arm cohesin peaks, are enriched in shugoshin and condensin.

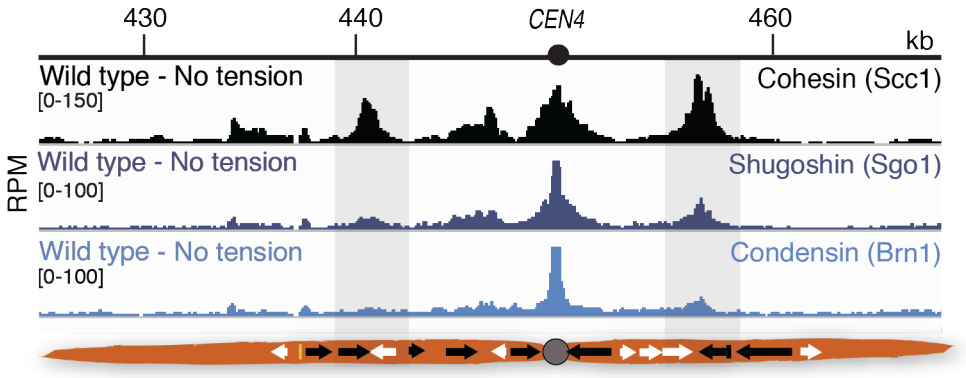

Figure 3.4.5.1. - Pericentromere borders are enriched in Shugoshin and condensin - Cohesin (Scc1-6HA), shugoshin (Sgo1-6HA) and condensin (Brn1-6HA) enrichment in metaphase-arrested cells in the presence of nocodazole in the pericentromeric region of chromosome IV.

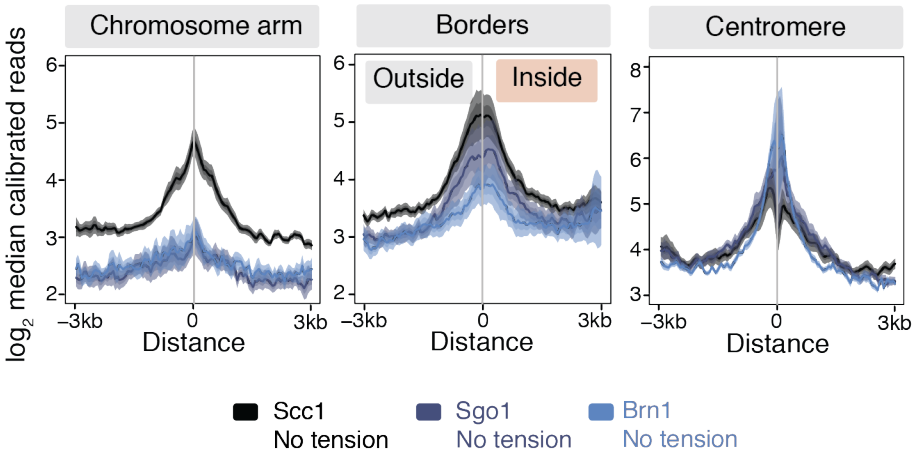

Figure 3.3.5.2. - Shugoshin and condensin localise to pericentrome borders - SeqPlots show median calibrated ChIP reads (solid line), standard error (dark shading) and 95% confidence interval (light shading) at borders and centromeres of all chromosomes for cohesin (Scc1), Shugoshin (Sgo1) and condensin (Brn1), in the absence of tension.

3.4 Discussion

Cohesin enrichment has been known to be a feature of budding yeast pericentromeres (Megee et al., 1999; Glynn et al., 2004; Weber et al., 2004; Eckert et al., 2007). However, what defines the limits of pericentromeric cohesin enrichment domains remained unknown. In order to investigate this, pericentromeric cohesin, shugoshin and condensin domains were mapped by ChIP-seq. Pericentromeric cohesin was further examined for changes in response to microtubule tension following biorientation, and in the absence of the kinetochore-driven cohesin loading pathway using calibrated ChIP-seq.

The data presented here indicates that the limits of tension-sensitive pericentromeric cohesin domains are marked by prominent cohesin enrichment sites (Figure 3.3.2.1, 3.3.2.4). Here we term these sites the borders of pericentromeres. While cohesin signal inside pericentromeres shows a Rad61/Wpl1-independent decrease (Figure 3.3.3.1) in the presence of microtubule based-tension, cohesin at borders does not. In the absence of centromeric cohesin loading, cohesin signal is diminished both inside pericentromeres and at the borders (Figure 3.3.4.1, 3.3.4.2), indicating that borders are functional in retaining cohesin that was loaded at the centromere. Finally, it was established that borders are enriched in other pericentromeric proteins, such as shugoshin and condensin (Figure 3.3.5.1, 3.3.5.2). Interestingly, it was found that pericentromere border regions form between centromere-flanking convergent genes (Figure 3.3.2.2). Although this was true for all 16 budding yeast chromosomes, no correlation between pericentromere size and chromosome size were found (Figure 3.3.2.3).

In summary, this chapter establishes the borders of pericentromeres as the most centromere-proximal chromosomal regions that retain high levels of cohesin under tension. Pericentromere borders form between centromere-flanking convergent gene pairs and are also characterised by the presence of

centromerically-loaded cohesin, as well as the pericentromeric proteins shugoshin and condensin.

Chapter 4 Pericentromere borders resist sister chromatid separation under tension

4.1 Introduction

Paradoxically, despite high cohesin density, sister centromeres transiently separate in pre-anaphase cells (Goshima and Yanagida, 2000; He et al., 2000; Tanaka et al., 2000). This is due to the attachment of sister kinetochores to opposite spindle poles during biorientation, which pulls sister centromeres apart while chromosome arms remain tightly cohesed. The region of separation was found to extend ~9 kb away from the centromere (He et al., 2000) which broadly coincides with the region of pericentromeric cohesin enrichment (Weber et al., 2004; Eckert et al., 2007; Fernius and Marston, 2009).

However, it has never been investigated if the region of separation solely depends on distance from the centromere or it is defined by the extent of the cohesin-rich pericentromere. It is possible, that pericentromere borders trap cohesin and resist sister chromatid separation under tension. Work presented in this chapter investigates if pericentromere borders identified by ChIP-seq also set the limits to the region of pre-anaphase separation of sisters upon biorientation.

4.1.1 The *tetO*/TerR-GFP system to label chromosomal loci

Sister chromatid cohesion and the pre-anaphase separation of centromere-proximal sequences can be studied by microscopy-based approaches that make use of the bacterial *lacO*/LacI (Straight et al., 1996) or *tetO*/TetR (Michaelis et al., 1997) interactions. Arrays of *tetO* or *lacO* operator sequences can be integrated at desired chromosomal loci and the interaction between the operators and their respective repressor produces bright fluorescent foci at

specific chromosomal loci in cells expressing TetR-GFP (binds *tetO*) or LacI-GFP (binds to *lacO*).

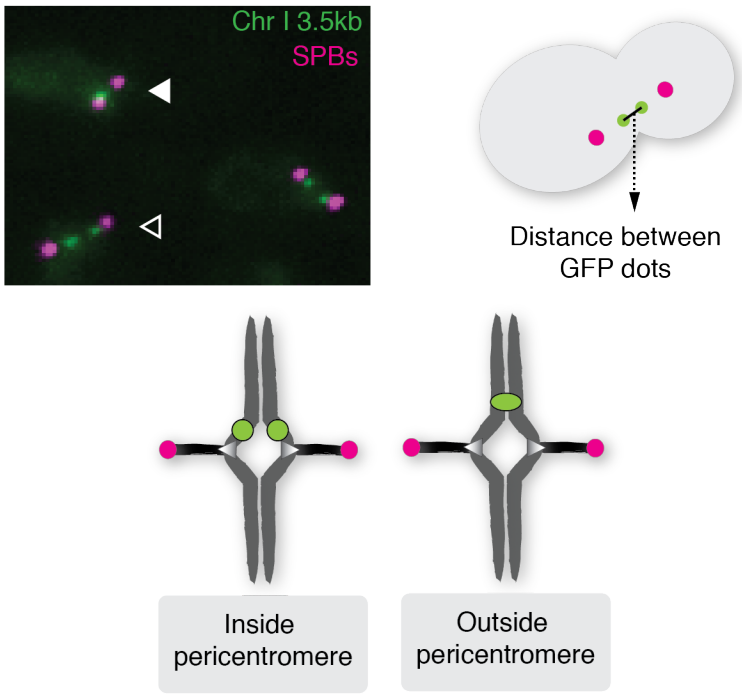

Figure 4.1.1.1. - Assay to measure separation of loci on sister chromatids in metaphase arrested cells - Cells carry *tetO*/TetR-GFP foci integrated at various positions, Spc42-tdTomato foci to mark spindle pole bodies and cells are arrested in metaphase by Cdc20 depletion. Representative image and schematic of distance measured is shown to the top. White and black arrows mark cells with a single GFP focus or split foci, respectively. Bottom schematic shows expected separation of GFP foci positioned inside and outside pericentromere loci. Green dots, *tetO*/TetR-GFP foci, Red dots, spindle pole bodies.

Employing the *tetO*/TetR system, this study investigates the role of pericentromere borders in defining the region of transient pre-anaphase separation of sister chromatids. Prior to biorientation, fluorescent *tetO*/TetR-GFP markers integrated to centromere-proximal loci appear as a single GFP focus due to the tight cohesion of sister chromatids. Once biorientation is achieved, tension-generating microtubule-kinetochore interactions split sister centromeres, resolving the *tetO*/TetR-GFP foci on the individual sister

chromatids. It was hypothesised that if pericentromere borders play a role in setting physical limits to the separating region, then *tetO*/TetR-GFP markers integrated to centromere-proximal side of borders will separate at high frequency, while markers integrated on the telomere side of the borders will not (Figure 4.1.1.1.).

4.2 Results

4.2.1 Mapping the region of pre-anaphase sister chromatid separation on chromosome I

According to the ChIP-seq analysis, chromosome I has a fairly small (13.1 kb) pericentromere with a clearly delineated border position. In order to understand the relationship between pericentromere borders and the transient pre-anaphase separation of sister chromatids, a series of TetR-GFP-expressing yeast strains were constructed, with *tetO* arrays integrated at various distances from the centromere on chromosome I.

TetO/TetR-GFP marked cells were pre-arrested in G1 using α-factor, released into a metaphase arrest by Cdc20 depletion, fixed in formaldehyde, mounted on glass slides and analysed by epifluorescence microscopy. Release from G1 arrest, and progression through S-phase to metaphase was verified by counting spindle pole bodies (SPBs) that duplicate in S-phase (labelled by Spc42-tdTomato). 200 cells were scored for the number of GFP foci and 100 cells were scored for the number of SPBs (Figure 4.2.1.1).

As expected, loci inside pericentromere borders (adjacent to *CEN1*, 3kb, 7kb) separated frequently (~70%), whereas the locus outside the border (12kb) almost always appeared as a single GFP dot. The marker within the pericentromeric cohesin peak (8kb) showed an intermediate level of separation. Altogether, these results indicate that the region of sister chromatid separation under tension shows good correlation with the pericentromeric domain defined by borders.

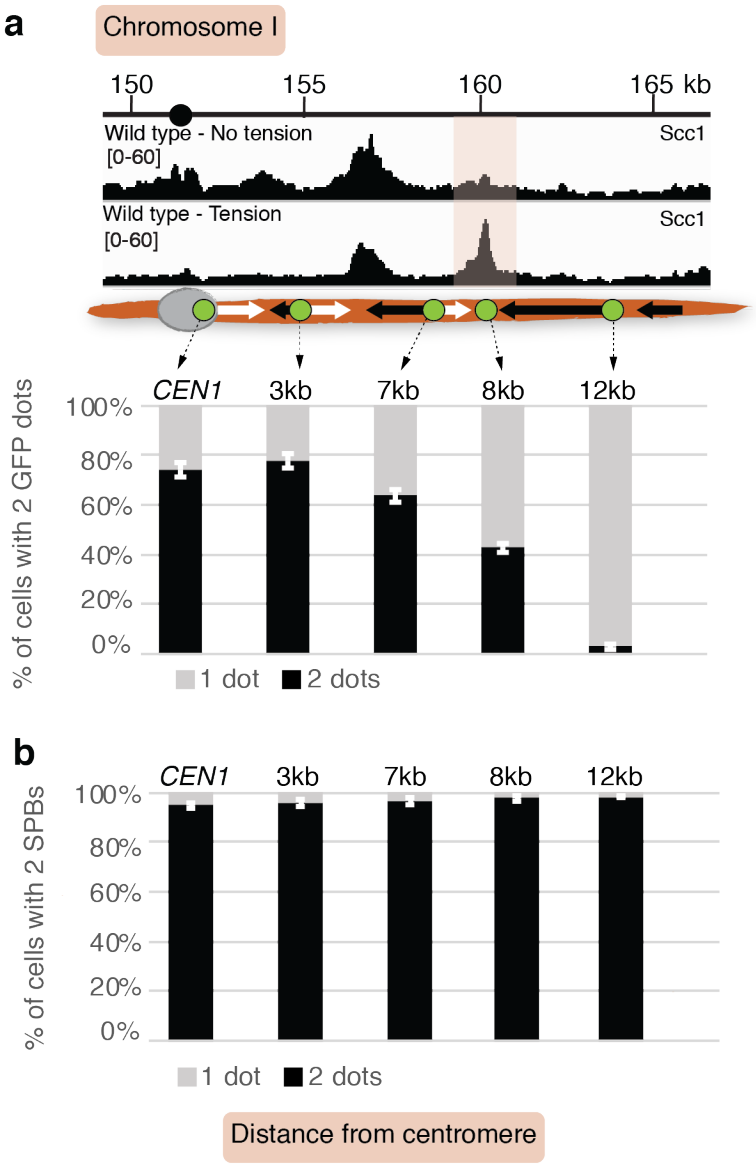

Figure 4.2.1.1. - Pericentromere borders resist sister chromatid separation under tension - **a**, The number of cells with 2 GFP foci were scored for the markers at the indicated loci on chromosome I (n = 200). Position of GFP foci and corresponding calibrated Scc1-6HA ChIP-seq profiles are shown for comparison. Error bars indicate standard error of three independent repeats. b, The number of cells with 2 SPBs were scored to confirm entry to mitosis (n=100). Error bars represent standard error of three independent repeats.

4.2.2 Mapping the region of pre-anaphase sister chromatid separation on chromosome III

Next, chromosome III was analysed for the relationship between pericentromere borders and sister chromatid separation. In contrast to the short, clearly defined pericentromere of chromosome I, chromosome III appeared to have a large (29.8 kb) and less defined pericentromere. If the region of separation does not only depend on distance from the centromere but also on borders, the difference in pericentromere size predicts differential behavior of markers on chromosome I and III integrated at equivalent distances from the centromere.

To assess this, chromosome III was labelled at varying distances from the centromere using *tetO*/TetR-GFP markers. As before, cells were synchronised in metaphase, fixed and scored for the number of GFP foci and SPBs (Figure 4.2.2.1).

Similar to chromosome I, markers inside pericentromere III (*CEN3*, 3.5kb, 7kb, 12kb) showed high levels of separation, while markers outside the pericentromere did not (18kb, 21kb, 23kb). Importantly, while the 12kb marker on chromosome I almost always appeared as a single GFP focus (<95%), the marker 12kb from *CEN3* frequently split (~50%). Only when markers were integrated >20kb away from *CEN3* was no separation observed, while no splitting was observed 12kb away from *CEN1*. This differential behaviour of the equivalent loci on chromosomes I and III indicates that the region of transient sister chromatid separation does scale with the pericentromere size defined by borders.

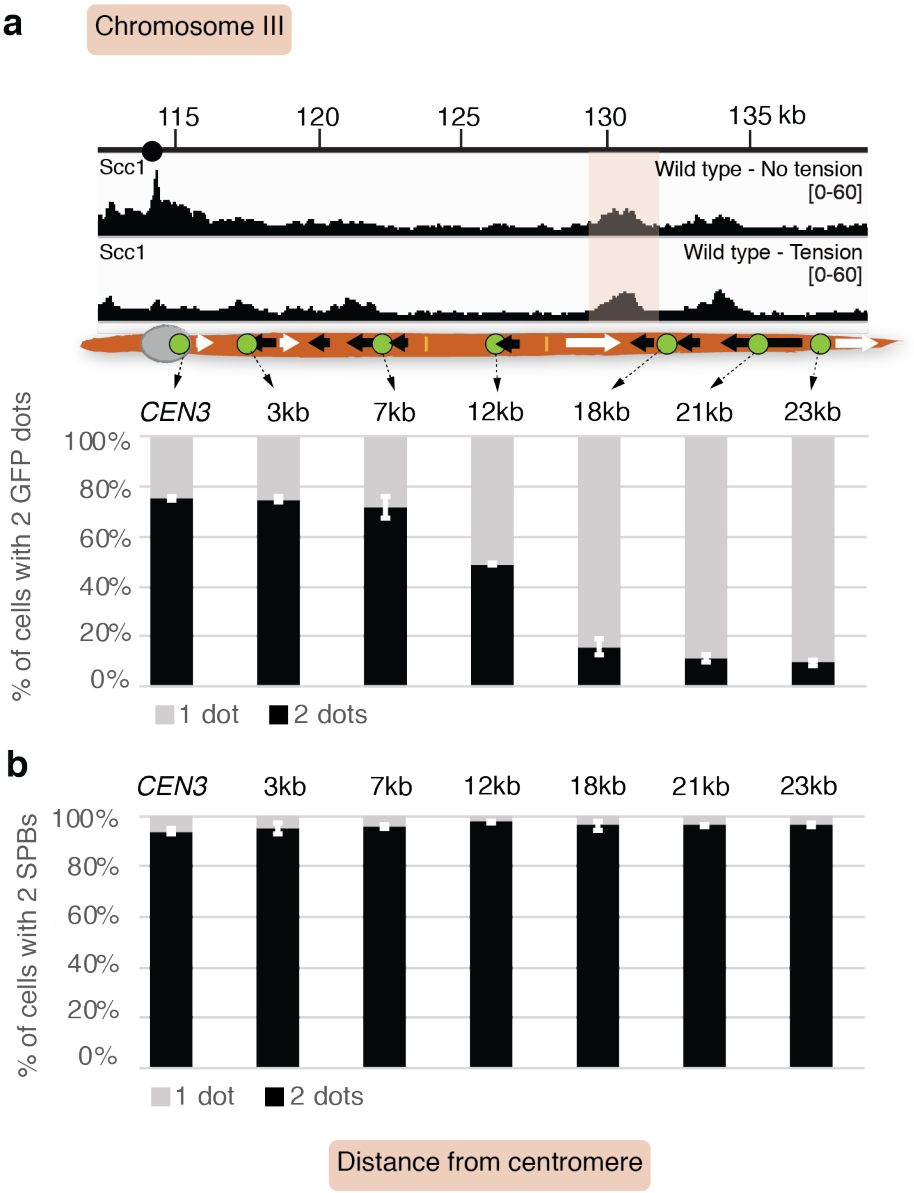

Figure 4.2.2.1 - Region of sister chromatid separation scales with pericentromere size - **a**, The number of cells with 2 GFP foci were scored for the markers at the indicated loci on chromosome III (n = 200). Position of GFP foci and corresponding calibrated Scc1-6HA ChIP-seq profiles are shown for comparison. Error bars indicate standard error of three independent repeats. **b**,The number of cells with 2 SPBs were scored to confirm entry to mitosis (n=100). Error bars represent standard error of three independent repeats.

4.2.3 Distances of GFP dot separation remain constant throughout the pericentromere

It was possible to measure changes in separation frequency between different *tetO*/TetR-GFP inserted on chromosome I and III, thus we reasoned that differences in separation distance between loci might be detectable. As during centromeric GFP dot splitting chromosome arms remain cohered, a decrease in separation distance might be detectable at loci close to the border. To this end, experiments similar to 4.2.2 were conducted. Instead of counting the number of GFP dots, images of cells were recorded and the distances between GFP foci were measured using a custom ImageJ plugin (Figure 4.2.3.1). Distance measurements confirmed the findings in 4.2.2. However, no decrease in separation distance was detected at loci integrated further away from the centromere, at each locus GFP foci being ~0.5-1 µm apart. This range of separation distance is in agreement with previous findings (Goshima and Yanagida, 2000).

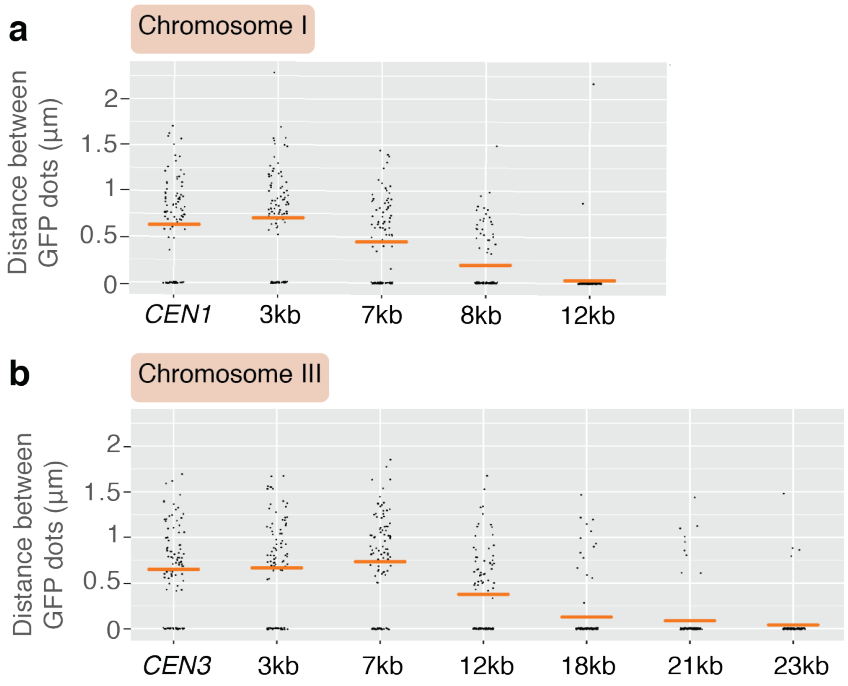

Figure 4.2.3.1 - Distance of sister chromatid separation remains constant in the pericentromere - The distance between GFP dots were measured (n = 100) on a, chromosome I and on b, chromosome III. Horizontal lines indicate mean.

4.3 Discussion

It was previously established that upon biorientation, cohesin-rich pericentromeres transiently separate prior to anaphase (Goshima and Yanagida, 2000; He et al., 2000; Tanaka et al., 2000) Work presented in this chapter investigated if the region of separation solely depends on distance from centromere or it is defined by pericentromere borders.

It was reasoned that if pericentromere borders play a role in determining the region of separation, *tetO*/TetR-GFP markers should show differential behaviour depending on whether they are located on the centromere-proximal or centromere-distal side of borders. Two chromosomes were chosen for detailed analysis: chromosome I and chromosome III, which based on the cohesin ChIP-seq profiles had small and large pericentromeres respectively. The difference in size between pericentromere I and III also predicted distinct behaviour for markers located equivalent distances from *CEN1* and *CEN3*.

Both of the above predictions were found to be true: on both chromosomes, loci inside the pericentromere separated frequently, loci outside did not. Importantly, the 12kb marker (that is inside the pericentromere on chromosome I but outside on chromosome III) displayed a much lower frequency of separation (<5%) on chromosome I compared to chromosome III (<50%). These observations indicate that the region of transient pre-anaphase separation does not only depend on distance from centromeres, but is scales with the pericentromere size defined by borders. Additionally, it was found that the distance between separated GFP foci did not vary largely between chromosomes and loci. However, it is possible that small differences in separation distance exist, but they are undetectable with the assay employed as the size of the integrated *tetO* arrays (~12kb) is comparable to the size of the entire pericentromere (12kb on chromosome I, 28kb on chromosome III).

Finally, although a clear correlation was found between the size of pericentromeres defined by borders and the region of separation, intermediate

rates of splitting at some loci suggest a certain level of stochasticity. For example, outside the border, the marker integrated at 18kb from *CEN3* separated in ~10% of cells, indicating that borders do not provide a fail-safe barrier to separation, leading to cell-to-cell variability in the extent of the region of separation.

Chapter 5 The pericentromere is a looped structure in mitosis which is converted to a V shape under tension

5.1 Introduction

Work in Chapters 3 and 4 established that cohesin accumulation at border regions defines the chromosomal domain that will separate under tension. Therefore, we hypothesized that cohesin loaded at centromeres together with borders define the structure of the pericentromere. This possibility is likely, as in addition to its canonical role in holding sister chromatids together, cohesin is a key determinant of chromosome conformation. In budding yeast cohesin has been shown to be involved in the mitotic (Schalbetter et al., 2017; Lazar-Stefanita et al., 2017) and meiotic compaction of chromosomes (Muller et al., 2018; Schalbetter et al., 2019). However, pericentromere structure has never been investigated in detail.

Pericentromeric cohesin facilitates biorientation and accurate chromosome segregation during mitosis (Eckert et al., 2007; Fernius and Marston, 2009; Ng et al., 2009). As sister chromatids are intrinsically biased to biorient on the mitotic spindle (Indjeian and Murray, 2007), cohesin at pericentromeres is thought to establish a preferred kinetochore geometry for capture by microtubules emanating from opposite spindle poles. Although the precise structure of pericentromeres is unknown, it is speculated that it is specialised and important for biorientation (Yeh et al., 2008). Therefore, work in this chapter set out to decipher pericentromere structure as well as its dependence on cohesin loaded at centromeres and pericentromeric condensin. Additionally, the separation of sister centromeres under spindle tension indicates that biorientation induces structural changes in centromere-proximal regions, so the chromosome conformational changes that occur upon

microtubule attachment will also be investigated. Finally, the results are examined in the context of the previously identified pericentromere borders.

5.1.1 Techniques to study chromosome conformation

Early studies on the spatial organisation of chromosomes mostly relied on *in situ* hybridisation techniques followed by imaging. Although these cytogenetic techniques revealed the first organisational principles of genomes, they generally suffered from low-resolution and low-throughput. To allow comprehensive analysis of the 3D folding of chromosomes at high resolution, 3C-based techniques have been developed. 3C approaches rely on chromatin crosslinking, fragmentation usually by restriction enzyme, and proximity-mediated ligation which generate chimeric DNA fragments, converting physical chromatin interactions into ligation products. The first such technique, 3C, allowed the detection of single ligation products using PCR primers annealing to the interacting fragments ("one-by-one") (Dekker et al., 2002). Later, 4C was developed which still generated interaction profiles for a single locus, but using inverse PCR, it allowed the detection of its genome-wide interactions ("one-by-all") (Simonis et al., 2006). Further improved, 5C was not anchored to a specific locus, and used microarrays or sequencing to detect millions of interactions over hundreds of kilobases ("many-by-many") (Dostie et al., 2006). As of today, the most widely used 3C-based approach is Hi-C, which allows comprehensive and unbiased detection of interactions genome-wide (Lieberman-Aiden et al., 2009). Instead of using specific primer sets to detect ligation products, ligation junctions are marked with biotinylated nucleotides, purified on streptavidin beads and sequenced directly using NGS. In the final Hi-C library, the abundance of certain chimeric products reflects the spatial proximity of loci. Over the years, a range of modifications to the original Hi-C method have been developed. Importantly, it was found that a higher degree of genome fragmentation gives higher resolution interaction maps. This high resolution method was implemented in this study.

5.2 Protocol optimisation

5.2.1 Lysis by spheroplasting yielded low-complexity Hi-C libraries

The resolution of Hi-C contact maps is ultimately limited by the degree of chromatin fragmentation prior to proximity ligation. As pericentromeres in budding yeast are small (<30 kb), a high resolution Hi-C protocol from (Schalbetter et al., 2019) was adapted. This protocol uses a 4-bp cutter restriction enzyme (*Dpn*II) to digest the yeast genome to ~250 bp fragments. With appropriate sequencing depth, this degree of fragmentation can produce Hi-C maps at 1 kb resolution, which are appropriate for studying budding yeast pericentromeres.

Initially, approximately 3.5 x 10^8 haploid cells were fixed and quenched, then cells were lysed using 100 µg/ml 100T zymolyase, for 15 minutes at 35°C. Hi-C protocol was the carried out as in (Schalbetter et al., 2019) with the following modifications: 1) instead of Covaris, chromatin was sheered using a Bioruptor Plus sonication device (Diagenode) for a total of 2x 30 cycles 30 seconds on/off at 'High' setting 2) instead of Blue Pippin (Sage), Hi-C libraries were fractionated using Ampure XP (Beckman) as described in Belton and Dekker (2015). The resulting Hi-C libraries were first assessed for quantity, quality and purity, then sequenced on the Illumina MiniSeq platform and analyzed using HiC-Pro (Daniel Robertson, Bioinformatics Core Facility). Quality control indicated that despite appropriate quality, the library was predominantly (82.8%) composed of invalid (self-circle and dangling end) Hi-C products resulting in low complexity (2.5M valid reads) (Figure 5.2.1.1). Additionally, 8% of valid reads were duplicates, indicating that the increasing sequencing depth would not increase library complexity.

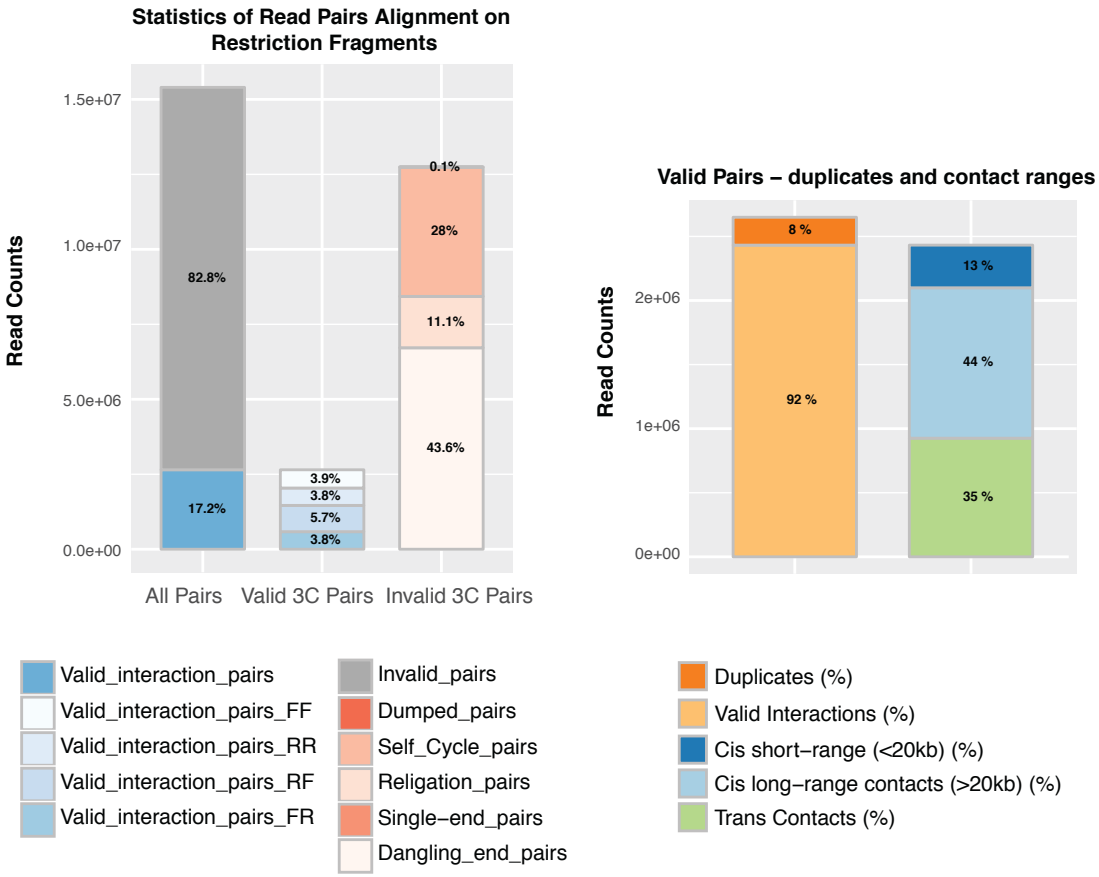

Figure 5.2.1.1. - HiC-Pro quality control of Hi-C library prepared from cells lysed by spheroplasting - Plots for read pair filtering (left) and contact ranges (right) show low complexity Hi-C library with predominantly invalid 3C pairs and high levels of sequencing duplicates. Analysis was performed by Daniel Robertson (WCCB Bioinformatics Core Facility).

5.2.2 Cell lysis by grinding improved Hi-C library quality

Methods to lyse yeast cells can be divided to two major types: enzymatic and mechanical disruption. As zymolyase digestion yielded poor results for mitotic samples, extracts were prepared by grinding cells with a chilled pestle and mortar for 15 minutes, a method that Belton and Dekker, 2015 used for mitotic cells. It was also speculated that the large number of dangling ends could be a result of using too many cells, saturating enzyme activities and resulting in incomplete reactions. This idea was supported by high DNA yield accompanied by high proportion of invalid Hi-C products in the previous attempt. Therefore, approximately 1.5 x 10^9 haploid cells were lysed, but $1/10^{th}$ of the lysed pellet weight was taken for further processing, lowering the number of cells used for Hi-C 2-3-fold. The protocol otherwise was left unchanged and Hi-C libraries were sequenced on Illumina MiniSeq to assess complexity (Figure 5.2.2.1a) which indicated a modest increase in valid Hi-C interactions (23.8%, 3M valid Hi-C pairs). Importantly, duplication level dropped to 1%, indicating that complexity could be improved by sequencing libraries at higher depth. Indeed, sequencing the Hi-C library on an Illumina NextSeq platform (EMBL Genomics Core, Heidelberg) resulted in a significant increase in detected valid Hi-C interactions (18M) which matched publication standards (Figure 5.2.2.1b). Afterwards, all Hi-C libraries were produced with these modifications implemented.

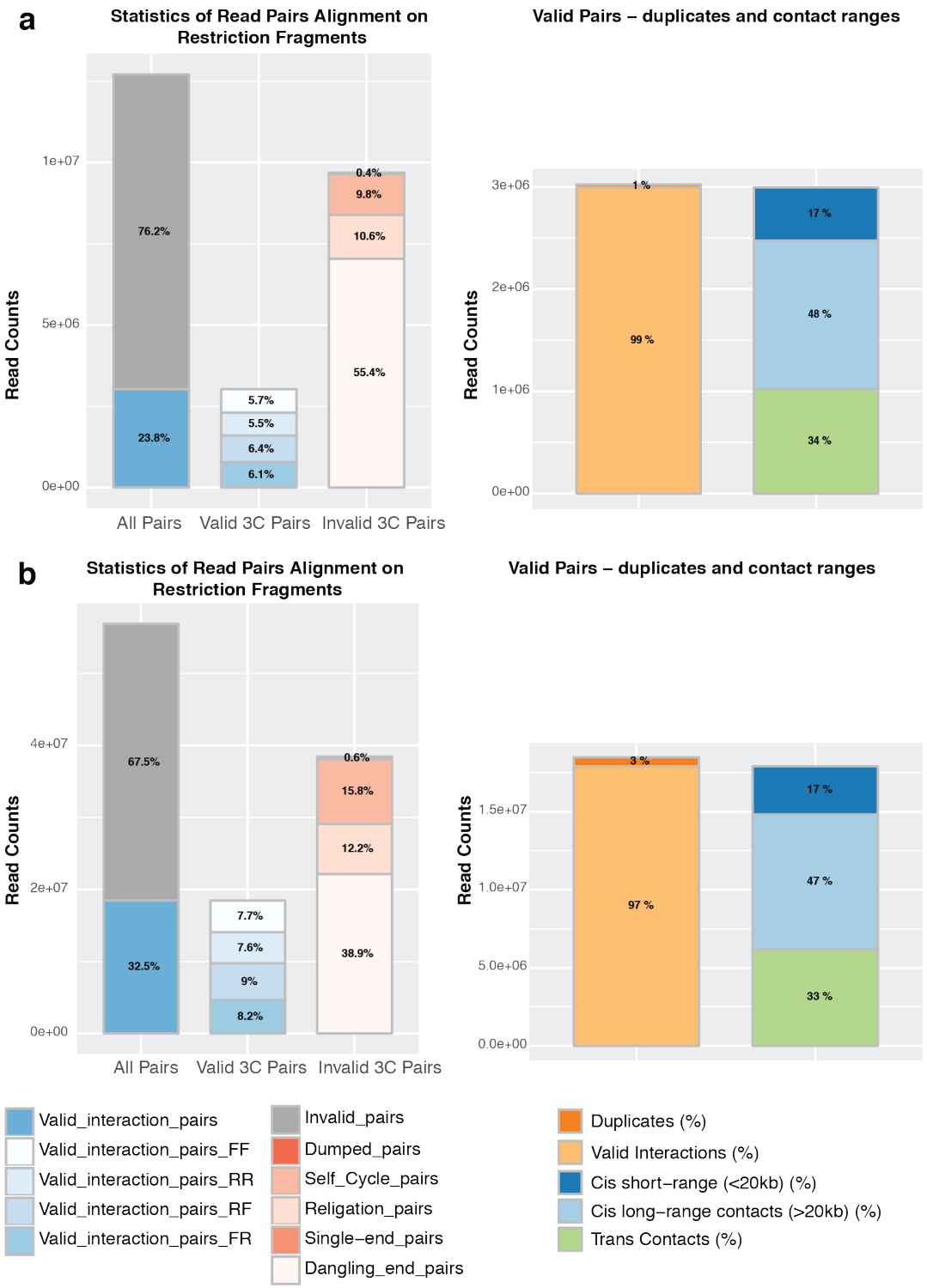

Figure 5.2.2.1. - HiC-Pro quality control of Hi-C library prepared from cells lysed by manual grinding - **a**, Plots for read pair filtering (left) and contact ranges (right) show modest increase in library complexity Hi-C library and a decrease in sequencing duplicates when sequenced on an Illumina MiniSeq platform **b**, Higher sequencing depth on Illumina NextNeq further increased the number of valid reads. Analyses and **a, b** were performed by Daniel Robertson (WCCB Bioinformatics Core Facility).

5.3 Results

5.3.1 Pericentromeric chromosome conformation changes when biorientation is established

In order to decipher pericentromeric chromosome conformation and how it changes in response to spindle tension, cells were synchronised in metaphase in the presence (no tension) or absence (tension) of microtubule drugs as previously described. Hi-C libraries were then prepared using the optimised protocol and sequenced on an Illumina NextSeq platform (EMBL Genomics Core, Heidelberg).

5.3.1.1 The pericentromere has a looped structure in the absence of spindle tension

Inspection of Hi-C contact maps in 50 kb regions surrounding centromeres revealed that in the absence of tension, core centromeres acted as strong insulators between the left and right chromosome arms, while making frequent contacts with the pericentromere on both sides (Figure 5.3.1.1.1a). As local Hi-C resolution varies depending on the distribution of *Dpn*II sites, this pattern was especially visible on some chromosomes, for example chromosomes IV, VII, X and XV.

In order to overcome differences in local resolution, *cis*-contacts surrounding all 16 centromeres were piled up (Figure 5.3.1.1.1b). Pile-up of contacts over longer distances (100 kb flanking centromeres) indicated high frequency interactions along chromosomes, consistent with compaction via *cis*-looping in mitosis (Schalbetter et al., 2017; Lazar-Stefanita et al., 2017) Shorter-range pericentromere pile-ups (25 kb flanking centromeres) confirmed the observation that the left and right sides of the pericentromere form distinct interaction domains that are in incomplete isolation from one another. This is consistent with a structure where either side of the pericentromere forms a

separate loop (Figure 5.3.1.1.1c). Finally, apparent on some chromosomes (IV, VII, X, XV), characteristic Hi-C stripes emanating from centromeres suggest that the looped structure of pericentromeres could be the result of chromatin loop extrusion by a centromere-anchored factor.

In summary, the high-quality high-resolution Hi-C maps produced here show patterns of mitotic chromosome arm compaction in the absence of tension, that are in agreement with previous findings. Close inspection of *cis*-contacts in the proximity of centromeres reveals a novel structure for the pericentromere, where the left and the right side form separate loops (Figure 5.3.1.1.1c), possibly via by loop extrusion.

5.3.1.2 Microtubule attachment extends pericentromere into a single open loop

Next, to understand what are the conformational changes that occur at the pericentromere when chromosomes biorient and centromeres move apart, Hi-C was performed in metaphase cells without the addition of microtubule drugs.

Inspection of individual pericentromeres revealed that under tension the insulator function of centromeres weakened (Figure 5.3.1.2.1a). This is indicated by contacts between the left and the right pericentromeres, in regions immediately flanking centromeres. In addition, contacts within pericentromeres were generally depleted, suggestive of the disruption of pericentromeric loops as sister centromeres are moved apart by the pulling forces of microtubules (best visible on chromosomes IV, VII, X, XV).

Contact across centromeres and the decrease in pericentromeric contacts were confirmed by pericentromere pile-ups (25 kb flanking centromeres) (Figure 5.3.1.2.1b). Importantly, pile-ups also showed that the *cis*-looping of chromosome arms remained unaffected. Altogether, these observations are consistent with the conversion of the pericentromere to a V-shape under tension, where the centromere is at the apex.

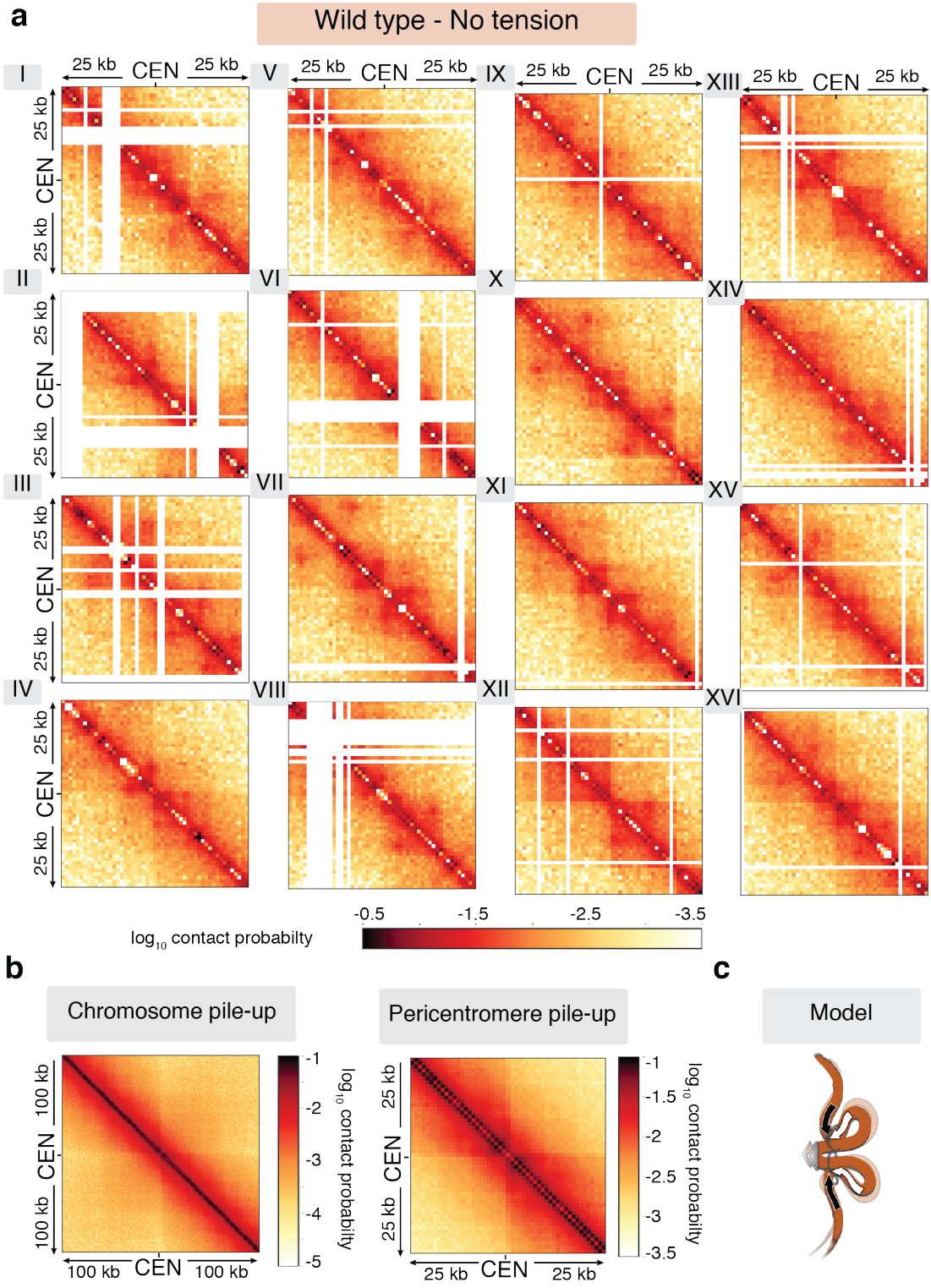

Figure 5.3.1.1.1. - The pericentromere has a multi-looped structure in the absence of tension - **a**, Hi-C contact maps (1kb bin) over a 50kb region surrounding all centromeres in wild type cells without tension. **b**, Pile-ups (bin size 1kb) of *cis* contacts 200kb (left panel) and 50kb (right panel) surrounding all 16 centromeres in absence of tension. **c**, Model for the multi-looped structure of the pericentoremre.

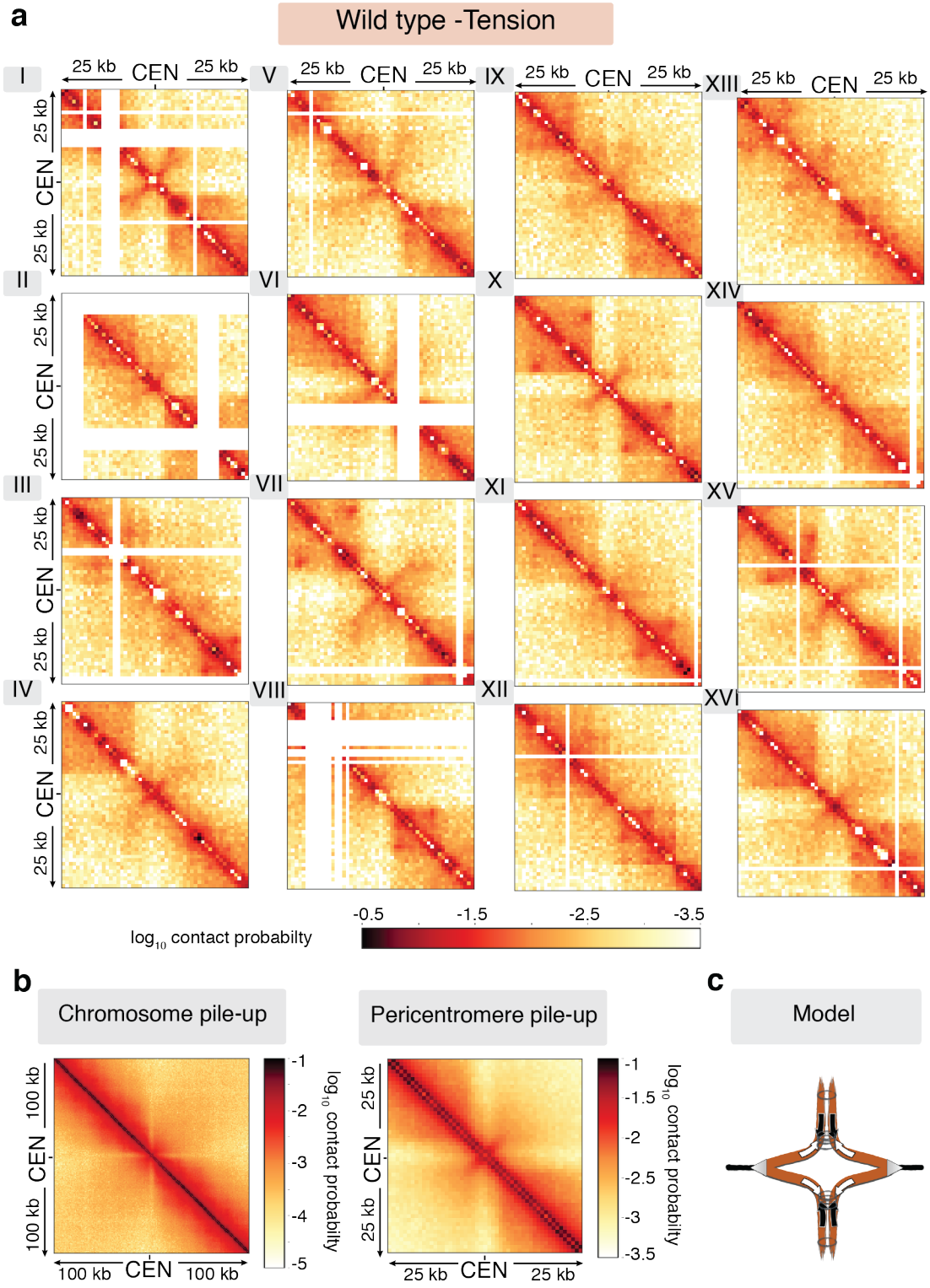

Figure 5.3.1.2.1 - The pericentromere is converted to a V-shape when biorientation is established - **a**, Hi-C contact maps (1kb bin) over a 50kb region surrounding all centromeres in wild type cells with tension. **b**, Pile-ups (bin size 1kb) of cis contacts 200kb (left panel) and 50kb (right panel) surrounding all 16 centromeres in the presence of tension. **c**, Model for pericentromere structure under tension.

To directly compare Hi-C profiles of pericentromeres in the absence and presence of tension, Hi-C difference maps were created by plotting the $\log_2$ difference between the tension and no tension pile-ups (Figure 5.3.1.2.2). This analysis confirmed that pericentromeric contacts substantially decreased as tension was exerted on chromosomes, as signified by the blue colours in pericentromeric regions on the difference maps. It was also confirmed that tension-dependent restructuring of chromosomes only affects pericentromeres, and not chromosome arms.

In summary, Hi-C in metaphase cells indicates that in the absence microtubule-kinetochore attachments each side of the pericentromere is organised into a separate loop. When biorientation is established, the attachment of microtubules converts this looped structure into a V-shape, extending a single pericentromeric loop.

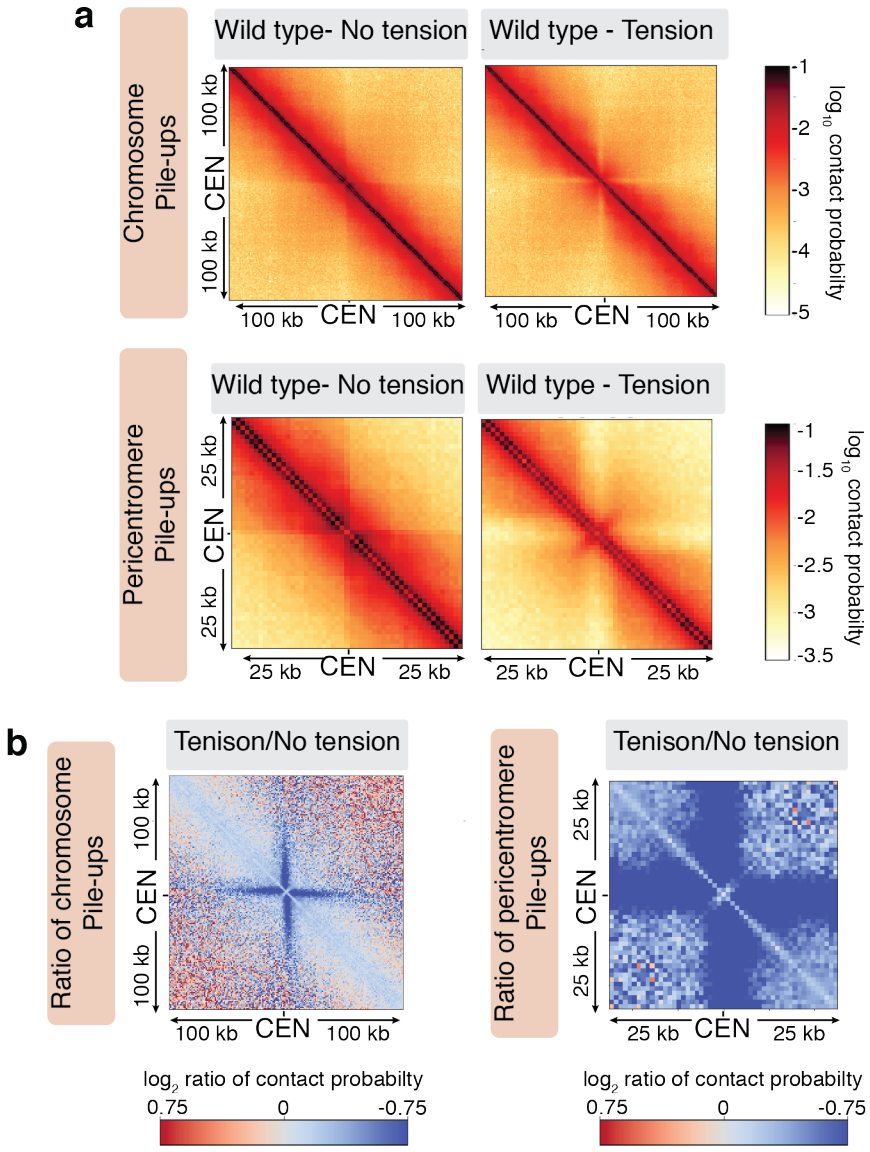

Figure 5.3.1.2.2 - The pericentromere undergoes a conformational change upon the establishment of bioreintation. a, Pile-ups (bin size 1kb) of cis contacts 100kb surrounding all 16 centromeres (top panel), pericentromere pile-ups (bottom panel, 25kb surrounding centromeres) in the absence or presence of spindle tension. **b**, Log2 difference between 100kb (left) and 25kb (right) pile-ups centered on the centromere in wild type cells in the absence and presence of tension. Blue colour signifies decrease in contacts under tension compared to no tension, red colour signifies increase in contacts under tension compared to no tension.

5.3.2 Pericentromeric chromosome conformation depends on kinetochore-driven cohesin loading

Next, in order to examine the dependence of pericentromere structure on pericentromeric cohesin, Hi-C was performed in *chl4Δ* cells that are defective in kinetochore-driven cohesin loading. This results in reduced cohesin levels at pericentromeres.

Both in the absence (Figure 5.3.2.1) and presence (Figure 5.3.2.2) of tension, the strength of Hi-C patterns decreased in the absence of centromeric cohesin loading. In the absence of tension, centromere-proximal loops were less defined, suggesting that cohesin loaded at the centromere promotes pericentromere looping. In the presence of tension, the region showing reduced *cis*-contacts expands in *chl4Δ.* This is consistent with the enlargement of the pericentromeric V-shape, indicating that cohesin loaded at the centromere restricts the size of the pericentromeric loop under tension.

The differences described above were most obvious on the $\log_2$ ratio plots between wild type and *chl4Δ* cells (Figure 5.3.2.3). Blue colour around centromeres signifies loss of contacts in *chl4Δ*, indicating an overall loss of structural organisation of pericentromeres in the absence of centromeric cohesin loading. The disruption of pericentromere structure is incomplete, which is consistent with the notion that although cohesin levels are reduced, there is still residual centromeric cohesin loading in *chl4Δ* (Fernius and Marston, 2009; Hinshaw et al., 2017).

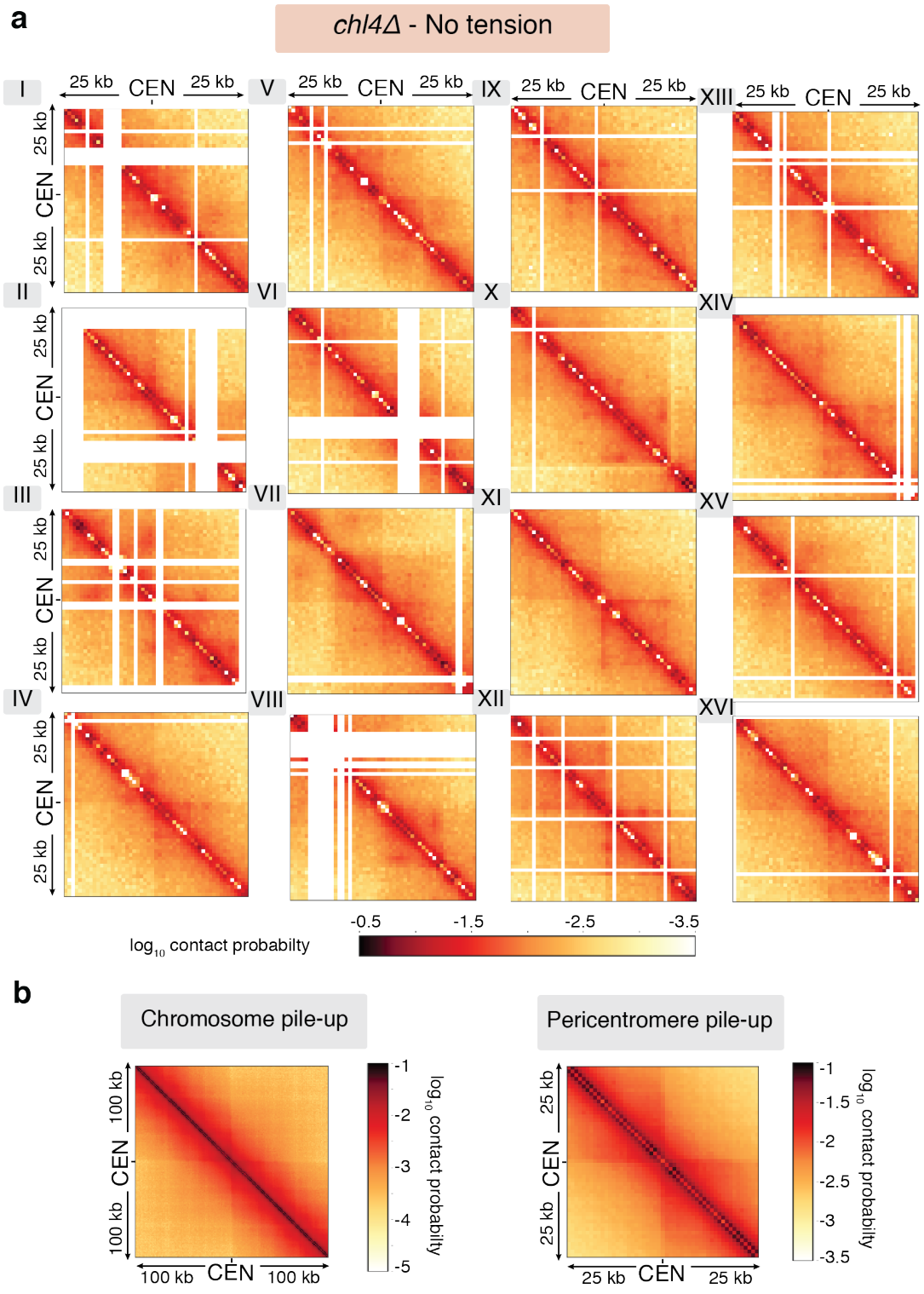

Figure 5.3.2.1. - Cohesin loaded at the centromere promotes pericentromere looping in the absence of tension - a, Hi-C contact maps (1kb bin) over a 50kb region surrounding all centromeres in *chl4Δ* cells without tension. **b**, Pile-ups (bin size 1kb) of cis contacts 200kb (left panel) and 50kb (right panel) surrounding all 16 centromeres in the absence of tension.

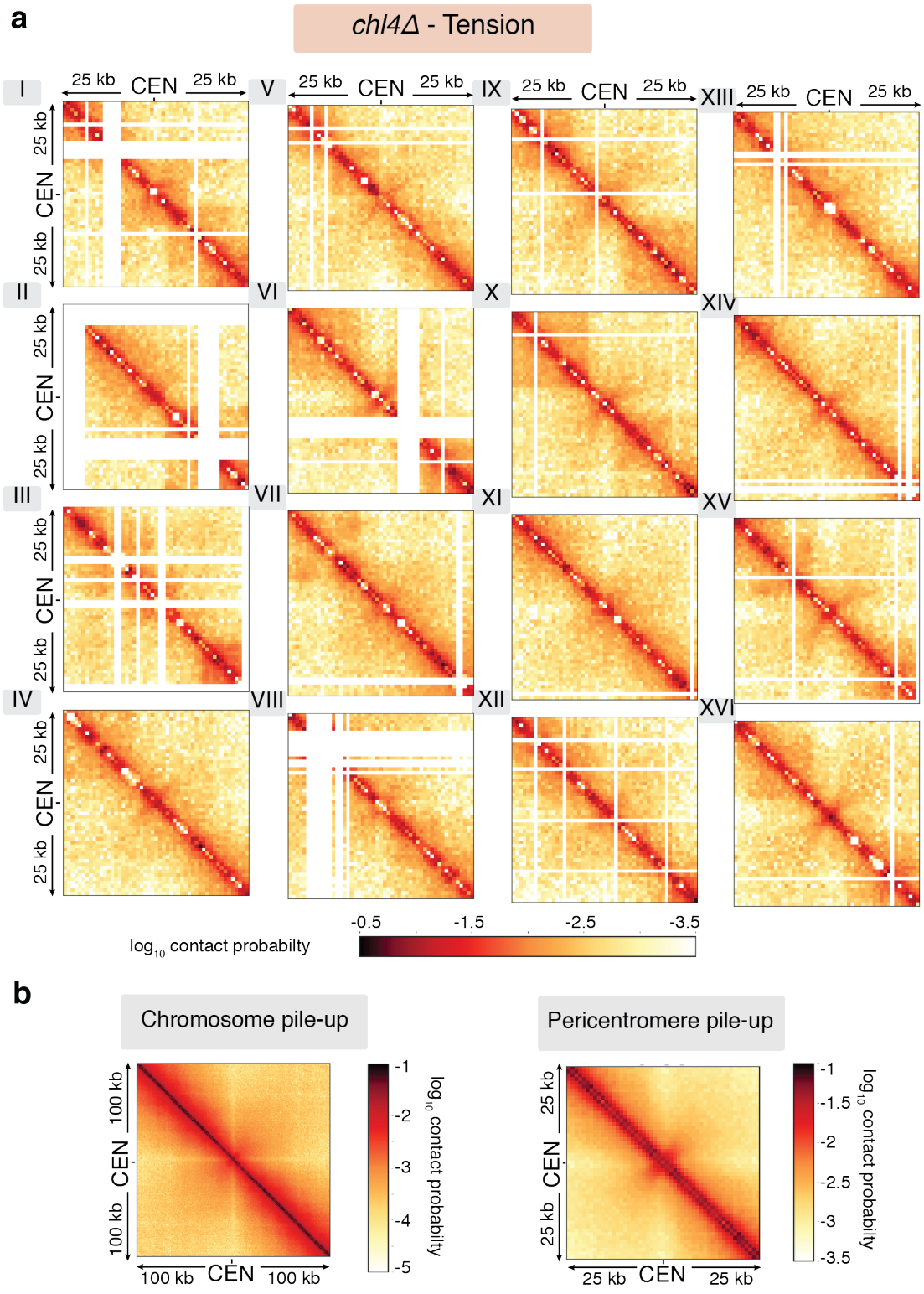

Figure 5.3.2.2. - Pericentromere loop strength under tension is conferrred by cohesin loaded at the centromere - **a**, Hi-C contact maps (1kb bin) over a 50kb region surrounding all centromeres in *chl4Δ* with tension. **b**, Pile-ups (bin size 1kb) of cis contacts 200kb (left panel) and 50kb (right panel) surrounding all 16 centromeres in the presence of tension.

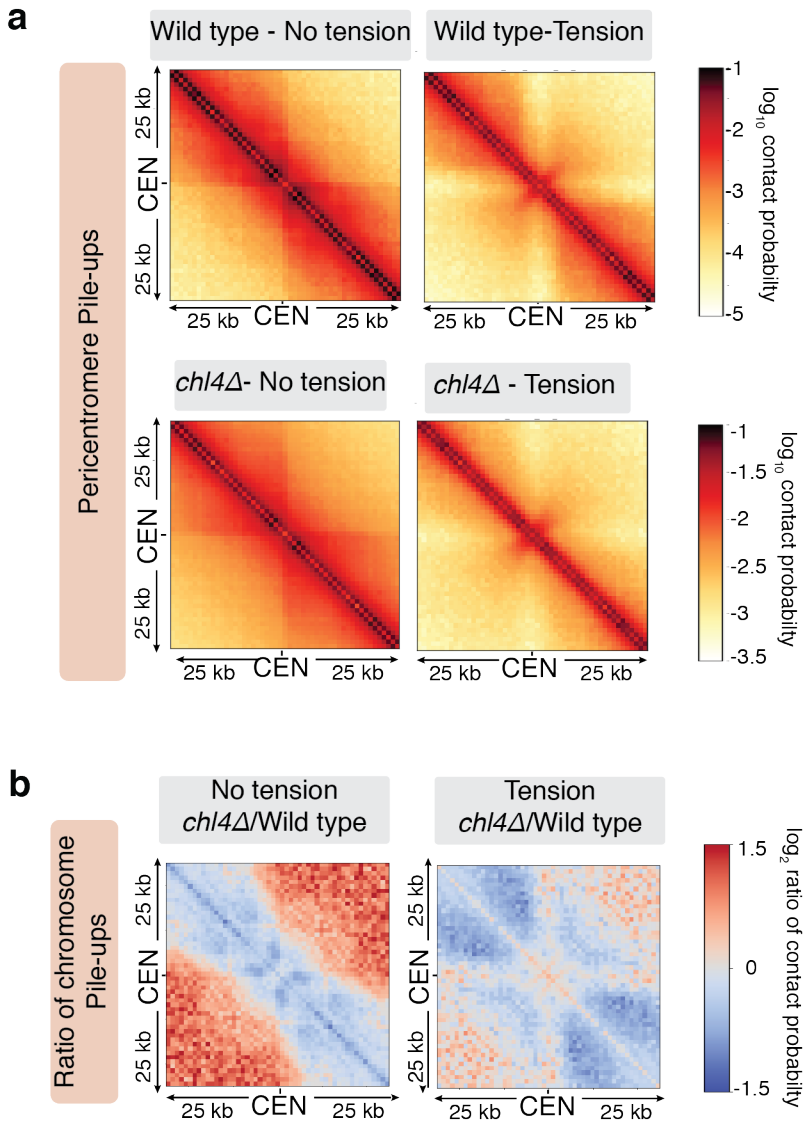

Figure 5.3.2.3. - Pericentromere structure changes in the absence of kintochore-driven cohesin loading. a, Pile-ups (bin size 1kb) of cis contacts 25kb surrounding all 16 centromeres in the absence or presence of spindle tension, in wild type (top panel) and in *chl4Δ* (bottom panel) cells. **b**, Log_2 difference between 100kb pile-ups centered on the centromere in wild type and *chl4Δ* cells, both in the absence (left panel) and presence (right panel) of tension. Blue colour signifies decrease in contacts in *chl4Δ* compared to wild type, red colour signifies increase in contacts in *chl4Δ* compared to wild type.

5.3.3 Shugoshin-dependent condensin recruitment does not influence chromosome conformation at pericentromeres

Besides cohesin, condensin is also enriched at pericentromeres (Peplowska et al., 2014; Verzijlbergen et al., 2014). As condensin also has a role in genome organisation in budding yeast (Schalbetter et al., 2017; Lazar-Stefanita et al., 2017), we next tested if condensin was involved in structuring pericentromeres. Because condensin localises to pericentromeres in a shugoshin-dependent manner (Peplowska et al., 2014; Verzijlbergen et al., 2014), which in turn is removed from pericentromeres in response to tension (Nerusheva et al., 2014), Hi-C was performed in *sgo1Δ* cells in the absence of tension to determine if condensin has a role in shaping the pericentromere. To separate any effect of *sgo1Δ* in pericentromere structure that might arise from failure to recruit PP2A rather than condensin, Hi-C was also performed in *sgo1-3A* mutants which recruit condensin to pericentromeres normally but fail to bind PP2A (Xu et al., 2009; Peplowska et al., 2014; Verzijlbergen et al., 2014).

Hi-C contact maps of *sgo1Δ* and *sgo1-3A* showed virtually no difference compared either to wild type or to each other (Figure 5.3.3.1). Therefore, it was concluded that pericentromeric condensin does not play a role in establishing the mloop structure of the pericentromere in the absence of tension.

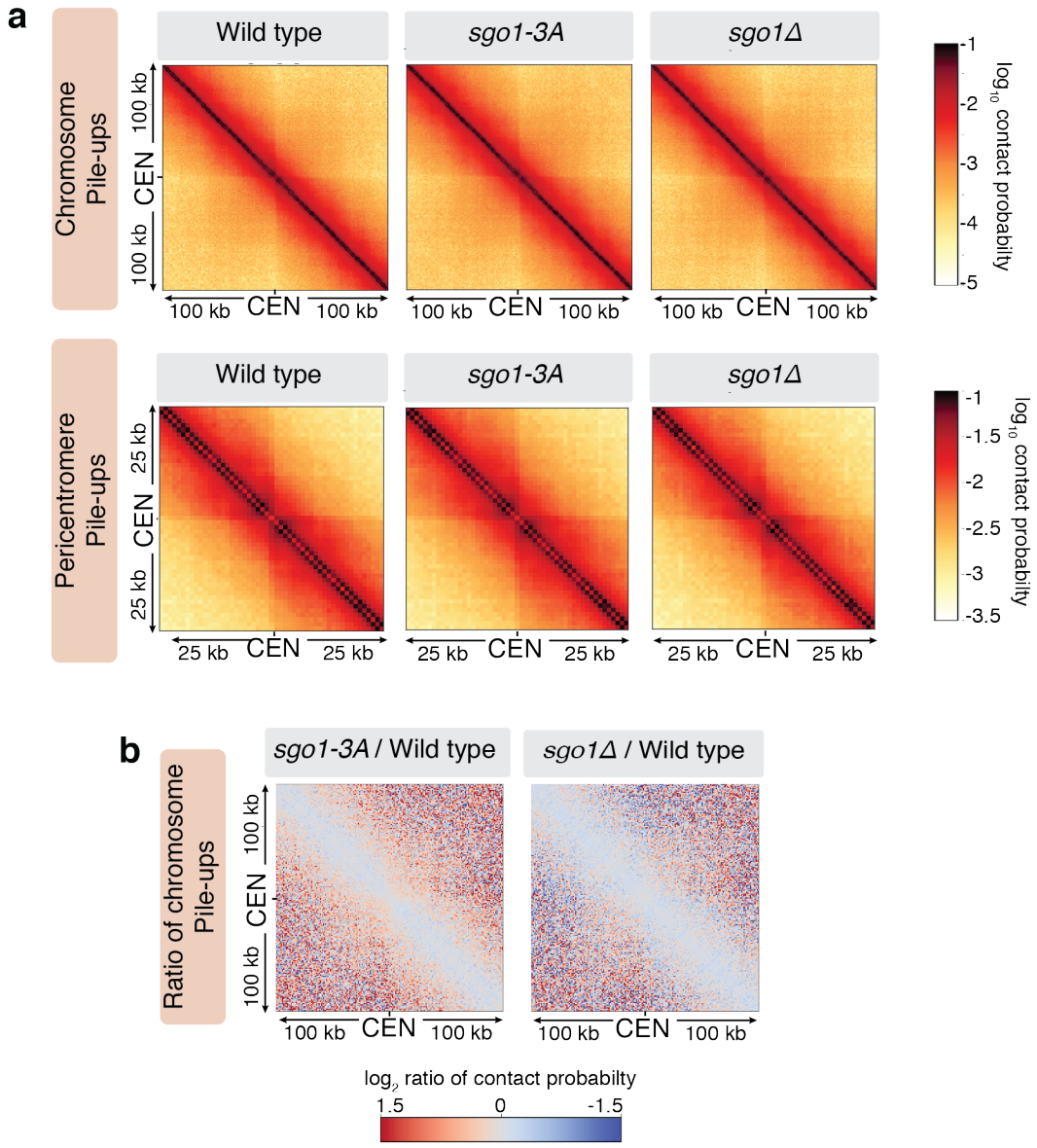

Figure 5.3.3.1. - The absence of Sgo1 does not grossly alter pericentromere structure at metaphase without tension. Hi-C analysis of *sgo1-3A* and *sgo1Δ* in metaphase-arrested cells in the absence of tension reveals similar patterns to wild type. **a**, Pile-ups (bin size 1kb) of *cis* contacts surrounding all 16 centromeres in absence of spindle tension for the indicated strains. **b**, Log_2 difference maps (bin size 1kb) of cis contacts surrounding all 16 pericentromeres.

5.3.4 Pericentromere borders act as boundaries between cohesed chromosome arms and tension-responsive pericentromeric domains

Pericentromere borders were found to be important to set the limits to pericentromeric cohesin enrichment as well as to define the region of pre-anaphase sister chromatid separation under tension. Next, the role of pericentromere borders in pericentromere structure was examined. To this end, cohesin ChIP-seq tracks were aligned with pericentromeric Hi-C maps, both on some individual chromosomes (IV, X) and on pericentromere pile-ups (Figure 5.3.4.1).

The following features were clearly visible: 1) the tension-sensitive pericentromeric cohesin domain aligns with the chromosomal region that shows conformational change in response to tension 2) high cohesin density and strong Hi-C signal coincide at border regions. Altogether, these observations suggest that borders define the size of the pericentromeric loops in the absence of tension. Conversely, in the presence of tension, borders will be at the base of the pericentromeric open loop or V-shape. Therefore, borders appear to separate the tension-responsive pericentromere from the cohered chromosome arms.

If borders separate pericentromeres from chromosome arms, then centring pile-ups on borders themselves (rather than centromeres) should show isolation of pericentromeric and chromosome arm regions. Indeed, both in the presence and absence of tension, contacts across borders, between chromosome arms and pericentromeres, were reduced (Figure 5.3.4.2), indicating that borders form a boundary between centromere-proximal and centromere-distal chromosomal domains. Boundary function of borders strikingly sharpened under tension and was dependent on *CHL4*.

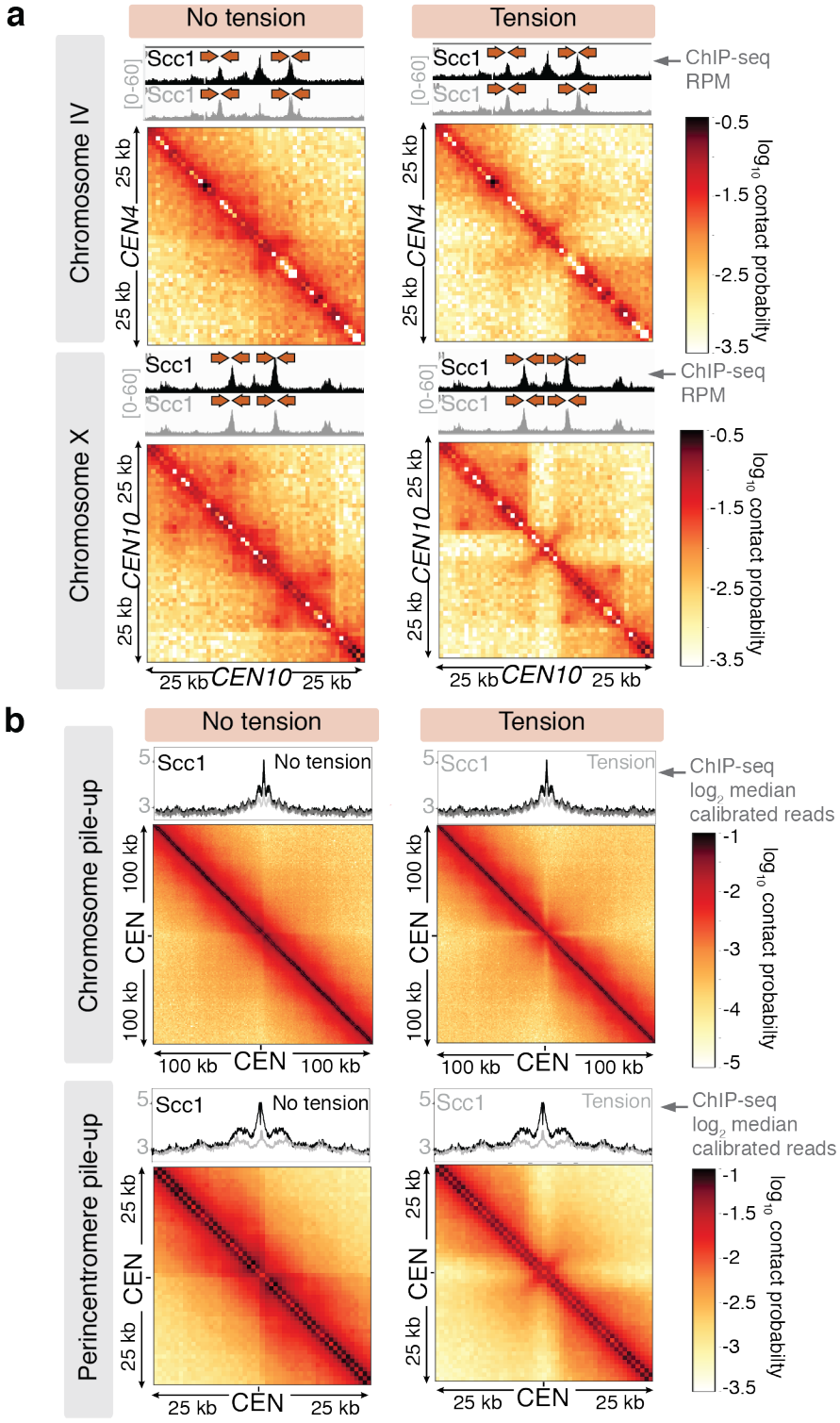

Figure 5.3.4.1. - Strong Hi-C signal and high cohesin densitiy coincide at pericentromere borders. a, Contact maps for pericentromere IV (top) and X (bottom) are shown for wild type cells in the absence (left) or presence (right) of spindle tension. Calibrated Scc1-6HA ChIP signal is shown above. **b**, Chromosome (top) and pericentromere (bottom) pile-ups in the absence (left) or presence (right) of spindle tension. Median calibrated Scc1-6HA ChIP signal is shown above.

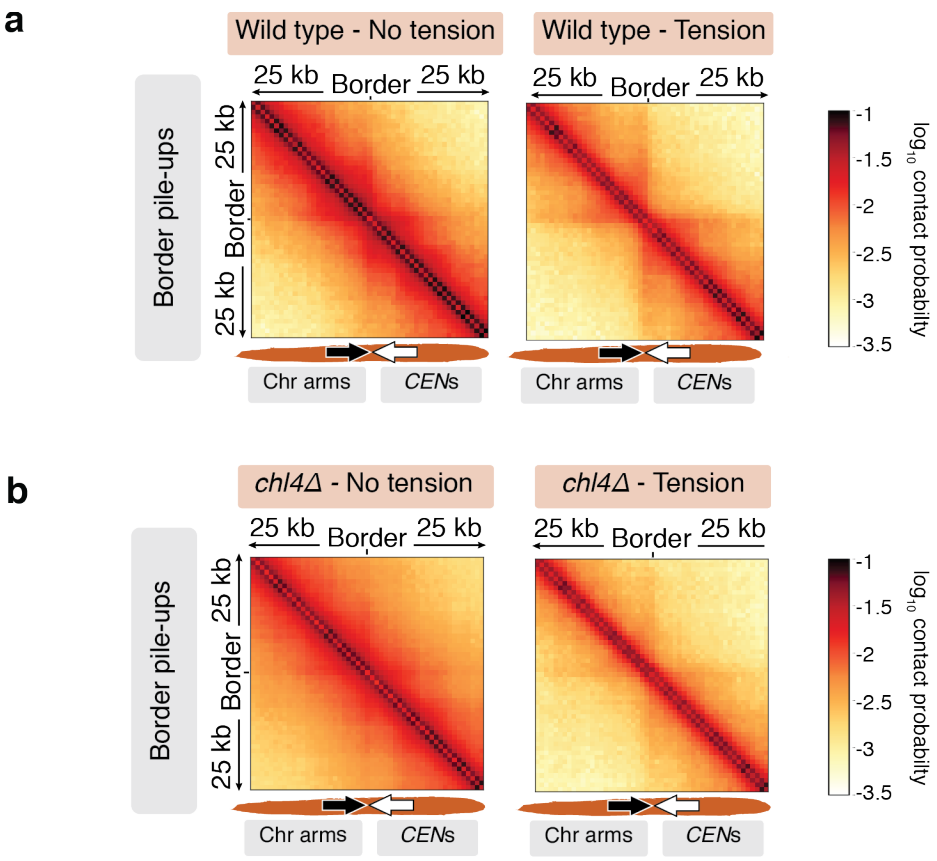

Figure 5.3.4.2. - Borders isolate pericentromeres from chromosome arms. Pile-ups (1kb bins) and of cis contacts surrounding pericentromere borders (25 kb) in wild type (**a**) and *chl4Δ* (**b**) cells.

5.4 Discussion

Using high-resolution Hi-C, work presented in this chapter deciphered pericentromeric chromosome conformation in metaphase, both the presence and absence of tension. It was found that in the absence of microtubule-kinetochore attachments, either side of the pericentromere folds into a separate loop that are in partial isolation from each other (Figure 5.3.1.1.1). Some evidence suggests that pericentromeric loops could be formed by loop extrusion, which is halted when pericentromere borders are encountered (Figure 5.3.4.1). When chromosomes biorient, the pulling forces of spindle microtubules extend a single loop, rendering the pericentromere into a V-shape, with borders at the base and core centromeres at the apex (Figure

5.3.1.2.1, 5.3.4.1). Accordingly, borders seem to act as boundaries between centromere-proximal (pericentromere) and centromere-distal (chromosome arm) regions (Figure 5.3.4.2). All the above structural features of the pericentromere are largely dependent on kinetochore-driven cohesin loading, as Hi-C maps of *chl4Δ* showed reduced pericentromeric looping in the absence of tension (Figure 5.3.2.1) and reduced boundary function (Figure 5.3.4.2), as well as an expansion of the pericentromeric V-conformation (Figure 5.3.2.2). This latter observation is consistent with the notion that *chl4Δ* cells have larger separation distance between centromeric GFP markers in the absence of tension (Fernius and Marston, 2009).

The apparent insulation between, and high-frequency interaction domains within the left and the right side of pericentromeres in the absence of tension argue against the presence of a single intramolecular loop at pericentromeres proposed by Yeh *et al*. (2008). Instead, we propose that each side of the pericentromere folds into a separate loop, and these loops are pulled out upon biorientation (Figure 5.4.1). Data presented here is in agreement with the proposition of Yeh *et al.* (2008) that pericentromeric cohesin – at least partly – establishes intra-sister rather than inter-sister linkages.

Interestingly, no role in pericentromere structure was found for condensin. This somewhat contradicts Schalbetter *et al.* (2017) where condensin inactivation was found to increase contacts between centromeres, and increase the isolation of centromere-proximal region from chromosome arms. However, this difference in findings can be explained by different experimental conditions and analysis. First, as opposed to global condensin inactivation used by Schalbetter et al. (2017), *sgo1Δ* employed in this study only affects condensin localisation to pericentromeric regions where it does not lead to complete condensin depletion. Thus, it is possible that the residual pericentromeric condensin *sgo1Δ* is sufficient for proper pericentromere structure. A second possibility is that while condensin has a structural role in presence of tension (Schalbetter et al., 2017), in the absence of tension it is dispensable for proper

pericentromere structure (this study). Third, we did not look at the frequency of *trans* contacts between centromeres, thus it is possible that pericentromeric condensin depletion by *sgo1Δ* leads to the over-clustering of centromeres as suggested in Schalbetter et al. (2017).

Finally, even in the light of the above findings it remains unclear precisely how pericentromere geometry facilitates biorientation. In order to understand this, the relative orientation of the two sisters in their looped conformation would have to be known, but Hi-C does not allow intra-sister interactions to be distinguished from inter-sister interactions.

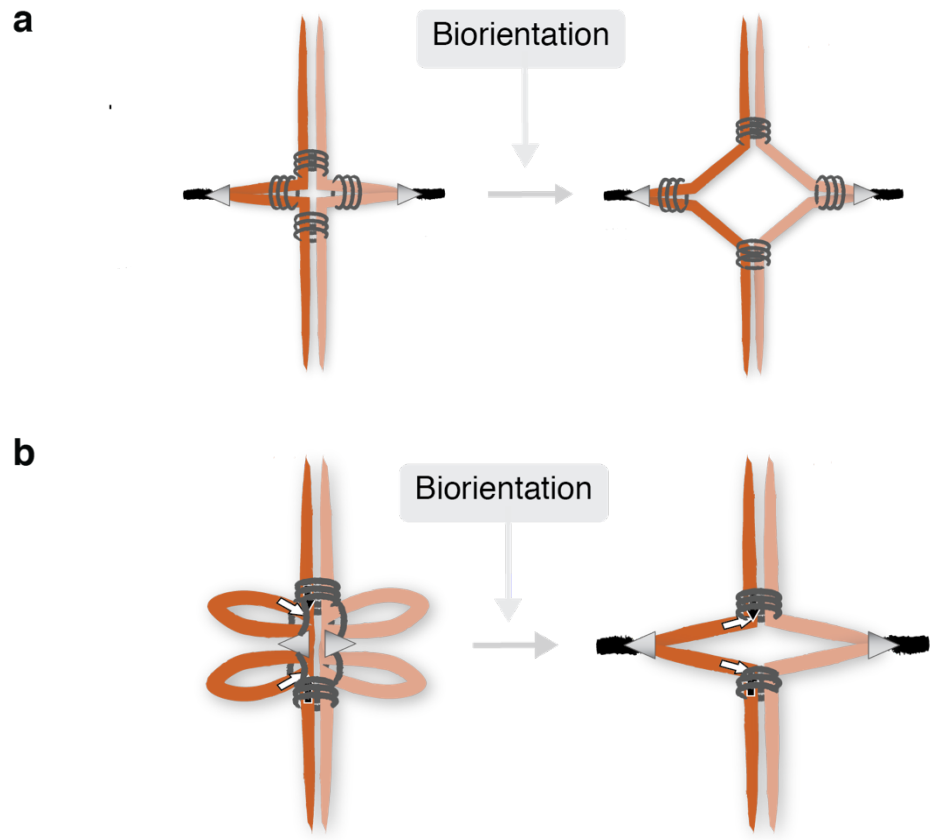

Figure 5.4.1. - Models for pericentromeric chromosome conformation. a, Cruciform structure formed by cohesin tethering the left and right sides of pericentromere together (Yeh *et al*. 2008) **b**, The separate looping of the left and right side of the pericentromere via loop extrusion, proposed in this study

Chapter 6 Gene orientation at borders affects pericentromere size, biorientation efficiency and cell viability

6.1 Introduction

It has been established in this study that pericentromere borders have an integral function in defining: 1) the region of pericentromeric cohesin enrichment, 2) the region of transient pre-anaphase sister chromatid separation, and 3) the region that undergoes a structural change upon biorientation. All these functions are anticipated to rely on the accumulation of high levels of cohesin at borders. What is the property of border regions that allows the retention of cohesin? It was found that pericentromere borders form between convergent genes. This is not surprising, as intergenic regions between convergent genes are known sites for cohesin accumulation, not only in budding yeast (Lengronne et al., 2004; Glynn et al., 2004) but in *S. pombe* (Lengronne et al., 2004; Gullerova and Proudfoot, 2008; Mizuguchi et al., 2014) and mammalian cells as well (Busslinger et al., 2017).

Previously, it has been shown that transcription can alter the chromosomal localisation of cohesin (Lengronne et al., 2004; Ocampo-Hafalla et al., 2016): transcriptional activation clears cohesin covering the gene, and causes it to accumulate at the 3' end. Therefore, in this chapter it is hypothesised that convergent transcription is the property of border regions that allows cohesin accumulation. To test this, the impact of convergent gene pairs on the function of pericentromere borders will be assessed. Finally, further experiments will establish the implications for chromosome segregation arising from the absence of border convergent genes.

6.2 Results

6.2.1 Border convergent genes are expressed

As cohesin localisation to the 3' end of convergent genes depends on active transcription (Lengronne et al., 2004; Ocampo-Hafalla et al., 2016), first the transcription of border convergent genes was checked. To this end, we obtained an Rpo21-CRAC dataset from (Bresson et al., 2017). Rpo21-CRAC allows the high-resolution mapping of the transcribing RNA polymerase II (RNAPII) through the UV-crosslinking of proteins with RNA. This indicated that sense transcripts could be detected for all genes at borders. Although transcription levels varied, border convergent genes overall showed moderate expression, and transcription at borders was typically higher towards than away from centromeres (Figure 6.2.1.1). This suggests that high transcription levels are not required for cohesin accumulation at convergent genes sites, and thus pericentromere border formation.

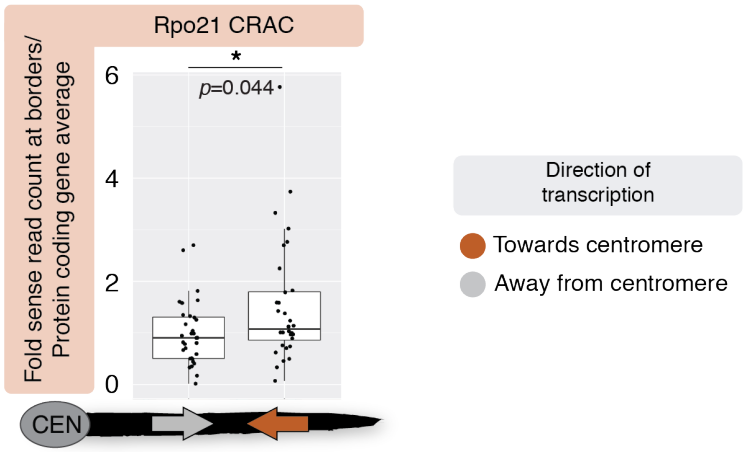

Figure 6.2.2.1. - Genes at pericentromeres are moderately expressed. Boxplot of transcription levels of genes at pericentromere borders based on RNA polymerase II (Rpo21) Cross-linking and analysis of cDNA (CRAC) from Besson *et al*. 2017. Rpo21 CRAC sense read counts of genes at borders were normalized to the protein coding gene average and genes at pericentromere borders were grouped by their relative orientation to centromeres. Data points correspond to the mean of three biological repeats. Centre line, median; box limits, second and third quartile; whiskers, first and fourth quartile (non-normal distribution, Shapiro-Wilk; *, p<0.05, two-sided Mann-Whitney test).

Second, previously we noted the presence of convergent genes inside pericentromere borders that did not seem to accumulate high levels of tension-insensitive cohesin and therefore did not form borders. It was found that, conversely to borders, transcription at non-border convergent genes inside pericentromeres was generally higher away from than towards centromeres (Figure 6.2.1.2). This suggests that a threshold level of centromere-oriented transcription might be required for border formation.

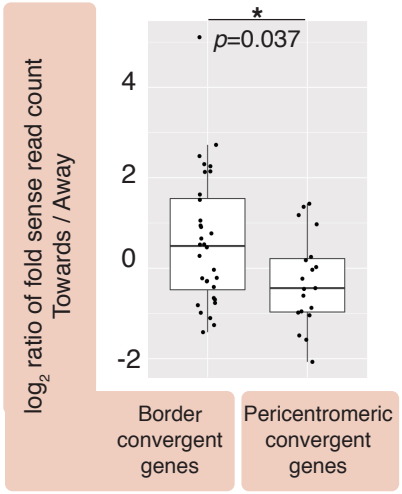

Figure 6.2.1.2. - At border convergent genes transcription towards the centromere tends to dominate. Boxplot of relative transcription levels of genes transcribed towards and away from centromeres, at pericentromere borders and at non-border convergent genes inside pericentromeres, based on RNA polymerase II (Rpo21) Cross-linking and analysis of cDNA (CRAC) from Besson *et al*. 2017. Rpo21 CRAC sense read counts of genes at borders were normalized to the protein coding gene average and genes at pericentromere borders were grouped by their relative orientation to centromeres. Data points correspond to the mean of three biological repeats. Centre line, median; box limits, second and third quartile; whiskers, first and fourth quartile (non-normal distribution, Shapiro-Wilk; *, p<0.05, two-sided Mann-Whitney test).

It has to be noted that Rpo21-CRAC was performed in exponentially growing cells. This however, did not impose a problem for the following reasons. First, the vast majority of genes at pericentromere border regions are constitutively expressed throughout the cell cycle, with only 4 out of 64 genes showing cell cycle regulation (Spellman et al., 1998). Second, it is unclear when

transcription at borders would be required: cohesin loading onto chromosomes starts in late G1 (Michaelis et al., 1997; Uhlmann and Nasmyth, 1998; Fernius et al., 2013) but pericentromere structure for biorientation is required at metaphase. Therefore, if transcription at borders indeed plays a role in pericentromere structure and function, transcription might be equally required for the establishment and/or maintenance of borders. However, this possibility was not investigated in more detail.

6.2.2 Gene reorientation at borders causes loss of cohesin, Shugoshin and condensin localisation

As transcription is able to change cohesin localisation on chromosomes, and pericentromere borders form at convergent gene sites, it is possible that convergent transcription positions pericentromere borders. If so, the cohesin enrichment sites at border regions should not form in the absence of convergent genes. In order to investigate if convergent genes are necessary for cohesin retention and border formation, a strain was created where border genes (along with promoters) on chromosome IV were re-arranged into a tandem orientation, transcribing away from the centromere. This allowed us to study the consequences specific to the absence of the convergent gene site, while minimally interfering with gene function. Strains carrying this modified chromosome IV will be referred to as ‘reoriented’ hereafter.

First, wild type and reoriented strains were arrested in metaphase in the absence or presence of tension (as previously described), and calibrated cohesin ChIP-seq was performed (Figure 6.2.2.1). Upon gene rearrangement, cohesin localisation was completely lost from border regions, indicating that the presence of convergent genes is the property of border regions that allows cohesin retention. Interestingly, additional small cohesin peaks appeared downstream of the tandem array of genes. This suggests that in the absence of convergent genes cohesin might be translocating further down on chromosome arms.

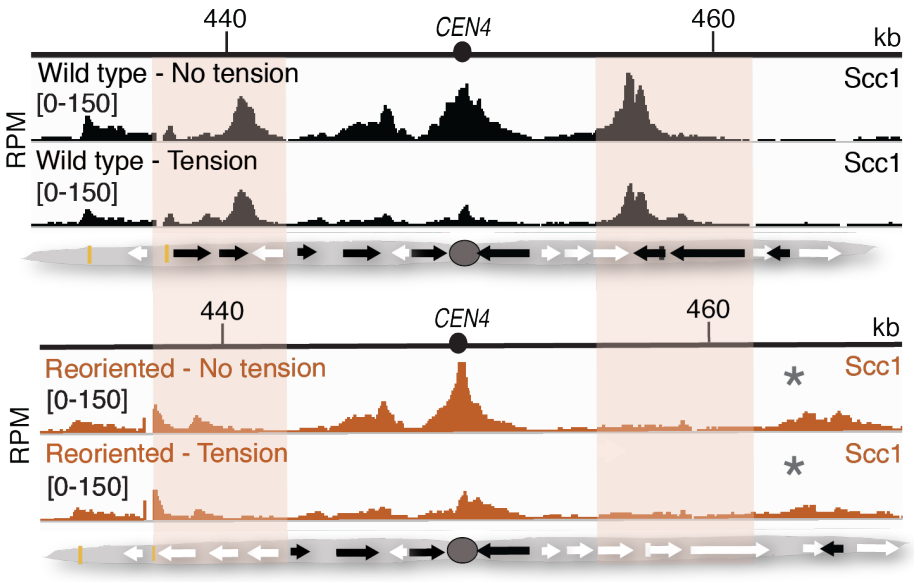

Figure 6.2.2.1 - Cohesin enrichment at pericentromre borders is lost in the absence of convergent genes. Cohesin enrichment in the pericentromeric region of chromosome IV in wild type and the reoriented strain. Shading indicates the position of the pericentromere borders in wild type cells. Asterisks indicate the position of new cohesin peaks in the reoriented strain. Schematics below show gene orientations: black and white arrows indicate genes transcribed towards and away from the centromere, respectively.

In addition to cohesin, pericentromere borders were found to be enriched in shugoshin and condensin. Therefore, I next tested if shugoshin and condensin localisation are also lost form pericentromere borders upon gene reorientation. Similar to cohesin, in the absence of border convergent genes, previous border regions were not enriched in shugoshin and condensin (Figure 6.2.2.2). Instead, shugoshin and condensin showed enrichment at the new downstream cohesin peak that formed upon gene reorientation.

In summary, when convergent genes at borders are rearranged into a tandem orientation transcribing away from centromeres, cohesin, Shugoshin and condensin localisation from original border positions is lost. Rather, all three proteins seem to accumulate at a new enrichment site, centromere-distal from the original border. Interestingly, the new cohesin, Shugoshin and condensin

peaks were found to form over *TRP1* and an overlapping ORF (*YDR008C*) on the opposite strand. Altogether, these observations indicate that the presence of convergent genes is required for cohesin retention, shugoshin and condensin localisation at pericentromere border regions.

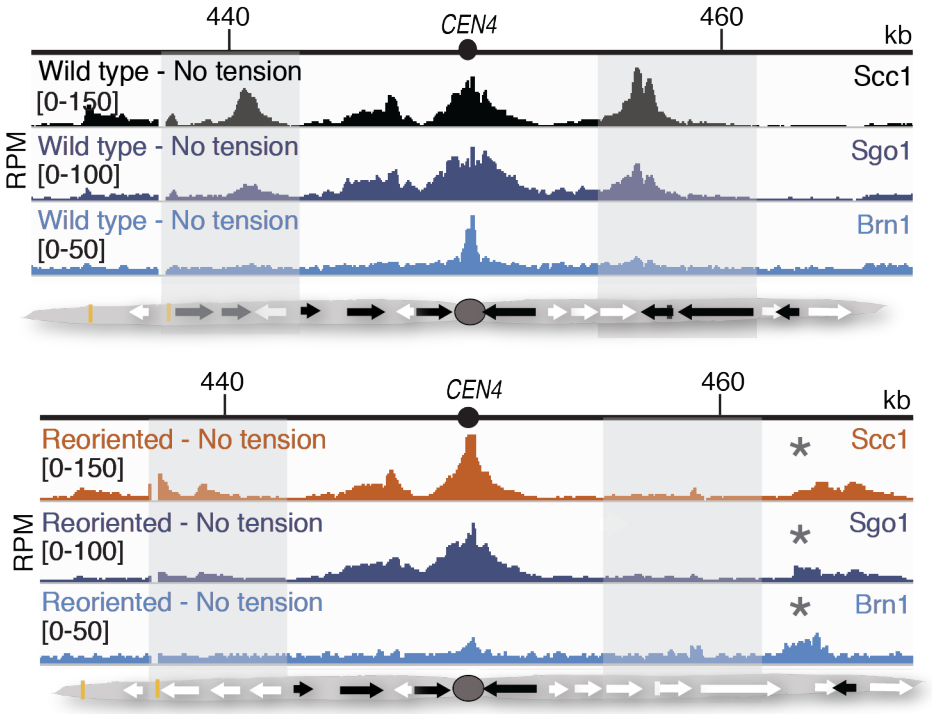

Figure 6.2.2.2. - Shugoshin and condensin localisation to borders is lost in the absence of convergent genes. Cohesin (Scc1), Shugoshin (Sgo1) and condensin (Brn1) enrichment in the pericentromeric region of chromosome IV in wild type (top panel) and the reoriented (bottom panel) strain. Shading indicates the position of the pericentromere borders in wild type cells. Asterisks indicate the position of new cohesin peaks in the reoriented strain. Schematics below show gene orientations: black and white arrows indicate genes transcribed towards and away from the centromere, respectively.

6.2.3 Gene reorientation at borders enlarges the pericentromere

On the reoriented chromosome IV, cohesin accumulation was observed centromere-distal to the original position of borders. This suggests that in the absence of convergent genes, instead of getting trapped at border regions, cohesin that was loaded at the centromere might translocate further down on chromosome arms. If so, this could be thought of as an expansion of the pericentromere which should be detectable with the GFP marker separation assay. Therefore, in order to test if pericentromere size increases in the absence of convergent genes, *tetO*/TetR-GFP markers were inserted inside and outside the pericentromere border, on both wild type and reoriented chromosome IV. Cells were then arrested in metaphase and the number of separated *tetO*/TetR-GFP markers were counted (Figure 6.2.3.1).

Wild type chromosome IV showed similar results to chromosome I and III: the marker inside pericentromere separated efficiently (~75%) while the marker outside separated infrequently (~15%). Strikingly, following gene reorientation, the markers inside and outside the original border behaved identically, both separating in ~70% of cells, indicating that the region of sister chromatid separation increases on the reoriented chromosome IV. Progression into metaphase was not affected by gene reorientation as SPBs separated identically in all strains. Finally, no increase in the distance between separated *tetO*/TetR-GFP was detected on the reoriented chromosome IV.

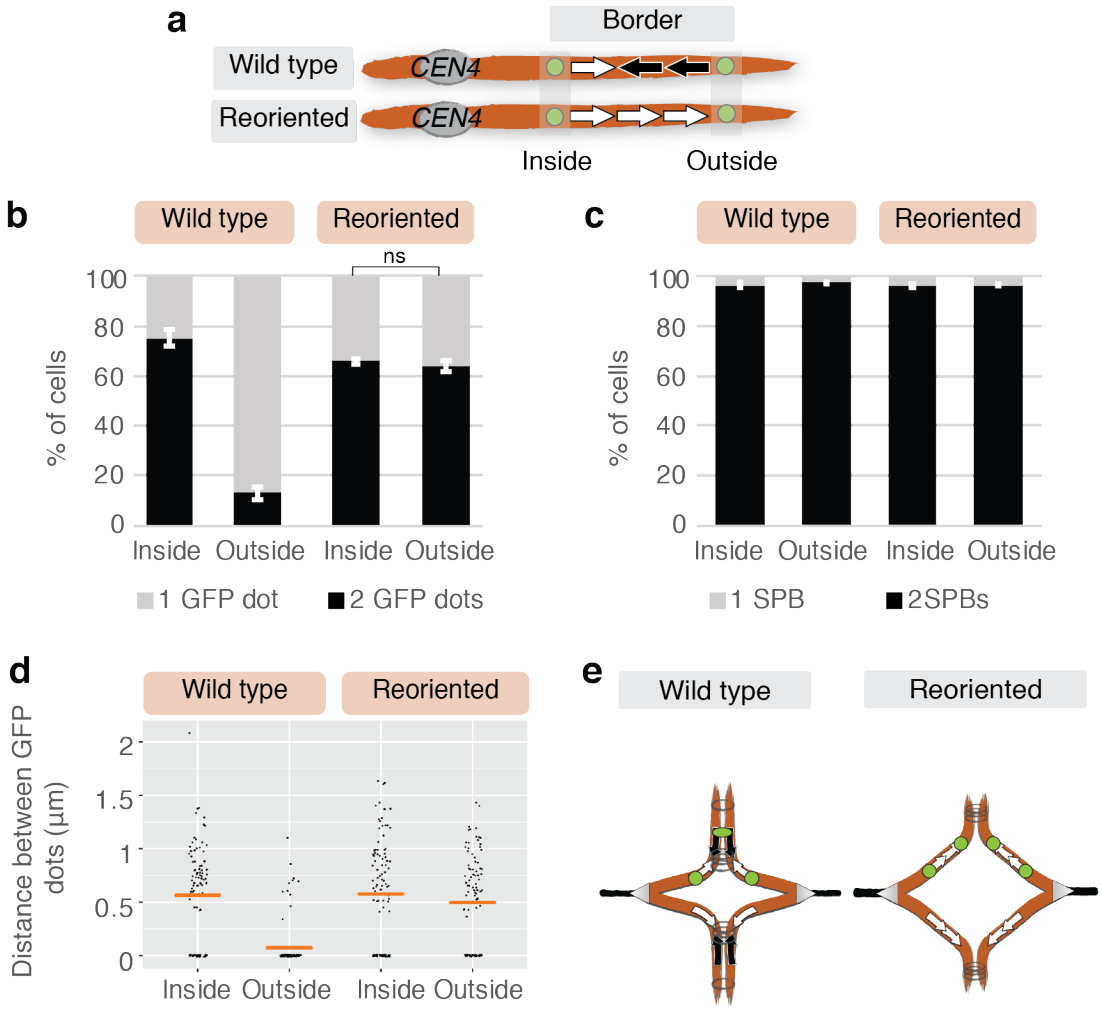

Figure 6.2.3.1. - Gene reorientation et borders enlarges the pericentromere. Strains with *tetO* arrays integrated at the indicated positions (**a**) were arrested in metaphase and the percentage of cells with 2 GFP foci (**b**) were scored (n = 200), and distances between the GFP foci (**d**) were measured (n = 100). Error bars indicate standard error (ns, p>0.05, t-test), orange lines indicate mean. Mitotic entry was confirmed by counting the number of SPBs (**c**). **e**, Model for pericentromere expansion in the absence of convergent genes.

In order to investigate how far sister chromatid separation extends upon gene reorientation, strains were created where wild type and reoriented chromosome IV were marked 23 kb away from *CEN4*. This marker was placed downstream of the new cohesin enrichment site that forms upon reorientation (~20 kb away from *CEN4*) and immediately downstream of the next convergent

gene site. The 23 kb marker had similar separation rate (~15%) on both wild type and reoriented chromosomes, indicating that separation does not extend beyond the next convergent gene site (Figure 6.2.3.2).

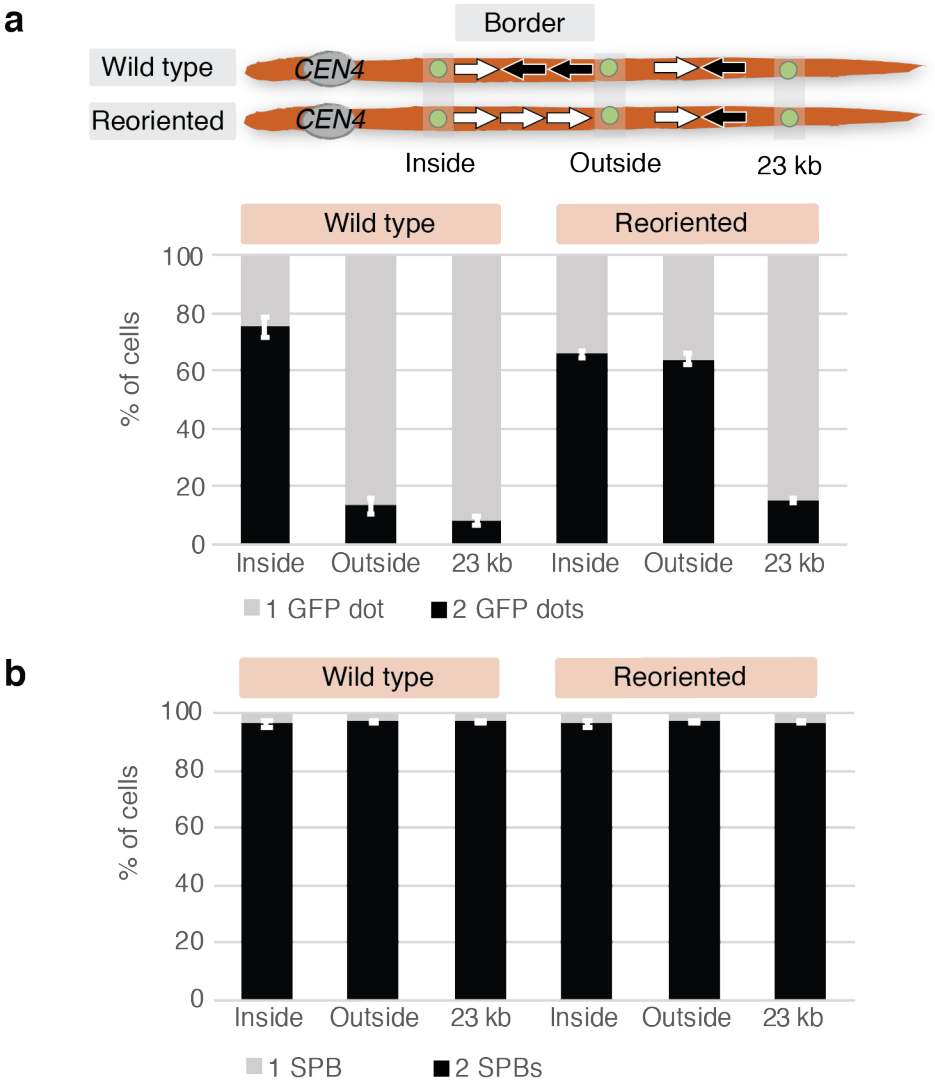

Figure 6.2.3.2. - Increased region of sister chromatid separation does not extend beyong the next convergent gene pair - **a**, Strains with tetO arrays integrated at the indicated positions were arrested in metaphase and the percentage of cells with 2 GFP foci were scored (n = 200). Error bars indicate standard error of three independent repeats. **b**, The number of cells with 2 SPBs were scored to confirm entry to mitosis (n=100).

Taken together, these findings signify that in the absence of convergent genes border regions lose their ability to 1) retain high level of cohesin and 2) resist the pulling forces of microtubules upon biorientation. Consequently, this leads to an increase in pericentromere size.

6.2.4 Re-introduction of convergent gene site partially restores pericentromere size

If increase in pericentromere size is caused by the loss of convergent genes from pericentromere borders, then re-introduction of convergent gene sites should restore pericentromere size. To test this, tandemly arranged *pURA3::AB1x2::TRP1* and *pURA3::PYLx2::HisMX6* model gene constructs, oriented towards the centromere, were integrated downstream of the centromere-proximal border gene, on wild type and reoriented chromosome IV. Following, the separation of *tetO*/TetR-GFP markers centromere-proximal and centromere-distal to border regions were assayed in metaphase (Figure 6.2.4.1). While separation of wild type chromosome IV was unaffected by the insertion of model genes at borders, pericentromere expansion was partially rescued on the reoriented chromosome IV: *tetO*/TetR-GFP markers inside and outside now separated at different frequencies (~60% without and ~40% with the inserted model genes). This result confirms that the presence of convergent genes is necessary and sufficient to restrict pericentromere size.

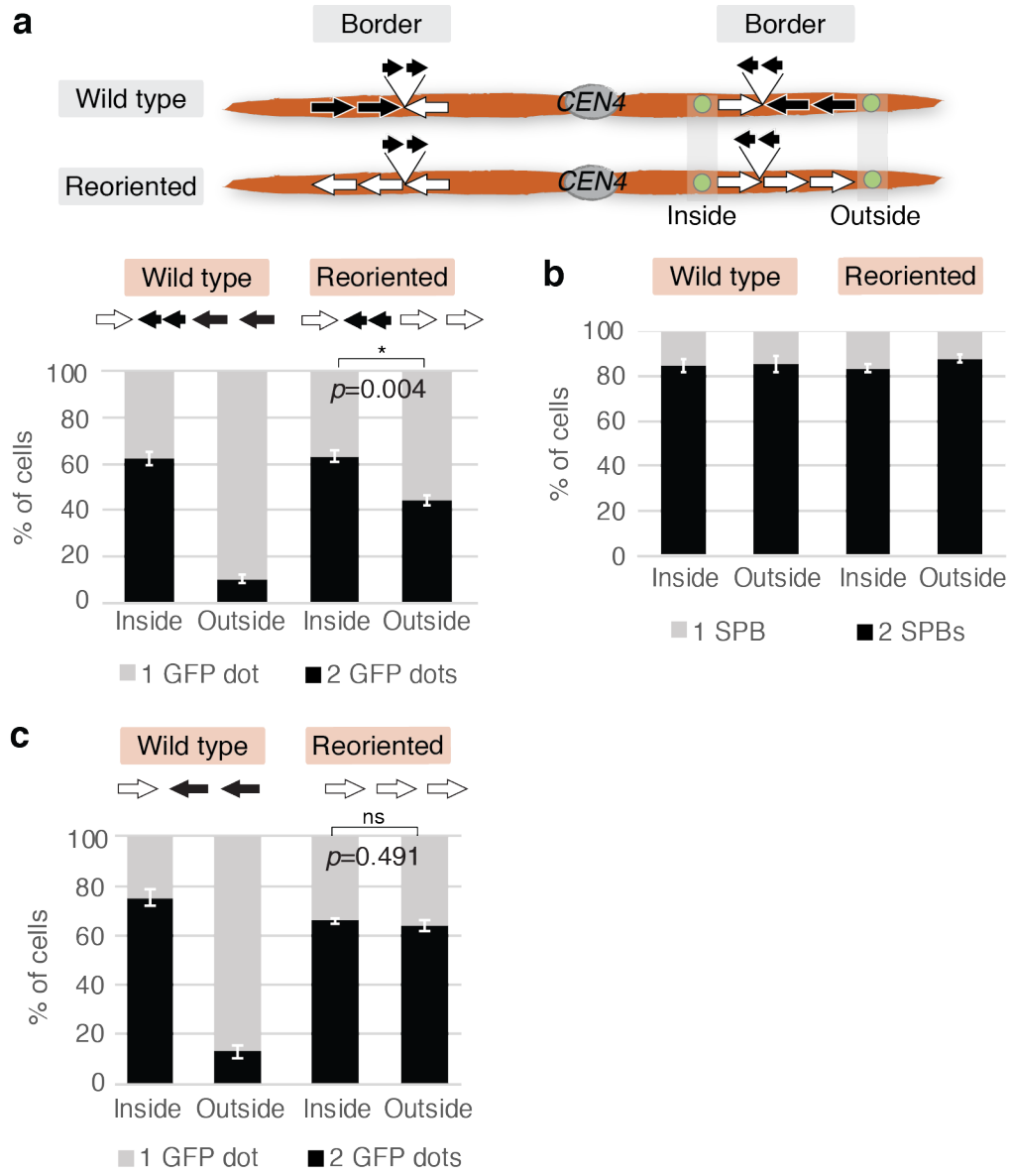

Figure 6.6.1. - Increase in pericentromere size can be partially rescued by the re-introduction of convergent gene sites. a, Construct carrying two short ORFs (ABIx2-TRP1 and PYLx2-HisMX6) were inserted downstream of the first genes (both on the left and right sides) at pericentromere IV in wild type and reoriented strains with *tetO* arrays at the indicated postitions. Cells were arrested in metaphase and the percentage of cells with 2 GFP foci were scored (n = 200). Error bars indicate standard error of three independent repeats (*, p<0.05, two-tailed t-test). **b**, The number of cells with 2 SPBs were scored to confirm entry to mitosis (n=100). **c**, Separation rate of GFP markers on wild type and reoriented chromosome IV from Fig. 6.3.1 is shown for comparison.

6.2.5 Pericentromeric chromosome conformation changes upon gene reorientation

It was found that gene reorientation at borders causes loss of cohesin accumulation at border regions, and this leads to an expansion of the region of transient sister chromatid separation upon biorientation. Next, I wanted to investigate if the third aspect of border function, the establishment of a specialised pericentromere structure was also disrupted in the reoriented strain. Accordingly, Hi-C was performed on the reoriented strain in the presence of spindle tension, and interaction maps around *CEN4* on wild type and reoriented chromosome IV were compared (Figure 6.2.5.1).

Hi-C demonstrated that gene reorientation at borders disrupts pericentromere structure: the insulator function of *CEN4* was lost, the region and frequency of pericentromeric contact increased, and boundaries at original border positions were diminished. Altogether, this suggests that the absence of convergent genes at borders changes pericentromere structure, causing it to adapt a more open and disorganised conformation.

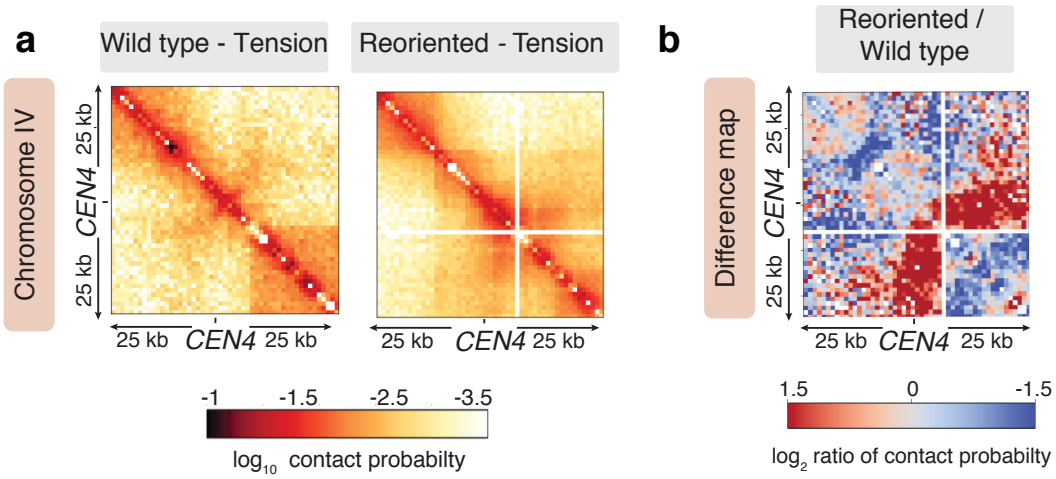

Figure 6.4.1. - Gene reorientation et borders changes chromosome structure. Hi-C contact maps (**a**) and log2 difference maps (**b**) (1kb bin) surrounding the centromere on chromosome IV in wild type and reoriented cells with tension.

6.2.6 Gene reorientation at borders impairs biorientation

Although it was examined in detail how the tandem reorientation of convergent genes at borders changes pericentromere size and structure, the functional importance of pericentromere borders was not studied. As the proposed function of pericentromeres is to facilitate chromosome segregation, the disruption of pericentromere borders should have implications for mitosis.

If pericentromere structure is important for biorientation, then gene reorientation at borders which disrupts pericentromere structure should cause defects in the process. To investigate this possibility, cells carrying *tetO*/TetR-GFP markers inside and outside the pericentromere border, on wild type and reoriented chromosome IV, were arrested in metaphase by Cdc20 depletion in the presence of nocodazole and benomyl. Subsequently, nocodazole was washed out, allowing microtubules to re-form while maintaining metaphase arrest. Starting from the time of nocodazole washout, samples were taken at 20 minute intervals for 2 hours, and at each time-point the proportion of cells with 2 GFP markers was counted. Instead of pericentromere size, here the separation GFP markers was used as a measure for biorientation (Figure 6.2.6.1). Wild type cells showed biorientation rates similar to what was previously observed (Verzijlbergen et al., 2014). Importantly, strains with reoriented chromosome IV, showed a consistent delay in, and reduced frequency of, the separation of *tetO*/TetR-GFP markers. This indicates that in the absence of border convergent genes, the disruption of pericentromere structure impairs biorientation, signifying the role of pericentromere borders for cellular processes.

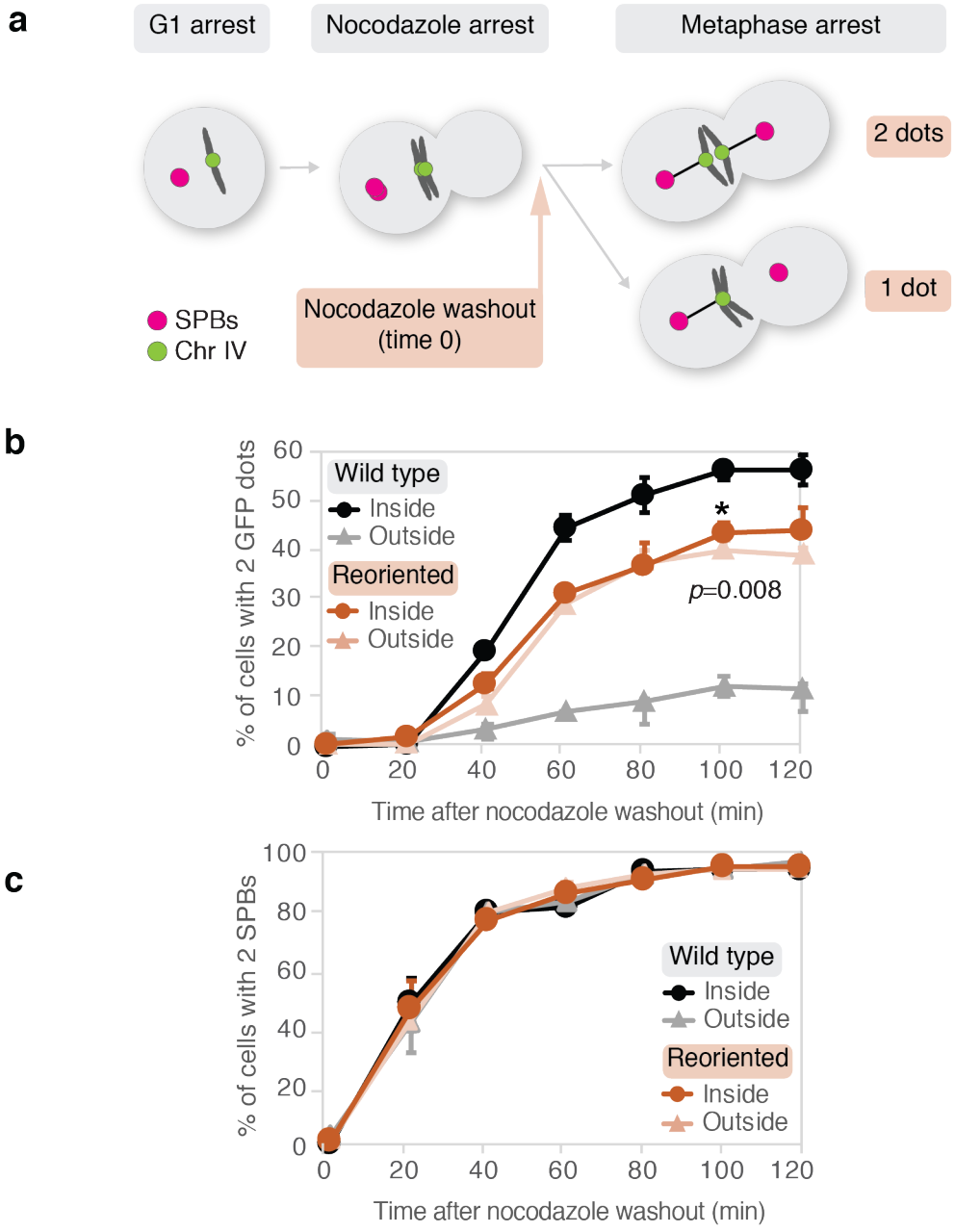

Figure 6.2.6.1 - Gene reorientation et borders impairs biorientation. a, Sister kinetochore biorientation following spindle re-polymerisation. Cells carrying the indicated chromosomal GFP labels, Spc42-tdTomato and *pMET-CDC20* were released from a G1 arrest and arrested in metaphase in the presence of nocodazole by depletion of Cdc20. Nocadazole was washed out while maintaining metaphase arrest by treatment with methionine. **b**, Percentage of cells with separated GFP foci (n=200 at each timepoint), mean of 3 biological replicates ±s.e.m. is shown; unpaired two-tailed t-test, * p<0.05 (p-values refer to wild type inside vs. reoriented inside). **c**, Percentage of cells with 2 SPBs was scored to monitor spindle repolymerisation (n=100), mean of 3 biological replicates ±s.e.m.

Next, a similar biorientation assay was performed on a microfluidics plate where cells were imaged live at 15-minute intervals for 3h. The analysis was extended to a strain where borders on chromosome IV were reoriented, but *tetO*/TetR-GFP markers were inserted adjacent to the centromere on chromosome III. Cells arrested by Cdc20 depletion in nocodazole and benomyl were loaded on microfluidics plates and nocodazole was washed out after images were taken for the first time-point. For each cell, biorientation time was calculated as the time between SPB separation and GFP marker separation (Figure 6.2.6.2). This confirmed results from fixed cells: reoriented chromosome IV showed a delay in biorientation. In addition, it was found that the biorientation delay was specific to reoriented chromosome IV, as chromosome III biorientation in the reoriented strain was similar to that of wild type chromosome IV.

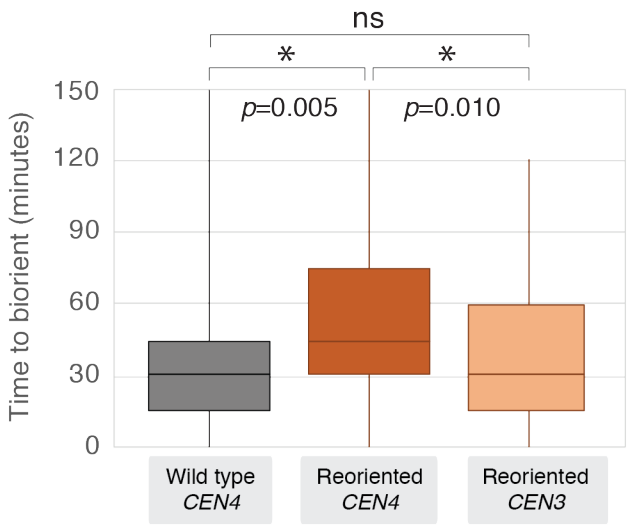

Figure 6.2.6.2 - Gene reorientation on chromosome IV delays biorienation of *CEN4* but not *CEN3*. Live-cell imaging of biorientation of chromosome IV in wild type and reoriented strains, and chromosome III in reoriented strain. Biorientation time was calculated as the time required for GFP dot separation from the separation of spindle pole bodies. Centre line, median; box limits, second and third quartile; whiskers, first and fourth quartiles for 120 cells split equally across two biological replicates; two-sided Mann-Whitney test, *, p<0.05

6.2.7 Cells that lack border convergent genes rely more on the error correction machinery

Cells lacking pericentromeric cohesin are slow to achieve biorientation and show greater reliance on the error correction machinery (Ng et al., 2009). If this is due to altered kinetochore geometry, which results in a decrease in biorientation efficiency, then the same effect might be observed upon gene reorientation. The absence of convergent genes was found to disrupt pericentromere structure and delay biorientation, so cells with the reoriented chromosome might rely more on the error correction machinery to destabilise incorrect microtubule-kinetochore attachments. To investigate this possibility, wild type and reoriented strains were tested for chromosome IV segregation in the temperature sensitive *ipl1-321* background (Biggins et al., 1999).

Cells were released from an alpha factor-induced G1 arrest into media pre-warmed to 32°C leading to partial Ipl1 inactivation in *ipl1-321* but not in *IPL1* cells. After 2 hours, cells were fixed and categorised based on cell morphology and the number of GFP foci. Following correct chromosome IV segregation, G1 cells with a single GFP marker are expected to be seen. However, after a single cell cycle, there was a modest decrease in G1 cells with 1 GFP marker in the reoriented strain. In parallel, an accumulation of metaphase cells (dumbbell-shaped cells with undivided nuclei) was observed in the reoriented strain. Both of these effects were specific to the *ipl1-321* background, suggesting that upon gene reorientation and pericentromere border disruption, cells indeed have a greater need for a functional error correction machinery in order to correctly segregate the reoriented chromosome IV.

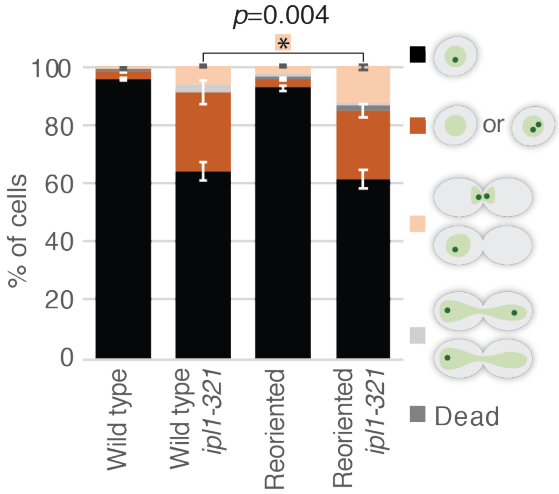

Figure 6.2.7.1. - Gene reorientation upon partial *ipl1-321* inactivation causes models increase in cells blocked in metaphase. Wild type or *ipl1-321* strains carrying wild type or reoriented chromosome IV were released from a G1 arrest into media pre-warmed to 32°C. Cells were fixed 2 hours after release and categorized for cell cycle stage based cell morphology, number of GFP foci and number of spindle pole bodies. Data show mean of 3 biological replicates ±s.e.m.; unpaired two-tailed t-test, *p<0.05.

Finally, to understand the consequences of gene reorientation to cell viability, wild type and reoriented cells (both in *IPL1* and *ipl1-321*) were challenged with nocodazole. Cells from exponentially growing cultures were plated on rich media right before, 2 hours and 4 hours following nocodazole treatment, and cells were grown at the permissive temperature for 2 days. After two days, the number of colonies on each plate were counted. Colony count at 2h and 4h was divided by that of pre-nocodazole (0h), to calculate the decline in cell viability following nocodazole treatment (Figure 6.7.2.2). Strikingly, there was a marked loss of viability, specific to the reoriented strain in the *ipl1-321* background, following nocodazole treatment. This indicates that border convergent genes enable a pericentromere structure that facilitates proper biorientation and error correction, and altogether these processes ensure accurate chromosome segregation required for cell viability.

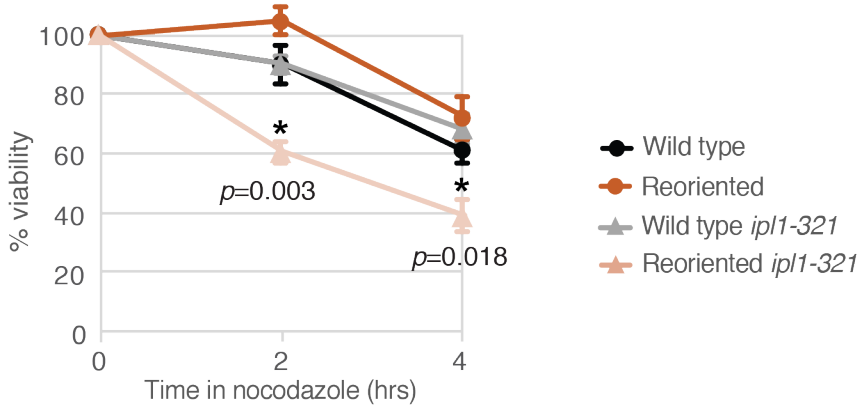

Figure 6.2.7.2. - Gene reorientation in *ipl1-321* background reduces cell vibility following nocodazole treatment. For each condition approximately 1000 cells were plated before (0h), 2 hours and 4 hours of nocodazole treatment and the number of colonies were scores. Viability was calculated as a percentage of colony count at 0h. Data are mean of 3 biological replicates ±s.e.m.; unpaired two-tailed t-test, *, p<0.05 (*p*-values refer to wild type *ipl1-321* vs. reoriented *ipl1-321*).

6.4 Discussion

This chapter explored the function of convergent genes at pericentromere borders. To do this, gene orientation at borders was manipulated: convergent gene sites were eliminated by the rearrangement of genes into tandem, all transcribing away from centromeres.

First, gene reorientation at borders resulted in the loss of cohesin, shugoshin and condensin enrichment from borders. This confirmed that convergent genes are required for cohesin accumulation at borders, and that shugoshin and condensin localisation also depend on the presence of convergent genes. These results were not entirely unexpected, as several studies have shown that there is an intrinsic relationship between transcription and the chromosomal localisation of cohesin (Lengronne et al., 2004; Ocampo-Hafalla et al., 2016), and that shugoshin (and therefore condensin) recruitment to pericentromeres is partially dependent on cohesin. Nevertheless, these results indicate that convergent gene sites are required for the formation of tension-insensitive cohesin peaks that mark pericentromere borders.

Second, the absence of convergent genes resulted in the expansion of the region of pre-anaphase sister chromatid separation. This suggests that upon the loss of cohesin from border regions, pericentromere borders lose the ability to resist sister chromatid separation under tension. Importantly, pericentromere size could be partially restored by the insertion of model genes that created a new convergent gene site at border regions. The effect of the rescue was small, potentially due to the very small size of the inserted model genes compared to endogenous border gene, as well as the expression level of model genes, which was not examined, relative to endogenous border genes.

Third, it was found that gene reorientation changes pericentromere structure under tension: Hi-C indicated that in the absence of convergent genes the pericentromeric V-shape is less defined, and the pericentromeric contact

domain expands. This suggests that convergent genes at borders have an inherent role is establishing orderly pericentromere structure.

Next, I investigated the implications of gene reorientation for chromosome segregation. Importantly, it was found that the reoriented chromosome IV showed a delay in and lower rates of biorientation compared to a chromosome IV where convergent gene sites at borders were intact. Biorientation delay was an effect specific to the reoriented chromosome, as chromosome III exhibited biorientation rates similar to wild type chromosome IV. Altogether, this demonstrates that convergent genes at pericentromere borders make chromosomes competent for biorientation, possibly through the establishment of a structure preferred for capture by spindle microtubules emanating from opposite spindle poles.

Finally, it was found that, similarly to cells lacking pericentromeric cohesin enrichment, disrupted pericentromere structure in addition to leading to reduced biorientation rate, also leads to a greater dependence on the error correction machinery which severs incorrect attachments to the spindle and thus facilitates accurate chromosome segregation. This was shown by looking at the segregation of fluorescent markers on wild type and reoriented strains, in the hypomorphic *ipl1-321* background under semi-permissive conditions. To demonstrate the effect of gene reorientation on cellular fitness, a cell viability assay was performed in the same strains, following nocodazole treatment. This showed a marked loss of viability in the reoriented strain in *ipl1-321* background, even at the permissive temperature. Collectively, this indicates that the disruption of pericentromere structure through the elimination of convergent gene sites from borders leads to a greater reliance on the error correction pathway to promote accurate chromosome segregation and cellular viability.

In summary, work in this chapter demonstrated that if convergent genes sites at pericentromere borders are disrupted through gene reorientation, all three

features of pericentromere border regions are lost: they no longer 1) accumulate high levels of cohesin, 2) resist the separation of sisters under tension, and 3) define orderly pericentromere structure. Moreover, it was found that, likely as a consequence of the disruption of pericentromere structure, cells in the absence of border convergent genes show defects in biorientation and efficient error correction. These observations indicate that pericentromere borders are required for pericentromere structure as well as function which is to facilitate biorientation and accurate chromosome segregation, and that pericentromere border formation requires centromere-flanking convergent gene sites.

Chapter 7 Discussion

The accurate inheritance of the genome during cell division relies on the establishment of proper connections between chromosomes and the microtubules that pull them apart. Much attention has focused on the interaction between kinetochores and microtubules, as well as the pathways that regulate this interaction to mediate accurate chromosome segregation. However, it has been long recognised that there are chromosomal factors important to this process which appear to be governed by high cohesin density in the pericentromere. This study identifies novel factors as key determinants of pericentromere structure and function: centromere-flanking convergent gene pairs that restrict cohesin accumulation to pericentromeres. These chromosomal regions, that we term “pericentromere borders”, were the focus of this study.

7.1 Implications of findings

7.1.1 Differential behaviour of pericentromeres

Pericentromeres, and cohesin that resides there, have been observed to show differential behaviour from chromosome arms, suggestive of specialised functions. Although enriched in cohesin, pericentromeres separate under spindle tension upon sister kinetochore biorientation, prior to anaphase. This is accompanied by a decrease in cohesin signal at the pericentromere, in the absence of any known cohesin removal pathway. Simultaneously, regions on chromosome arms remain tightly linked and cohesin levels remain unchanged. This project shows that the identified pericentromere border regions set the limit to both of these differential behaviours: on the centromere-proximal side of borders sister chromatids separate and cohesin levels are diminished under tension, while on the centromere-distal side of borders neither of these are true. Hence, pericentromere borders, that we define as the most centromere-proximal cohesin peaks that do not decrease under tension, define the region

of tension-sensitive cohesin as well as the region of pre-anaphase sister chromatid separation. Importantly, it was also shown for the first time, that the extent of transient sister chromatid separation under tension does not solely depend on distance from the centromere and varies between chromosomes.

7.1.2 Cohesin accumulation at the pericentromere

Despite its importance, in budding yeast the definition of the pericentromere is vague: centromere-proximal chromosomal regions that accumulate high levels of cohesin. It was not understood however, how pericentromeric cohesin enrichment, that is a result of kinetochore-driven cohesin, is spatially confined to the vicinity of centromeres. We find that this is conferred by convergent genes at pericentromere borders that accumulate high levels of cohesin. Cohesin at pericentromere borders at least partially originates from the centromeric loading site as cohesin association with borders diminishes when kinetochore-driven cohesin loading is compromised. Cohesin sites centromere-distal to borders remain unaffected by the absence of centromeric cohesin loading, indicating that pericentromere border regions restrict cohesin enrichment to pericentromeres. Thus, this study offers new insight into how pericentromeric cohesin domains are defined, as well as how the linear order of genes on chromosomes can be an important determinant of chromosomal domain organisation. Additionally, the precise genome-wide mapping carried out in this study also provides a more precise definition for pericentromeric domains on each budding yeast chromosome.

7.1.3 Structural changes in the pericentromere

The project also uncovered details of the tension-dependent restructuring of pericentromeres that happens when biorientation is achieved, and sister centromeres are moved apart. We find that in the absence of tension the left and right side of pericentromeres fold into separate loops, with the centromere sitting in between them. Some characteristic features of interaction maps suggest that the looping might be mediated by loop extrusion, by a centromere-

anchored loop extruding factor. As looping is diminished in the absence of kinetochore-driven cohesin loading, we speculate that loop extrusion is mediated by cohesin that is loaded at the centromere, and it is halted when convergent genes at pericentromere borders are encountered. This suggests that cohesin loaded at the centromere might not function in holding sister chromatids together, instead – as proposed before – its main function is to structure the pericentromere. It follows that, when sister chromatids come under tension during biorientation, the pericentromeric loops are disrupted and the resulting pulling forces extend chromatin outwards until pericentromere borders are encountered. Thus, pericentromere borders prevent further unzipping of sister chromatids under tension. Importantly, the tension-dependent disruption of pericentromere loops postulates an attractive explanation for the concomitant tension-dependent removal of cohesin from the pericentromere: loop-extruding cohesin can be passively evicted from chromosomes by chromatin stretching under tension.

7.1.4 The role of convergent genes at pericentromere borders

The study showed that the presence of convergent genes was the key property of pericentromere border function. In the absence of convergent gene sites, border regions lost their characteristic features: cohesin no longer accumulated at borders, pre-anaphase sister chromatid separation extended beyond borders and pericentromere structure was compromised. Crucially, I found that the disruption of the pericentromere through the elimination of convergent gene sites lead to impairment in biorientation and error correction. Thus, pericentromere structure defined by pericentromere borders, together with cohesin loaded at the centromere, enable efficient sister kinetochore biorientation and proficient error correction which is critical for cellular fitness. As this depends on the presence of centromere-flanking convergent gene sites, our study provides a conceptual advance, identifying the linear arrangement of transcriptional units as an important parameter governing genome transmission.

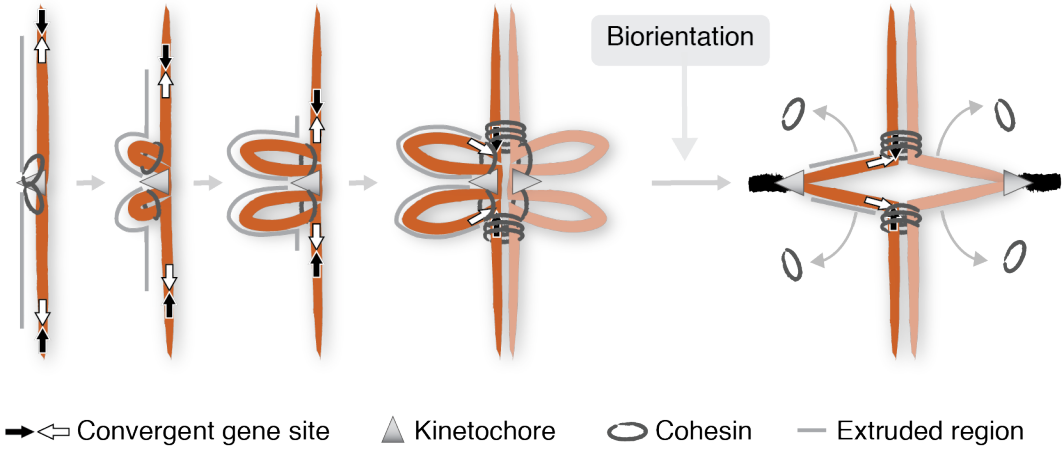

Figure 7.1.3.1 - Model of loop extrusion at pericentromeres - Cohesin rings loaded at kinetochores make extrude a single chromatin loop at either side of the pericentromere until halted by a convergent gene site at pericentromere borders. Intramolecular cohesin at the base of loops is passively removed from chromosomes when biorientation extends pericentromeric chromatin outwards, converting centromere-flanking cis-loops to a V-shaped structure.

7.2 Open questions

7.2.1 How are border convergent genes selected?

First, it is currently unclear exactly how it is specified whether or not a convergent gene site will form a pericentromere border region. Rather than the identity of the convergent genes, their relative position to the centromere appears to be the main determinant of border formation: an ectopic centromere establishes new borders on chromosome arms, with convergent gene pairs flanking the ectopic centromere accumulating increased levels of cohesin (work by Bonnie Alver, available in Paldi et al. (2019)). However, pericentromere borders do not always form at the most centromere-proximal convergent gene site, indicating that other factors might be involved. Such a potential factor is the level of transcription. We briefly investigated this and found that transcriptional activity towards the centromere is higher on average than transcriptional activity away from the centromere in the border convergent gene pairs, the opposite of what is seen at the convergent genes within the pericentromere that do not form borders. Therefore, the level of transcription, particularly towards the centromere, is likely to be important in defining the pericentromere border. However, it would be interesting to see for example if changes in transcriptional states of border convergent genes could lead to changes in the position of pericentromere borders.

Second, it appears that the usage of convergent genes as borders is somewhat stochastic. This is indicated by the intermediate separation rates of chromosomal markers integrated nearby borders, as well as the presence of pericentromere loops that extend beyond borders. This notion is consistent with the idea that while preferred sites exist, pericentromere borders do not provide absolute barriers to loop extrusion and tension-dependent sister chromatid separation, leading to a certain level of cell-to-cell variability.

7.2.2 Does convergent transcription have a conserved role in structuring pericentromeres?

Euchromatic budding yeast pericentromeres are fundamentally different from that of other organisms that harbour large domains of heterochromatin. However, in most organisms pericentromeres are not devoid of transcription as heterochromatin establishment is mediated by long non-coding RNAs, transcribed from pericentromeres often both in sense and antisense directions. As cohesin enrichment is a general feature of all pericentromeres, it is tempting to speculate that transcription-mediated cohesin positioning might structure pericentromeres in organisms other than budding yeast as well. Suggestive of a potential conserved function are the set of inverted repeats surrounding the central domain of fission yeast centromeres. Interestingly, transcription from pericentromeric repeats in fission yeast is upregulated in S-phase (Chen et al., 2008), which is the time when cohesion establishment occurs. Moreover, in *Cryptococcus neoformans* pericentromeric heterochromatin is flanked by convergent genes (Heitman and Yadav, 2019), posing the question if convergent genes could function as boundaries to pericentromeres in this organism. Altogether, these suggest that the role of convergent transcription might have a conserved role in structuring pericentromeres.

7.2.3 How does transcription position cohesin?

Although cohesin localisation on chromosomes and transcription are closely linked, it is not fully understood how transcription alters cohesin distribution. One possibility is that the large size of the transcription machinery simply imposes steric constraints to cohesin translocation on chromosomes. Indeed, in single molecule studies, cohesin diffusion along DNA was halted by transcription (Davidson et al., 2016), indicating that the transcription machinery might be too large to pass inside the cohesin ring. Another possibility is that cohesin localisation on chromosomes is altered by transcription indirectly, through DNA supercoiling. Due to the unwinding of the double helix,

transcription changes the structure of the DNA making it over-twisted (positive supercoil) in front of the polymerase, and under-twisted (negative supercoil) behind it. Consequently, convergent gene sites accumulate high levels of positive supercoils forming secondary structures which could act as a barrier to cohesin sliding and/or loop extrusion (reviewed in Björkegren and Baranello, 2018).

7.2.4 What is the relative orientation of sister chromatids?

Findings in this study provide a novel understanding of pericentromere structure in mitosis. However, how the looped pericentromere structure facilitates the establishment of biorientation cannot be conclusively determined in the absence of information on the relative orientation of sister chromatids. This requires a Hi-C-based technique that allows to distinguish sister chromatids from one another. Due to the semi-conservative nature of DNA replication such a technique is very possible, and although it is not publicly available yet, it is currently being developed (Mitter, 2019). Once feasible, it would be intriguing to complement this study with the conformation of sister chromatids as well as how it changes in the absence of convergent gene sites at pericentromere borders.

Bibliography

Akiyoshi, B., Sarangapani, K.K., Powers, A.F., Nelson, C.R., Reichow, S.L., Arellano-Santoyo, H., Gonen, T., Ranish, J.A., Asbury, C.L. and Biggins, S. 2010. Tension directly stabilizes reconstituted kinetochore-microtubule attachments. *Nature*. **468**(7323), pp.576–579.

Alipour, E. and Marko, J.F. 2012. Self-organization of domain structures by DNA-loop-extruding enzymes. *Nucleic Acids Research*. **40**(22), pp.11202–11212.

Allshire, R.C. and Karpen, G.H. 2008. Epigenetic regulation of centromeric chromatin: Old dogs, new tricks? *Nature Reviews Genetics*. **9**(12), pp.923–937.

Anderson, M., Haase, J., Yeh, E. and Bloom, K. 2009. Function and assembly of DNA looping, clustering, and microtubule attachment complexes within a eukaryotic kinetochore. *Molecular Biology of the Cell*. **20**(19), pp.4131–4139.

De Antoni, A., Pearson, C.G., Cimini, D., Canman, J.C., Sala, V., Nezi, L., Mapelli, M., Sironi, L., Faretta, M., Salmon, E.D. and Musacchio, A. 2005. The Mad1/Mad2 complex as a template for Mad2 activation in the spindle assembly checkpoint. *Current biology : CB*. **15**(3), pp.214–25.

Arumugam, P., Gruber, S., Tanaka, K., Haering, C.H., Mechtler, K. and Nasmyth, K. 2003. ATP Hydrolysis Is Required for Cohesin's Association with Chromosomes. *Current Biology*. **13**(22), pp.1941–1953.

Arumugam, P., Nishino, T., Haering, C.H., Gruber, S. and Nasmyth, K. 2006. Cohesin's ATPase Activity Is Stimulated by the C-Terminal Winged-Helix Domain of Its Kleisin Subunit. *Current Biology*. **16**(20), pp.1998–2008.

Baxter, J., Oliver, A.W. and Schalbetter, S.A. 2019. Are SMC Complexes

Loop Extruding Factors? Linking Theory With Fact. *BioEssays : news and reviews in molecular, cellular and developmental biology*. **41**(1), p.e1800182.

Beckouët, F., Srinivasan, M., Roig, M.B., Chan, K.L., Scheinost, J.C., Batty, P., Hu, B., Petela, N., Gligoris, T., Smith, A.C., Strmecki, L., Rowland, B.D. and Nasmyth, K. 2016. Releasing Activity Disengages Cohesin's Smc3/Scc1 Interface in a Process Blocked by Acetylation. *Molecular Cell*. **61**(4), pp.563–574.

Belton, J.M. and Dekker, J. 2015. Hi-C in budding yeast. *Cold Spring Harbor Protocols*. **2015**(7), pp.649–662.

Ben-Shahar, T.R., Heeger, S., Lehane, C., East, P., Flynn, H., Skehel, M. and Uhlmann, F. 2008. Eco1-dependent cohesin acetylation during establishment of sister chromatid cohesion. *Science*. **321**(5888), pp.563–566.

Bernard, P., Maure, J.F., Partridge, J.F., Genier, S., Javerzat, J.P. and Allshire, R.C. 2001. Requirement of heterochromatin for cohesion at centromeres. *Science*. **294**(5551), pp.2539–2542.

Biggins, S. and Murray, A.W. 2001. The budding yeast protein kinase Ipl1/Aurora allows the absence of tension to activate the spindle checkpoint. *Genes and Development*. **15**(23), pp.3118–3129.

Biggins, S., Severin, F.F., Bhalla, N., Sassoon, I., Hyman, A.A. and Murray, A.W. 1999. The conserved protein kinase Ipl1 regulates microtubule binding to kinetochores in budding yeast. *Genes and Development*. **13**(5), pp.532–544.

Birkenbihl, R.P. and Subramani, S. 1992. Cloning and characterization of *rad21* an essential gene of *Schizosaccharomyces pombe* involved in DNA double-strand-break repair. *Nucleic Acids Research*. **20**(24),

pp.6605–6611.

Björkegren, C. and Baranello, L. 2018. DNA supercoiling, topoisomerases, and cohesin: Partners in regulating chromatin architecture? *International Journal of Molecular Sciences*. **19**(3).

Blat, Y. and Kleckner, N. 1999. Cohesins bind to preferential sites along yeast chromosome III, with differential regulation along arms versus the centric region. *Cell*. **98**(2), pp.249–259.

Bloom, K. and Costanzo, V. 2017. Centromere Structure and Function. *Progress in molecular and subcellular biology*. **56**, pp.515–539.

Bokros, M. and Wang, Y. 2016. Spindle assembly checkpoint silencing and beyond. *Cell Cycle*. **15**(13), pp.1661–1662.

Bresson, S., Tuck, A., Staneva, D. and Tollervey, D. 2017. Nuclear RNA Decay Pathways Aid Rapid Remodeling of Gene Expression in Yeast. *Molecular Cell*. **65**(5), pp.787-800.e5.

Burton, J.L. and Solomon, M.J. 2007. Mad3p, a pseudosubstrate inhibitor of APCCdc20 in the spindle assembly checkpoint. *Genes and Development*. **21**(6), pp.655–667.

Busslinger, G.A., Stocsits, R.R., Van Der Lelij, P., Axelsson, E., Tedeschi, A., Galjart, N. and Peters, J.M. 2017. Cohesin is positioned in mammalian genomes by transcription, CTCF and Wapl. *Nature*. **544**(7651), pp.503–507.

Canudas, S. and Smith, S. 2009. Differential regulation of telomere and centromere cohesion by the Scc3 homologues SA1 and SA2, respectively, in human cells. *Journal of Cell Biology*. **187**(2), pp.165–173.

Carmena, M., Wheelock, M., Funabiki, H. and Earnshaw, W.C. 2012. The

chromosomal passenger complex (CPC): From easy rider to the godfather of mitosis. *Nature Reviews Molecular Cell Biology*. **13**(12), pp.789–803.

Chapard, C., Jones, R., van Oepen, T., Scheinost, J.C. and Nasmyth, K. 2019. Sister DNA Entrapment between Juxtaposed Smc Heads and Kleisin of the Cohesin Complex. *Molecular Cell*. **75**(2), pp.224-237.e5.

Chen, E.S., Zhang, K., Nicolas, E., Cam, H.P., Zofall, M. and Grewal, S.I.S. 2008. Cell cycle control of centromeric repeat transcription and heterochromatin assembly. *Nature*. **451**(7179), pp.734–737.

Ciosk, R., Shirayama, M., Shevchenko, Anna, Tanaka, T., Toth, A., Shevchenko, Andrej and Nasmyth, K. 2000. Cohesin's binding to chromosomes depends on a separate complex consisting of Scc2 and Scc4 proteins. *Molecular Cell*. **5**(2), pp.243–254.

Ciosk, R., Zachariae, W., Michaelis, C., Shevchenko, A., Mann, M. and Nasmyth, K. 1998. An ESP1/PDS1 complex regulates loss of sister chromatid cohesion at the metaphase to anaphase transition in yeast. *Cell*. **93**(6), pp.1067–1076.

Clarke, L. and Carbon, J. 1980. Isolation of a yeast centromere and construction of functional small circular chromosomes. *Nature*. **287**(5782), pp.504–509.

Cohen-Fix, O., Peters, J.M., Kirschner, M.W. and Koshland, D. 1996. Anaphase initiation in *Saccharomyces cerevisiae* is controlled by the APC-dependent degradation of the anaphase inhibitor Pds1p. *Genes & Development*. **10**(24), pp.3081–93.

Cuylen, S., Metz, J. and Haering, C.H. 2011. Condensin structures chromosomal DNA through topological links. *Nature Structural and Molecular Biology*. **18**(8), pp.894–901.

Darwiche, N., Freeman, L.A. and Strunnikov, A. 1999. Characterization of the components of the putative mammalian sister chromatid cohesion complex. *Gene*. **233**(1–2), pp.39–47.

Davidson, I.F., Bauer, B., Goetz, D., Tang, W., Wutz, G. and Peters, J.-M. 2019. DNA loop extrusion by human cohesin. *Science*. **66**(6471), pp.1338-1345.

Davidson, I.F., Goetz, D., Zaczek, M.P., Molodtsov, M.I., Huis in 't Veld, P.J., Weissmann, F., Litos, G., Cisneros, D.A., Ocampo-Hafalla, M., Ladurner, R., Uhlmann, F., Vaziri, A. and Peters, J. 2016. Rapid movement and transcriptional re-localization of human cohesin on DNA. *The EMBO Journal*. **35**(24), pp.2671–2685.

Dedon, P.C., Soults, J.A., David Allis, C. and Gorovsky, M.A. 1991. A simplified formaldehyde fixation and immunoprecipitation technique for studying protein-DNA interactions. *Analytical Biochemistry*. **197**(1), pp.83–90.

Dekker, J., Rippe, K., Dekker, M. and Kleckner, N. 2002. Capturing chromosome conformation. *Science*. **295**(5558), pp.1306–1311.

Dewar, H., Tanaka, K., Nasmyth, K. and Tanaka, T.U. 2004. Tension between two kinetochores suffices for their bi-orientation on the mitotic spindle. *Nature*. **428**(6978), pp.93–97.

Diebold-Durand, M.L., Lee, H., Ruiz Avila, L.B., Noh, H., Shin, H.C., Im, H., Bock, F.P., Bürmann, F., Durand, A., Basfeld, A., Ham, S., Basquin, J., Oh, B.H. and Gruber, S. 2017. Structure of Full-Length SMC and Rearrangements Required for Chromosome Organization. *Molecular Cell*. **67**(2), pp.334-347.e5.

Dixon, J.R., Selvaraj, S., Yue, F., Kim, A., Li, Y., Shen, Y., Hu, M., Liu, J.S. and Ren, B. 2012. Topological domains in mammalian genomes

identified by analysis of chromatin interactions. *Nature*. **485**(7398), pp.376–380.

Dorsett, D. and Merkenschlager, M. 2013. Cohesin at active genes: A unifying theme for cohesin and gene expression from model organisms to humans. *Current Opinion in Cell Biology*. **25**(3), pp.327–333.

Dorsett, D. and Ström, L. 2012. The ancient and evolving roles of cohesin in gene expression and DNA repair. *Current Biology*. **22**(7).

Dostie, J., Richmond, T.A., Arnaout, R.A., Selzer, R.R., Lee, W.L., Honan, T.A., Rubio, E.D., Krumm, A., Lamb, J., Nusbaum, C., Green, R.D. and Dekker, J. 2006. Chromosome Conformation Capture Carbon Copy (5C): A massively parallel solution for mapping interactions between genomic elements. *Genome Research*. **16**(10), pp.1299–1309.

Dunham, M.J., Badrane, H., Ferea, T., Adams, J., Brown, P.O., Rosenzweig, F. and Botstein, D. 2002. Characteristic genome rearrangements in experimental evolution of *Saccharomyces cerevisiae. Proceedings of the National Academy of Sciences of the United States of America*. **99**(25), pp.16144–16149.

Duro, E. and Marston, A.L. 2015. From equator to pole: Splitting chromosomes in mitosis and meiosis. *Genes and Development*. **29**(2), pp.109–122.

Eckert, C.A., Gravdahl, D.J. and Megee, P.C. 2007. The enhancement of pericentromeric cohesin association by conserved kinetochore components promotes high-fidelity chromosome segregation and is sensitive to microtubule-based tension. *Genes and Development*. **21**(3), pp.278–291.

Eshleman, H.D. and Morgan, D.O. 2014. Sgo1 recruits PP2A to chromosomes to ensure sister chromatid bi-orientation during mitosis.

Journal of cell science. **127**(Pt 22), pp.4974–83.

Fernius, J. and Hardwick, K.G. 2007. Bub1 kinase targets Sgo1 to ensure efficient chromosome biorientation in budding yeast mitosis. *PLoS Genetics*. **3**(11), pp.2312–2325.

Fernius, J. and Marston, A.L. 2009. Establishment of cohesion at the pericentromere by the Ctf19 kinetochore subcomplex and the replication fork-associated factor, Csm3. *PLoS Genetics*. **5**(9).

Fernius, J., Nerusheva, O.O., Galander, S., Alves, F.D.L., Rappsilber, J. and Marston, A.L. 2013. Cohesin-dependent association of Scc2/4 with the centromere initiates pericentromeric cohesion establishment. *Current Biology*. **23**(7), pp.599–606.

Filipski, J. and Mucha, M. 2002. Structure, function and DNA composition of *Saccharomyces cerevisiae* chromatin loops *Gene*., pp.63–68.

Freeman, L., Aragon-Alcaide, L. and Strunnikov, A. 2000. The condensin complex governs chromosome condensation and mitotic transmission of rDNA. *The Journal of cell biology*. **149**(4), pp.811–24.

Ganji, M., Shaltiel, I.A., Bisht, S., Kim, E., Kalichava, A., Haering, C.H. and Dekker, C. 2018. Real-time imaging of DNA loop extrusion by condensin. *Science*. **360**(6384), pp.102–105.

Garcia-Luis, J., Lazar-Stefanita, L., Gutierrez-Escribano, P., Thierry, A., Cournac, A., García, A., González, S., Sánchez, M., Jarmuz, A., Montoya, A., Dore, M., Kramer, H., Karimi, M.M., Antequera, F., Koszul, R. and Aragon, L. 2019. FACT mediates cohesin function on chromatin. *Nature Structural & Molecular Biology*. **26**(10), pp.970–979.

Gerlich, D., Hirota, T., Koch, B., Peters, J.M. and Ellenberg, J. 2006. Condensin I stabilizes chromosomes mechanically through a dynamic

interaction in live cells. *Current Biology*. **16**(4), pp.333–344.

Gerlich, D., Koch, B., Dupeux, F., Peters, J.M. and Ellenberg, J. 2006. Live-Cell Imaging Reveals a Stable Cohesin-Chromatin Interaction after but Not before DNA Replication. *Current Biology*. **16**(15), pp.1571–1578.

Gillett, E.S., Espelin, C.W. and Sorger, P.K. 2004. Spindle checkpoint proteins and chromosome-microtubule attachment in budding yeast. *Journal of Cell Biology*. **164**(4), pp.535–546.

Gligoris, T.G., Scheinost, J.C., Bürmann, F., Petela, N., Chan, K.L., Uluocak, P., Beckouët, F., Gruber, S., Nasmyth, K. and Löwe, J. 2014. Closing the cohesin ring: Structure and function of its Smc3-kleisin interface. *Science*. **346**(6212), pp.963–967.

Glynn, E.F., Megee, P.C., Yu, H.G., Mistrot, C., Unal, E., Koshland, D.E., DeRisi, J.L. and Gerton, J.L. 2004. Genome-wide mapping of the cohesin complex in the yeast *Saccharomyces cerevisiae*. *PLoS Biology*. **2**(9).

Goloborodko, A., Marko, J.F. and Mirny, L.A. 2016. Chromosome Compaction by Active Loop Extrusion. *Biophysical Journal*. **110**(10), pp.2162–2168.

Goshima, G. and Yanagida, M. 2000. Establishing biorientation occurs with precocious separation of the sister kinetochores, but not the arms, in the early spindle of budding yeast. *Cell*. **100**(6), pp.619–633.

Gruber, S., Arumugam, P., Katou, Y., Kuglitsch, D., Helmhart, W., Shirahige, K. and Nasmyth, K. 2006. Evidence that Loading of Cohesin Onto Chromosomes Involves Opening of Its SMC Hinge. *Cell*. **127**(3), pp.523–537.

Gruber, S., Haering, C.H. and Nasmyth, K. 2003. Chromosomal cohesin

forms a ring. *Cell*. **112**(6), pp.765–777.

Guacci, V. and Koshland, D. 2012. Cohesin-independent segregation of sister chromatids in budding yeast. *Molecular biology of the cell*. **23**(4), pp.729–39.

Guacci, V., Koshland, D. and Strunnikov, A. 1997. A direct link between sister chromatid cohesion and chromosome condensation revealed through the analysis of MCD1 in *S. cerevisiae*. *Cell*. **91**(1), pp.47–57.

Guacci, V., Stricklin, J., Bloom, M.S., Guō, X., Bhatter, M. and Koshland, D. 2015. A novel mechanism for the establishment of sister chromatid cohesion by the ECO1 acetyltransferase. *Molecular biology of the cell*. **26**(1), pp.117–33.

Gullerova, M. and Proudfoot, N.J. 2008. Cohesin Complex Promotes Transcriptional Termination between Convergent Genes in *S. pombe*. *Cell*. **132**(6), pp.983–995.

Haarhuis, J.H.I., Elbatsh, A.M.O. and Rowland, B.D. 2014. Cohesin and its regulation: On the logic of X-shaped chromosomes. *Developmental Cell*. **31**(1), pp.7–18.

Haering, C.H., Farcas, A.M., Arumugam, P., Metson, J. and Nasmyth, K. 2008. The cohesin ring concatenates sister DNA molecules. *Nature*. **454**(7202), pp.297–301.

Haering, C.H., Löwe, J., Hochwagen, A. and Nasmyth, K. 2002. Molecular architecture of SMC proteins and the yeast cohesin complex. *Molecular Cell*. **9**(4), pp.773–788.

Hardwick, K.G., Johnston, R.C., Smith, D.L. and Murray, A.W. 2000. MAD3 encodes a novel component of the spindle checkpoint which interacts with Bub3p, Cdc20p, and Mad2p. *The Journal of cell biology*. **148**(5),

pp.871–82.

Hartman, T., Stead, K., Koshland, D. and Guacci, V. 2000. Pds5p is an essential chromosomal protein required for both sister chromatid cohesion and condensation in *Saccharomyces cerevisiae*. *Journal of Cell Biology*. **151**(3), pp.613–626.

He, X., Asthana, S. and Sorger, P.K. 2000. Transient Sister Chromatid Separation and Elastic Deformation of Chromosomes during Mitosis in Budding Yeast. *Cell*. **101**(7), pp.763–775.

Hinshaw, S.M., Makrantoni, V., Harrison, S.C. and Marston, A.L. 2017. The Kinetochore Receptor for the Cohesin Loading Complex. *Cell*. **171**(1), pp.72-84.e13.

Hinshaw, S.M., Makrantoni, V., Kerr, A., Marston, A.L. and Harrison, S.C. 2015. Structural evidence for Scc4-dependent localization of cohesin loading. *eLife*. **4**(JUNE), pp.1–15.

Hirano, M. and Hirano, T. 2006. Opening closed arms: Long-distance activation of SMC ATPase by hinge-DNA interactions. *Molecular Cell*. **21**(2), pp.175–186.

Hirano, T. 2016. Condensin-Based Chromosome Organization from Bacteria to Vertebrates. *Cell*. **164**(5), pp.847–857.

Hirano, T. 2012. Condensins: Universal organizers of chromosomes with diverse functions. *Genes and Development*. **26**(15), pp.1659–1678.

Hornung, P., Troc, P., Malvezzi, F., Maier, M., Demianova, Z., Zimniak, T., Litos, G., Lampert, F., Schleiffer, A., Brunner, M., Mechtler, K., Herzog, F., Marlovits, T.C. and Westermann, S. 2014. A cooperative mechanism drives budding yeast kinetochore assembly downstream of CENP-A. *Journal of Cell Biology*. **206**(4), pp.509–524.

Hsieh, T.H.S., Fudenberg, G., Goloborodko, A. and Rando, O.J. 2016. Micro-C XL: Assaying chromosome conformation from the nucleosome to the entire genome. *Nature Methods*. **13**(12), pp.1009–1011.

Hsieh, T.H.S., Weiner, A., Lajoie, B., Dekker, J., Friedman, N. and Rando, O.J. 2015. Mapping Nucleosome Resolution Chromosome Folding in Yeast by Micro-C. *Cell*. **162**(1), pp.108–119.

Hu, B., Itoh, T., Mishra, A., Katoh, Y., Chan, K.-L., Upcher, W., Godlee, C., Roig, M.B., Shirahige, K. and Nasmyth, K. 2011. ATP hydrolysis is required for relocating cohesin from sites occupied by its Scc2/4 loading complex. *Current biology : CB*. **21**(1), pp.12–24.

Hu, B., Petela, N., Kurze, A., Chan, K.L., Chapard, C. and Nasmyth, K. 2015. Biological chromodynamics: A general method for measuring protein occupancy across the genome by calibrating ChIP-seq. *Nucleic Acids Research*. **43**(20).

Indjeian, V.B. and Murray, A.W. 2007. Budding Yeast Mitotic Chromosomes Have an Intrinsic Bias to Biorient on the Spindle. *Current Biology*. **17**(21), pp.1837–1846.

Indjeian, V.B., Stern, B.M. and Murray, A.W. 2005. The centromeric protein Sgo1 is required to sense lack of tension on mitotic chromosomes. *Science*. **307**(5706), pp.130–133.

Irniger, S., Piatti, S., Michaelis, C. and Nasmyth, K. 1995. Genes involved in sister chromatid separation are needed for b-type cyclin proteolysis in budding yeast. *Cell*. **81**(2), pp.269–277.

Ivanov, D. and Nasmyth, K. 2005. A topological interaction between cohesin rings and a circular minichromosome. *Cell*.

Ivanov, D., Schleiffer, A., Eisenhaber, F., Mechtler, K., Haering, C.H. and

Nasmyth, K. 2002. Eco1 is a novel acetyltransferase that can acetylate proteins involved in cohesion. *Current Biology*. **12**(4), pp.323–328.

Iyer, V.R., Horak, C.E., Scafe, C.S., Botstein, D., Snyder, M. and Brown, P.O. 2001. Genomic binding sites of the yeast cell-cycle transcription factors SBF and MBF. *Nature*. **409**(6819), pp.533–538.

Johnson, D.S., Mortazavi, A., Myers, R.M. and Wold, B. 2007. Genome-wide mapping of in vivo protein-DNA interactions. *Science*. **316**(5830), pp.1497–1502.

Kakui, Y., Rabinowitz, A., Barry, D.J. and Uhlmann, F. 2017. Condensin-mediated remodeling of the mitotic chromatin landscape in fission yeast. *Nature Genetics*. **49**(10), pp.1553–1557.

Kawashima, S.A., Yamagishi, Y., Honda, T., Lshiguro, K.I. and Watanabe, Y. 2010. Phosphorylation of H2A by Bub1 prevents chromosomal instability through localizing shugoshin. *Science*. **327**(5962), pp.172–177.

Kerpedjiev, P., Abdennur, N., Lekschas, F., McCallum, C., Dinkla, K., Strobelt, H., Luber, J.M., Ouellette, S.B., Azhir, A., Kumar, N., Hwang, J., Lee, S., Alver, B.H., Pfister, H., Mirny, L.A., Park, P.J. and Gehlenborg, N. 2018. HiGlass: Web-based visual exploration and analysis of genome interaction maps. *Genome Biology*. **19**(1).

Kerrebrock, A.W., Miyazaki, W.Y., Birnby, D. and Orr-Weaver, T.L. 1992. The Drosophila mei-S332 gene promotes sister-chromatid cohesion in meiosis following kinetochore differentiation. *Genetics*. **130**(4), pp.827–41.

Kojic, A., Cuadrado, A., De Koninck, M., Giménez-Llorente, D., Rodríguez-Corsino, M., Gómez-López, G., Le Dily, F., Marti-Renom, M.A. and Losada, A. 2018. Distinct roles of cohesin-SA1 and cohesin-SA2 in 3D chromosome organization. *Nature Structural and Molecular Biology*.

25(6), pp.496–504.

Koshland, D. and Hartwell, L.H. 1987. The structure of sister minichromosome DNA before anaphase in *Saccharomyces cerevisiae*. *Science*. **238**(4834), pp.1713–1716.

Krantz, I.D., McCallum, J., DeScipio, C., Kaur, M., Gillis, L.A., Yaeger, D., Jukofsky, L., Wasserman, N., Bottani, A., Morris, C.A., Nowaczyk, M.J.M., Toriello, H., Bamshad, M.J., Carey, J.C., Rappaport, E., Kawauchi, S., Lander, A.D., Calof, A.L., Li, H.H., Devoto, M. and Jackson, L.G. 2004. Cornelia de Lange syndrome is caused by mutations in NIPBL, the human homolog of *Drosophila melanogaster* Nipped-B. *Nature Genetics*. **36**(6), pp.631–635.

Kueng, S., Hegemann, B., Peters, B.H., Lipp, J.J., Schleiffer, A., Mechtler, K. and Peters, J.M. 2006. Wapl Controls the Dynamic Association of Cohesin with Chromatin. *Cell*. **127**(5), pp.955–967.

Ladurner, R., Kreidl, E., Ivanov, M.P., Ekker, H., Idarraga-Amado, M.H., Busslinger, G.A., Wutz, G., Cisneros, D.A. and Peters, J. 2016. Sororin actively maintains sister chromatid cohesion. *The EMBO Journal*. **35**(6), pp.635–653.

Laloraya, S., Guacci, V. and Koshland, D. 2000. Chromosomal addresses of the cohesin component Mcd1p. *Journal of Cell Biology*. **151**(5), pp.1047–1056.

Lavoie, B.D., Tuffo, K.M., Oh, S., Koshland, D. and Holm, C. 2000. Mitotic chromosome condensation requires Brn1p, the yeast homologue of Barren. *Molecular biology of the cell*. **11**(4), pp.1293–304.

Lazar-Stefanita, L., Scolari, V.F., Mercy, G., Muller, H., Guérin, T.M., Thierry, A., Mozziconacci, J. and Koszul, R. 2017. Cohesins and condensins orchestrate the 4D dynamics of yeast chromosomes during the

cell cycle. *The EMBO Journal*. **36**(18), pp.2684–2697.

Lee, J., Kitajima, T.S., Tanno, Y., Yoshida, K., Morita, T., Miyano, T., Miyake, M. and Watanabe, Y. 2008. Unified mode of centromeric protection by shugoshin in mammalian oocytes and somatic cells. *Nature Cell Biology*. **10**(1), pp.42–52.

Lengronne, A., Katou, Y., Mori, S., Yokabayashi, S., Kelly, G.P., Ito, T., Watanabe, Y., Shirahige, K. and Uhlmann, F. 2004. Cohesin relocation from sites of chromosomal loading to places of convergent transcription. *Nature*. **430**(6999), pp.573–578.

Lengronne, A., McIntyre, J., Katou, Y., Kanoh, Y., Hopfner, K.-P., Shirahige, K. and Uhlmann, F. 2006. Establishment of sister chromatid cohesion at the *S. cerevisiae* replication fork. *Molecular cell*. **23**(6), pp.787–99.

Li, X. and Nicklas, R.B. 1995. Mitotic forces control a cell-cycle checkpoint. *Nature*. **373**(6515), pp.630–2.

Liang, C., Chen, Q., Yi, Q., Zhang, M., Yan, H., Zhang, B., Zhou, L., Zhang, Z., Qi, F., Ye, S. and Wang, F. 2018. A kinase-dependent role for Haspin in antagonizing Wapl and protecting mitotic centromere cohesion. *EMBO reports*. **19**(1), pp.43–56.

Lieberman-Aiden, E., Van Berkum, N.L., Williams, L., Imakaev, M., Ragoczy, T., Telling, A., Amit, I., Lajoie, B.R., Sabo, P.J., Dorschner, M.O., Sandstrom, R., Bernstein, B., Bender, M.A., Groudine, M., Gnirke, A., Stamatoyannopoulos, J., Mirny, L.A., Lander, E.S. and Dekker, J. 2009. Comprehensive mapping of long-range interactions reveals folding principles of the human genome. *Science*. **326**(5950), pp.289–293.

Litwin, I., Pilarczyk, E. and Wysocki, R. 2018. The emerging role of cohesin in the DNA damage response. *Genes*. **9**(12).

Liu, D., Vleugel, M., Backer, C.B., Hori, T., Fukagawa, T., Cheeseman, I.M. and Lampson, M.A. 2010. Regulated targeting of protein phosphatase 1 to the outer kinetochore by KNL1 opposes Aurora B kinase. *The Journal of cell biology*. **188**(6), pp.809–20.

Liu, H., Jia, L. and Yu, H. 2013. Phospho-H2A and cohesin specify distinct tension-regulated sgo1 pools at kinetochores and inner centromeres. *Current Biology*. **23**(19), pp.1927–1933.

Liu, J. and Krantz, I.D. 2008. Cohesin and Human Disease. *Annual Review of Genomics and Human Genetics*. **9**(1), pp.303–320.

London, N. and Biggins, S. 2014. Signalling dynamics in the spindle checkpoint response. *Nature Reviews Molecular Cell Biology*. **15**(11), pp.735–747.

London, N., Ceto, S., Ranish, J.A. and Biggins, S. 2012. Phosphoregulation of Spc105 by Mps1 and PP1 regulates Bub1 localization to kinetochores. *Current Biology*. **22**(10), pp.900–906.

Lopez-Serra, L., Kelly, G., Patel, H., Stewart, A. and Uhlmann, F. 2014. The Scc2-Scc4 complex acts in sister chromatid cohesion and transcriptional regulation by maintaining nucleosome-free regions. *Nature Genetics*. **46**(10), pp.1147–1151.

Lopez-Serra, L., Lengronne, A., Borges, V., Kelly, G. and Uhlmann, F. 2013. Budding yeast Wapl controls sister chromatid cohesion maintenance and chromosome condensation. *Current Biology*. **23**(1), pp.64–69.

Losada, A., Yokochi, T., Kobayashi, R. and Hirano, T. 2000. Identification and characterization of SA/Scc3p subunits in the *Xenopus* and human cohesin complexes. *Journal of Cell Biology*. **150**(3), pp.405–416.

Marcos-Alcalde, Í., Mendieta-Moreno, J.I., Puisac, B., Gil-Rodríguez, M.C.,

Hernández-Marcos, M., Soler-Polo, Di., Ramos, F.J., Ortega, J., Pié, J., Mendieta, J. and Gómez-Puertas, P. 2017. Two-step ATP-driven opening of cohesin head. *Scientific Reports*. **7**(1).

Maresca, T.J. and Salmon, E.D. 2009. Intrakinetochore stretch is associated with changes in kinetochore phosphorylation and spindle assembly checkpoint activity. *Journal of Cell Biology*. **184**(3), pp.373–381.

Marko, J.F. and Siggia, E.D. 1997. Polymer models of meiotic and mitotic chromosomes. *Molecular biology of the cell*. **8**(11), pp.2217–31.

Marston, A.L. 2015. Shugoshins: Tension-Sensitive Pericentromeric Adaptors Safeguarding Chromosome Segregation. *Molecular and Cellular Biology*. **35**(4), pp.634–648.

Megee, P.C., Mistrot, C., Guacci, V. and Koshland, D. 1999. The centromeric sister chromatid cohesion site directs Mcd1p binding to adjacent sequences. *Molecular Cell*. **4**(3), pp.445–450.

Meluh, P.B., Yang, P., Glowczewski, L., Koshland, D. and Smith, M.M. 1998. Cse4p is a component of the core centromere of *Saccharomyces cerevisiae*. *Cell*. **94**(5), pp.607–613.

Merkenschlager, M. and Nora, E.P. 2016. CTCF and Cohesin in Genome Folding and Transcriptional Gene Regulation. *Annual Review of Genomics and Human Genetics*. **17**(1), pp.17–43.

Michaelis, C., Ciosk, R. and Nasmyth, K. 1997. Cohesins: Chromosomal proteins that prevent premature separation of sister chromatids. *Cell*. **91**(1), pp.35–45.

Mizuguchi, T., Fudenberg, G., Mehta, S., Belton, J.M., Taneja, N., Folco, H.D., FitzGerald, P., Dekker, J., Mirny, L., Barrowman, J. and Grewal, S.I.S. 2014. Cohesin-dependent globules and heterochromatin shape 3D

genome architecture in *S. pombe*. *Nature*. **516**(7531), pp.432–435.

Muller, H., Scolari, V.F., Agier, N., Piazza, A., Thierry, A., Mercy, G., Descorps-Declere, S., Lazar-Stefanita, L., Espeli, O., Llorente, B., Fischer, G., Mozziconacci, J. and Koszul, R. 2018. Characterizing meiotic chromosomes' structure and pairing using a designer sequence optimized for Hi-C. *Molecular Systems Biology*. **14**(7).

Muñoz, S., Minamino, M., Casas-Delucchi, C.S., Patel, H. and Uhlmann, F. 2019. A Role for Chromatin Remodeling in Cohesin Loading onto Chromosomes. *Molecular Cell*. **74**(4), pp.664-673.e5.

Murayama, Y. and Uhlmann, F. 2014. Biochemical reconstitution of topological DNA binding by the cohesin ring. *Nature*. **505**(7483), pp.367–371.

Murayama, Y. and Uhlmann, F. 2015. DNA Entry into and Exit out of the Cohesin Ring by an Interlocking Gate Mechanism. *Cell*. **163**(7), pp.1628–1640.

Nasmyth, K. 1996. At the heart of the budding yeast cell cycle. *Trends in Genetics*. **12**(10), pp.405–412.

Nasmyth, K. 2001. Disseminating the genome: joining, resolving, and separating sister chromatids during mitosis and meiosis. *Annual review of genetics*. **35**, pp.673–745.

Natsume, T., Müller, C.A., Katou, Y., Retkute, R., Gierliński, M., Araki, H., Blow, J.J., Shirahige, K., Nieduszynski, C.A. and Tanaka, T.U. 2013. Kinetochores coordinate pericentromeric cohesion and early DNA replication by Cdc7-Dbf4 kinase recruitment. *Molecular Cell*. **50**(5), pp.661–674.

Naumova, N., Imakaev, M., Fudenberg, G., Zhan, Y., Lajoie, B.R., Mirny, L.A.

and Dekker, J. 2013. Organization of the mitotic chromosome. *Science*. **342**(6161), pp.948–953.

Nerusheva, O.O., Galander, S., Fernius, J., Kelly, D. and Marston, A.L. 2014. Tension-dependent removal of pericentromeric shugoshin is an indicator of sister chromosome biorientation. *Genes and Development*. **28**(12), pp.1291–1309.

Ng, T.M., Waples, W.G., Lavoie, B.D. and Biggins, S. 2009. Pericentromeric sister chromatid cohesion promotes kinetochore biorientation. *Molecular Biology of the Cell*. **20**(17), pp.3818–3827.

Nicklas, R.B. and Koch, C.A. 1969. Chromosome micromanipulation. 3. Spindle fiber tension and the reorientation of mal-oriented chromosomes. *The Journal of cell biology*. **43**(1), pp.40–50.

Nishida, H., Suzuki, T., Ookawa, H., Tomaru, Y. and Hayashizaki, Y. 2005. Comparative analysis of expression of histone H2a genes in mouse. *BMC Genomics*. **6**.

Nishiyama, T. 2019. Cohesion and cohesin-dependent chromatin organization. *Current Opinion in Cell Biology*. **58**, pp.8–14.

Nishiyama, T., Ladurner, R., Schmitz, J., Kreidl, E., Schleiffer, A., Bhaskara, V., Bando, M., Shirahige, K., Hyman, A.A., Mechtler, K. and Peters, J.M. 2010. Sororin mediates sister chromatid cohesion by antagonizing Wapl. *Cell*. **143**(5), pp.737–749.

Nonaka, N., Kitajima, T., Yokobayashi, S., Xiao, G., Yamamoto, M., Grewal, S.I.S. and Watanabe, Y. 2002. Recruitment of cohesin to heterochromatic regions by Swi6/HP1 in fission yeast. *Nature Cell Biology*. **4**(1), pp.89–93.

Ocampo-Hafalla, M., Muñoz, S., Samora, C.P. and Uhlmann, F. 2016.

Evidence for cohesin sliding along budding yeast chromosomes. *Open Biology*. **6**(6).

Ocampo-Hafalla, M.T., Katou, Y., Shirahige, K. and Uhlmann, F. 2007. Displacement and re-accumulation of centromeric cohesin during transient pre-anaphase centromere splitting. *Chromosoma*. **116**(6), pp.531–544.

Oliveira, R.A., Coelho, P.A. and Sunkel, C.E. 2005. The condensin I subunit Barren/CAP-H is essential for the structural integrity of centromeric heterochromatin during mitosis. *Molecular and cellular biology*. **25**(20), pp.8971–84.

Onn, I. and Koshland, D. 2011. In vitro assembly of physiological cohesin/DNA complexes. *Proceedings of the National Academy of Sciences of the United States of America*. **108**(30), pp.12198–12205.

Ono, T., Losada, A., Hirano, M., Myers, M.P., Neuwald, A.F. and Hirano, T. 2003. Differential contributions of condensin I and condensin II to mitotic chromosome architecture in vertebrate cells. *Cell*. **115**(1), pp.109–121.

Orlando, V., Strutt, H. and Paro, R. 1997. Analysis of chromatin structure by in vivo formaldehyde cross-linking. *Methods: A Companion to Methods in Enzymology*.

Paldi, F., Alver, B., Robertson, D., Schalbetter, S.A., Kerr, A., Kelly, D.A., Neale, M.J., Baxter, J. and Marston, A.L. 2019. Convergent genes shape budding yeast pericentromeres. *bioRxiv*., p.592782.

Peplowska, K., Wallek, A.U. and Storchova, Z. 2014. Sgo1 Regulates Both Condensin and Ipl1/Aurora B to Promote Chromosome Biorientation. *PLoS Genetics*. **10**(6).

Petela, N.J., Gligoris, T.G., Metson, J., Lee, B.G., Voulgaris, M., Hu, B.,

Kikuchi, S., Chapard, C., Chen, W., Rajendra, E., Srinivisan, M., Yu, H., Löwe, J. and Nasmyth, K.A. 2018. Scc2 Is a Potent Activator of Cohesin's ATPase that Promotes Loading by Binding Scc1 without Pds5. *Molecular Cell*. **70**(6), pp.1134-1148.e7.

Potapova, T. and Gorbsky, G. 2017. The Consequences of Chromosome Segregation Errors in Mitosis and Meiosis. *Biology*. **6**(4), p.12.

Primorac, I. and Musacchio, A. 2013. Panta rhei: the APC/C at steady state. *The Journal of cell biology*. **201**(2), pp.177–89.

Rankin, S., Ayad, N.G. and Kirschner, M.W. 2005. Sororin, a substrate of the anaphase- promoting complex, is required for sister chromatid cohesion in vertebrates. *Molecular Cell*. **18**(2), pp.185–200.

Rao, S.S.P., Huntley, M.H., Durand, N.C., Stamenova, E.K., Bochkov, I.D., Robinson, J.T., Sanborn, A.L., Machol, I., Omer, A.D., Lander, E.S. and Aiden, E.L. 2014. A 3D map of the human genome at kilobase resolution reveals principles of chromatin looping. *Cell*. **159**(7), pp.1665–1680.

Ren, B., Robert, F., Wyrick, J.J., Aparicio, O., Jennings, E.G., Simon, I., Zeitlinger, J., Schreiber, J., Hannett, N., Kanin, E., Volkert, T.L., Wilson, C.J., Bell, S.P. and Young, R.A. 2000. Genome-wide location and function of DNA binding proteins. *Science*. **290**(5500), pp.2306–2309.

Ribeiro, S.A., Gatlin, J.C., Dong, Y., Joglekar, A., Cameron, L., Hudson, D.F., Farr, C.F., McEwen, B.F., Salmon, E.D., Earnshaw, W.C. and Vagnarelli, P. 2009. Condensin regulates the stiffness of vertebrate centromeres. *Molecular Biology of the Cell*. **20**(9), pp.2371–2380.

Ricke, R.M. and Van Deursen, J.M. 2013. Aneuploidy in health, disease, and aging. *Journal of Cell Biology*. **201**(1), pp.11–21.

Rieder, C.L., Cole, R.W., Khodjakov, A. and Sluder, G. 1995. The checkpoint

delaying anaphase in response to chromosome monoorientation is mediated by an inhibitory signal produced by unattached kinetochores. *Journal of Cell Biology*. **130**(4), pp.941–948.

Robertson, G., Hirst, M., Bainbridge, M., Bilenky, M., Zhao, Y., Zeng, T., Euskirchen, G., Bernier, B., Varhol, R., Delaney, A., Thiessen, N., Griffith, O.L., He, A., Marra, M., Snyder, M. and Jones, S. 2007. Genome-wide profiles of STAT1 DNA association using chromatin immunoprecipitation and massively parallel sequencing. *Nature Methods*. **4**(8), pp.651–657.

Rowland, B.D., Roig, M.B., Nishino, T., Kurze, A., Uluocak, P., Mishra, A., Beckouët, F., Underwood, P., Metson, J., Imre, R., Mechtler, K., Katis, V.L. and Nasmyth, K. 2009. Building Sister Chromatid Cohesion: Smc3 Acetylation Counteracts an Antiestablishment Activity. *Molecular Cell*. **33**(6), pp.763–774.

van Ruiten, M.S. and Rowland, B.D. 2018. SMC Complexes: Universal DNA Looping Machines with Distinct Regulators. *Trends in Genetics*. **34**(6), pp.477–487.

Sakuno, T., Tada, K. and Watanabe, Y. 2009. Kinetochore geometry defined by cohesion within the centromere. *Nature*. **458**(7240), pp.852–858.

Sanborn, A.L., Rao, S.S.P., Huang, S.-C., Durand, N.C., Huntley, M.H., Jewett, A.I., Bochkov, I.D., Chinnappan, D., Cutkosky, A., Li, J., Geeting, K.P., Gnirke, A., Melnikov, A., McKenna, D., Stamenova, E.K., Lander, E.S. and Aiden, E.L. 2015. Chromatin extrusion explains key features of loop and domain formation in wild-type and engineered genomes. *Proceedings of the National Academy of Sciences of the United States of America*. **112**(47), pp.E6456-65.

Schalbetter, S.A., Fudenberg, G., Baxter, J., Pollard, K.S. and Neale, M.J. 2019. Principles of meiotic chromosome assembly revealed in *S.*

cerevisiae. Nature Communications. **10**(1).

Schalbetter, S.A., Goloborodko, A., Fudenberg, G., Belton, J.M., Miles, C., Yu, M., Dekker, J., Mirny, L. and Baxter, J. 2017. SMC complexes differentially compact mitotic chromosomes according to genomic context. *Nature Cell Biology*. **19**(9), pp.1071–1080.

Sedeño Cacciatore, Á. and Rowland, B.D. 2019. Loop formation by SMC complexes: turning heads, bending elbows, and fixed anchors. *Current Opinion in Genetics and Development*. **55**, pp.11–18.

Servant, N., Varoquaux, N., Lajoie, B.R., Viara, E., Chen, C.J., Vert, J.P., Heard, E., Dekker, J. and Barillot, E. 2015. HiC-Pro: An optimized and flexible pipeline for Hi-C data processing. *Genome Biology*. **16**(1).

Sheu, Y.J. and Stillman, B. 2010. The Dbf4-Cdc7 kinase promotes S phase by alleviating an inhibitory activity in Mcm4. *Nature*. **463**(7277), pp.113–117.

Shukla, M., Tong, P., White, S.A., Singh, P.P., Reid, A.M., Catania, S., Pidoux, A.L. and Allshire, R.C. 2018. Centromere DNA Destabilizes H3 Nucleosomes to Promote CENP-A Deposition during the Cell Cycle. *Current Biology*. **28**(24), pp.3924-3936.e4.

Simonis, M., Klous, P., Splinter, E., Moshkin, Y., Willemsen, R., De Wit, E., Van Steensel, B. and De Laat, W. 2006. Nuclear organization of active and inactive chromatin domains uncovered by chromosome conformation capture-on-chip (4C). *Nature Genetics*. **38**(11), pp.1348–1354.

Sjögren, C. and Nasmyth, K. 2001. Sister chromatid cohesion is required for postreplicative double-strand break repair in *Saccharomyces cerevisiae. Current Biology*. **11**(12), pp.991–995.

Skibbens, R. V, Corson, L.B., Koshland, D. and Hieter, P. 1999. Ctf7p is essential for sister chromatid cohesion and links mitotic chromosome structure to the DNA replication machinery. *Genes & development*. **13**(3), pp.307–19.

Smurova, K. and De Wulf, P. 2018. Centromere and Pericentromere Transcription: Roles and Regulation in Sickness and in Health. *Frontiers in Genetics*. **9**.

Solomon, M.J., Larsen, P.L. and Varshavsky, A. 1988. Mapping proteinDNA interactions in vivo with formaldehyde: Evidence that histone H4 is retained on a highly transcribed gene. *Cell*. **53**(6), pp.937–947.

Sonoda, E., Matsusaka, T., Morrison, C., Vagnarelli, P., Hoshi, O., Ushiki, T., Nojima, K., Fukagawa, T., Waizenegger, I.C., Peters, J.M., Earnshaw, W.C. and Takeda, S. 2001. Scc1/Rad21/Mcd1 Is Required for Sister Chromatid Cohesion and Kinetochore Function in Vertebrate Cells. *Developmental Cell*. **1**(6), pp.759–770.

Spellman, P.T., Sherlock, G., Zhang, M.Q., Iyer, V.R., Anders, K., Eisen, M.B., Brown, P.O., Botstein, D. and Futcher, B. 1998. Comprehensive identification of cell cycle-regulated genes of the yeast *Saccharomyces cerevisiae* by microarray hybridization. *Molecular Biology of the Cell*. **9**(12), pp.3273–3297.

Srinivasan, M., Scheinost, J.C., Petela, N.J., Gligoris, T.G., Wissler, M., Ogushi, S., Collier, J.E., Voulgaris, M., Kurze, A., Chan, K.L., Hu, B., Costanzo, V. and Nasmyth, K.A. 2018. The Cohesin Ring Uses Its Hinge to Organize DNA Using Non-topological as well as Topological Mechanisms. *Cell*. **173**(6), pp.1508-1519.e18.

Stempor, P. and Ahringer, J. 2016. SeqPlots - Interactive software for exploratory data analyses, pattern discovery and visualization in genomics. *Wellcome Open Research*. **1**, p.14.

Stephens, A.D., Haase, J., Vicci, L., Taylor, R.M. and Bloom, K. 2011. Cohesin, condensin, and the intramolecular centromere loop together generate the mitotic chromatin spring. *Journal of Cell Biology*. **193**(7), pp.1167–1180.

Stoler, S., Keith, K.C., Curnick, K.E. and Fitzgerald-Hayes, M. 1995. A mutation in CSE4, an essential gene encoding a novel chromatin-associated protein in yeast, causes chromosome nondisjunction and cell cycle arrest at mitosis. *Genes and Development*. **9**(5), pp.573–586.

Straight, A.F., Belmont, A.S., Robinett, C.C. and Murray, A.W. 1996. GFP tagging of budding yeast chromosomes reveals that protein-protein interactions can mediate sister chromatid cohesion. *Current Biology*. **6**(12), pp.1599–1608.

Strick, T.R., Kawaguchi, T. and Hirano, T. 2004. Real-time detection of single-molecule DNA compaction by condensin I. *Current biology : CB*. **14**(10), pp.874–80.

Ström, L., Lindroos, H.B., Shirahige, K. and Sjögren, C. 2004. Postreplicative recruitment of cohesin to double-strand breaks is required for DNA repair. *Molecular Cell*. **16**(6), pp.1003–1015.

Strunnikov, A. V, Hogan, E. and Koshland, D. 1995. SMC2, a *Saccharomyces cerevisiae* gene essential for chromosome segregation and condensation, defines a subgroup within the SMC family. *Genes & development*. **9**(5), pp.587–99.

Sudakin, V., Chan, G.K.T. and Yen, T.J. 2001. Checkpoint inhibition of the APC / C in HeLa cells. *Cell*. **154**(5), pp.925–936.

Sumara, I., Vorlaufer, E., Gieffers, C., Peters, B.H. and Peters, J.M. 2000. Characterization of vertebrate cohesin complexes and their regulation in prophase. *Journal of Cell Biology*. **151**(4), pp.749–761.

Sutani, T., Kawaguchi, T., Kanno, R., Itoh, T. and Shirahige, K. 2009. Budding Yeast Wpl1(Rad61)-Pds5 Complex Counteracts Sister Chromatid Cohesion-Establishing Reaction. *Current Biology*. **19**(6), pp.492–497.

Sutani, T., Yuasa, T., Tomonaga, T., Dohmae, N., Takio, K. and Yanagida, M. 1999. Fission yeast condensin complex: Essential roles of non-SMC subunits for condensation and Cdc2 phosphorylation of Cut3/SMC4. *Genes and Development*. **13**(17), pp.2271–2283.

Szabo, Q., Bantignies, F. and Cavalli, G. 2019. Principles of genome folding into topologically associating domains. *Science Advances*. **5**(4).

Tanaka, T., Cosma, M.P., Wirth, K. and Nasmyth, K. 1999. Identification of cohesin association sites at centromeres and along chromosome arms. *Cell*. **98**(6), pp.847–858.

Tanaka, T., Fuchs, J., Loidl, J. and Nasmyth, K. 2000. Cohesin ensures bipolar attachment of microtubules to sister centromeres and resists their precocious separation. *Nature Cell Biology*. **2**(8), pp.492–499.

Tanaka, T.U. 2010. EMBO Member's Review Kinetochore-microtubule interactions: steps towards bi-orientation. *The EMBO Journal*. **29**, pp.4070–4082.

Tanaka, T.U., Rachidi, N., Janke, C., Pereira, G., Galova, M., Schiebel, E., Stark, M.J.R. and Nasmyth, K. 2002. Evidence that the Ipl1-Sli15 (Aurora Kinase-INCENP) complex promotes chromosome bi-orientation by altering kinetochore-spindle pole connections. *Cell*. **108**(3), pp.317–329.

Tomonaga, T., Nagao, K., Kawasaki, Y., Furuya, K., Murakaini, A., Morishita, J., Yuasa, T., Sutani, T., Kearsey, S.E., Uhlmann, F., Nasmyth, K. and Yanagida, M. 2000. Characterization of fission yeast cohesin: Essential

anaphase proteolysis of Rad21 phosphorylated in the S phase. *Genes and Development*. **14**(21), pp.2757–2770.

Tonkin, E.T., Wang, T.J., Lisgo, S., Bamshad, M.J. and Strachan, T. 2004. NIPBL, encoding a homolog of fungal Scc2-type sister chromatid cohesion proteins and fly Nipped-B, is mutated in Cornelia de Lange syndrome. *Nature Genetics*. **36**(6), pp.636–641.

Tóth, A., Ciosk, R., Uhlmann, F., Galova, M., Schleiffer, A. and Nasmyth, K. 1999. Yeast cohesin complex requires a conserved protein, Eco1p(Ctf7), to establish cohesion between sister chromatids during DNA replication. *Genes and Development*. **13**(3), pp.320–333.

Uchida, K.S.K., Takagaki, K., Kumada, K., Hirayama, Y., Noda, T. and Hirota, T. 2009. Kinetochore stretching inactivates the spindle assembly checkpoint. *Journal of Cell Biology*. **184**(3), pp.383–390.

Uhlmann, F. 2016. SMC complexes: From DNA to chromosomes. *Nature Reviews Molecular Cell Biology*. **17**(7), pp.399–412.

Uhlmann, F., Lottspeich, F. and Nasmyth, K. 1999. Sister-chromatid separation at anaphase onset is promoted by cleavage of the cohesin subunit Scc1. *Nature*. **400**(6739), pp.37–42.

Uhlmann, F. and Nasmyth, K. 1998. Cohesion between sister chromatids must be established during DNA replication. *Current Biology*. **8**(20), pp.1095–1102.

Uhlmann, F., Wernic, D., Poupart, M.A., Koonin, E. V. and Nasmyth, K. 2000. Cleavage of cohesin by the CD clan protease separin triggers anaphase in yeast. *Cell*. **103**(3), pp.375–386.

Unal, E., Heidinger-Pauli, J.M., Kim, W., Guacci, V., Onn, I., Gygi, S.P. and Koshland, D.E. 2008. A molecular determinant for the establishment of

sister chromatid cohesion. *Science (New York, N.Y.)*. **321**(5888), pp.566–9.

Verzijlbergen, K.F., Nerusheva, O.O., Kelly, D., Kerr, A., Clift, D., Alves, F. de L., Rappsilber, J. and Marston, A.L. 2014. Shugoshin biases chromosomes for biorientation through condensin recruitment to the pericentromere. *eLife*. **2014**(3).

Voordeckers, K., Kominek, J., Das, A., Espinosa-Cantú, A., De Maeyer, D., Arslan, A., Van Pee, M., van der Zande, E., Meert, W., Yang, Y., Zhu, B., Marchal, K., DeLuna, A., Van Noort, V., Jelier, R. and Verstrepen, K.J. 2015. Adaptation to High Ethanol Reveals Complex Evolutionary Pathways. *PLoS Genetics*. **11**(11).

Wang, X., Brandão, H.B., Le, T.B.K., Laub, M.T. and Rudner, D.Z. 2017. *Bacillus subtilis* SMC complexes juxtapose chromosome arms as they travel from origin to terminus. *Science*. **355**(6324), pp.524–527.

Warren, W.D., Steffensen, S., Lin, E., Coelho, P., Loupart, M.L., Cobbe, N., Lee, J.Y., McKay, M.J., Orr-Weaver, T., Heck, M.M.S. and Sunkel, C.E. 2000. The *Drosophila* RAD21 cohesin persists at the centromere region in mitosis. *Current Biology*. **10**(22), pp.1463–1466.

Weber, S.A., Gerton, J.L., Polancic, J.E., DeRisi, J.L., Koshland, D. and Megee, P.C. 2004. The kinetochore is an enhancer of pericentric cohesin binding. *PLoS Biology*. **2**(9).

Welburn, J.P.I., Vleugel, M., Liu, D., Yates, J.R., Lampson, M.A., Fukagawa, T. and Cheeseman, I.M. 2010. Aurora B Phosphorylates Spatially Distinct Targets to Differentially Regulate the Kinetochore-Microtubule Interface. *Molecular Cell*. **38**(3), pp.383–392.

Wendt, K.S., Yoshida, K., Itoh, T., Bando, M., Koch, B., Schirghuber, E., Tsutsumi, S., Nagae, G., Ishihara, K., Mishiro, T., Yahata, K., Imamoto,

F., Aburatani, H., Nakao, M., Imamoto, N., Maeshima, K., Shirahige, K. and Peters, J.M. 2008. Cohesin mediates transcriptional insulation by CCCTC-binding factor. *Nature*. **451**(7180), pp.796–801.

Winey, M., Mamay, C.L., O'Toole, E.T., Mastronarde, D.N., Giddings, T.H., McDonald, K.L. and McIntosh, J.R. 1995. Three-dimensional ultrastructural analysis of the *Saccharomyces cerevisiae* mitotic spindle. *Journal of Cell Biology*. **129**(6), pp.1601–1615.

Xu, Z., Cetin, B., Anger, M., Cho, U.S., Helmhart, W., Nasmyth, K. and Xu, W. 2009. Structure and Function of the PP2A-Shugoshin Interaction. *Molecular Cell*. **35**(4), pp.426–441.

Yeh, E., Haase, J., Paliulis, L. V., Joglekar, A., Bond, L., Bouck, D., Salmon, E.D. and Bloom, K.S. 2008. Pericentric Chromatin Is Organized into an Intramolecular Loop in Mitosis. *Current Biology*. **18**(2), pp.81–90.

Yi, Q., Chen, Q., Liang, C., Yan, H., Zhang, Z., Xiang, X., Zhang, M., Qi, F., Zhou, L. and Wang, F. 2018. HP 1 links centromeric heterochromatin to centromere cohesion in mammals. *EMBO reports*. **19**(4).

Zheng, H. and Xie, W. 2019. The role of 3D genome organization in development and cell differentiation. *Nature Reviews Molecular Cell Biology*. **20**(9), pp.535–550.

Appendix I – Plasmids used in this study

Plasmid	Characteristics
AMp326	*pURA3::TETR-GFP::LEU2*
AMp327	*pRS306(tetOx224)*
AMp884	*pFA6a-FRB-HISMX6*
AMp887	*pFA6a-2xFKBP12-TRP1*
AMp1298	*pMAF1-MAF2 LoxP-KanMX6-LoxP*
AMp1302	*pPTC1-PTC1 LoxP-KanMX6-LoxP*
AMp1332	*pRPT2-RPT2 LoxP-KanMX6-LoxP*
AMp1360	*pSOK1-SOK1 LoxP-kanMX6-LoxP*
AMp1411	*pRS306(tetOx224) + 502bp genomic sequence (2901bp right of centromere 3) to integrate tetOs ~3kb to right of CEN3*
AMp1412	*pRS306(tetOx224) + 635bp genomic sequence (6453bp right of centromere 3) to integrate tetOs ~7kb to right of CEN3*
AMp1413	*pRS306(tetOx224) + 514bp genomic sequence (17546bp right of centromere 3) to integrate tetOs ~18kb to right of CEN3*
AMp1433	*pRS306(tetOx224) + 676bp genomic sequence (674bp right of centromere 1) to integrate tetOs ~1kb to right of CEN1*

Plasmid	Characteristics
AMp1436	*pRS306(tetOx224) + 443bp genomic sequence (7123bp right of centromere 1) to integrate tetOs ~7kb to right of CEN1*
AMp1437	*pRS306(tetOx224) + 377bp genomic sequence (3456bp right of centromere 1) to integrate tetOs ~3kb to right of CEN1*
AMp1460	*ABI1-V5-HIS*
AMp1461	*PYL-FLAG*
AMp1538	*pRS306(tetOx224) + 442bp genomic sequence (8105bp right of centromere 1) to integrate tetOs ~8kb to right of CEN1*
AMp1539	*pRS306(tetOx224) + 632bp genomic sequence (23137bp right of centromere 3) to integrate tetOs ~18kb to right of CEN3*
AMp1562	*pRS306(tetOx224) + 611bp genomic sequence (20810bp right of centromere 3) to integrate tetOs ~21kb to right of CEN3*
AMp1669	*pRS306(tetOx224) + 505bp genomic sequence (12611bp right of centromere 1) to integrate tetOs ~12kb to right of CEN1*
AMp1670	*pRS306(tetOx224) + 375bp genomic sequence (11156bp right of centromere 3) to integrate tetOs ~12kb to right of CEN3*
AMp1676	*pRS306(tetOx224) + 535bp genomic sequence (3765bp right of centromere 4) to integrate tetOs ~4kb to right of CEN4*

Plasmid	Characteristics
AMp1677	*pRS306(tetOx224) + 594bp genomic sequence (11426bp right of centromere 4) to integrate tetOs ~11kb to right of CEN4*
AMp1678	*pRS306(tetOx224) + 560bp genomic sequence (13745bp right of centromere 4) to integrate tetOs ~14kb to right of CEN4 in MAF1-SOK1 reversed orientation strain*
AMp1776	*pRS306(tetOx224) + 505bp genomic sequence (20660bp right of centromere 4) to integrate tetOs ~21kb to right of CEN4*
AMp1781	*pURA3::ABIx2-V5::TRP1*
AMp1792	*pRS306(tetOx224) + 585bp genomic sequence (576bp right of centromere 3) to integrate tetOs ~0,5kb to right of CEN3*
AMp1796	*pURA3::PYLx2-FLAG::HISMX6*

All plasmids except AMp326, AMp884, AMp887, AMp327, AMp1298, AMp1302, Amp1332, AMp1360, AMp1460 and AMp1461 were generated in this study.

Appendix II – Budding yeast strains used in this study

Strain	Relevant genotype
AMy1105	*MATa cdc20::URA3::pMET-CDC20 SCC1-6HA*
AMy1145	*MATa SCC1-6HA*
AMy2508	*MATa, cdc20::URA3::pMET-CDC20*
AMy3950	*MATa cdc20::URA3::pMET-CDC20 SCC1-6HA chl4Δ::KanMX6*
AMy6389	*MATa cdc20::URA3::pMET-CDC20 SGO1-6HA::TRP1*
AMy6471	*MATa, cdc20::URA3::pMET-CDC20 Spc42-tdTomato::NAT his3::PURA3::tetR-GFP::HIS3 ~1kbR_CEN3::tetOx224::URA3*
AMy6884	*MATa cdc20::URA3::pMET-CDC20 SCC1-6HA sgo1(Y47A;Q50A;S52A)::hphMX4*
AMy7217	*MATa cdc20::URA3::pMET-CDC20 SCC1-6HA sgo1Δ::KanMX6*
AMy8955	*MATa cdc20::URA3::pMET-CDC20 BRN1-6HA::TRP1*
AMy22078	*MATa cdc20::URA3::pMET-CDC20 SCC1-6HA pMAF1-MAF1::loxp (reversed orientation) pPTC1-PTC1::loxp (reversed orientation) pRPT2-RPT2::loxp (reversed orientation) pSOK1-SOK1-loxp-KANMX-loxp (reversed orientation)*

Strain	Relevant genotype
AMy22900	*MATa, cdc20::URA3::pMET-CDC20 Spc42-tdTomato::NAT leu2::tetR-GFP::LEU2 ~7kbR_CEN3::tetOx224::URA3*
AMy22936	*MATa cdc20::URA3::pMET-CDC20 Spc42-tdTomato::NAT leu2::tetR-GFP::LEU2 ~3kbR_CEN3::tetOx224::URA3*
AMy23081	*MATa, cdc20::URA3::pMET-CDC20 Spc42-tdTomato::NAT leu2::tetR-GFP::LEU2 ~3kbR_CEN1::tetOx224::URA3*
AMy23082	*MATa, cdc20::URA3::pMET-CDC20 Spc42-tdTomato::NAT leu2::tetR-GFP::LEU2 ~1kbR_CEN1::tetOx224::URA3*
AMy23125	*MATa, cdc20::URA3::pMET-CDC20 Spc42-tdTomato::NAT leu2::tetR-GFP::LEU2~7kbR_CEN1::tetOx224::URA3*
AMy23185	*MATa, cdc20::URA3::pMET-CDC20 Spc42-tdTomato::NAT leu2::tetR-GFP::LEU2 ~18kbR_CEN3::tetOx224::URA3*
AMy25236	*MATa, cdc20::URA3::pMET-CDC20 Spc42-tdTomato::NAT leu2::tetR-GFP::LEU2 ~23kbR_CEN3::tetOx224::URA3*
AMy25297	*MATa, cdc20::URA3::pMET-CDC20 Spc42-tdTomato::NAT leu2::tetR-GFP::LEU2 ~8kbR_CEN1::tetOx224::URA3*
AMy25298	*MATa cdc20::URA3::pMET-CDC20 SCC1-6HA pMAF1-MAF1::loxp (reversed orientation) pPTC1-PTC1::loxp (reversed orientation) pRPT2-RPT2::loxp (reversed*

Strain	Relevant genotype
	orientation) pSOK1-SOK1-loxp-KANMX-loxp (reversed orientation) SGO1-6HIS-3FLAG::URA3
AMy25299	*MATa cdc20::URA3::pMET-CDC20 SCC1-6HA pMAF1-MAF1::loxp (reversed orientation) pPTC1-PTC1::loxp (reversed orientation) pRPT2-RPT2::loxp (reversed orientation) pSOK1-SOK1-loxp-KANMX-loxp (reversed orientation) BRN1-6HIS-3FLAG::NATMX6*
AMy25379	*MATa cdc20::URA3::pMET-CDC20 SCC1-6HA BRN1-6HIS-3FLAG::NATMX6*
AMy25409	*MATa cdc20::URA3::pMET-CDC20 SCC1-6HA SGO1-6HIS-3FLAG::URA3*
AMy25764	*MATa, cdc20::URA3::pMET-CDC20 Spc42-tdTomato::NAT leu2::tetR-GFP::LEU2 ~21kbR_CEN3::tetOx224::URA3*
AMy26822	*MATa, cdc20::URA3::pMET-CDC20 chl4Δ::KanMX6*
AMy26964	*MATa, cdc20::URA3::pMET-CDC20 Spc42-tdTomato::NAT leu2::tetR-GFP::LEU2 ~12kbR_CEN1::tetOx224::URA3*
AMy26965	*MATa, cdc20::URA3::pMET-CDC20 Spc42-tdTomato::NAT leu2::tetR-GFP::LEU2 ~12kbR_CEN3::tetOx224::URA3*
AMy26966	*MATa, cdc20::URA3::pMET-CDC20 SCC1-6HA rad61Δ::TRP1*
AMy27213	*MATa, cdc20::URA3::pMET-CDC20 Spc42-tdTomato::NAT leu2::tetR-GFP::LEU2 ~4kbR_CEN4::tetOx224::URA3*

Strain	Relevant genotype
AMy27214	*MATa, cdc20::URA3::pMET-CDC20 Spc42-tdTomato::NAT leu2::tetR-GFP::LEU2 ~11.5kbR_CEN4::tetOx224::URA3*
AMy27215	*MATa, cdc20::URA3::pMET-CDC20 Spc42-tdTomato::NAT leu2::tetR-GFP::LEU2 pMAF1-MAF1::loxp (reversed orientation) pPTC1-PTC1::loxp (reversed orientation) pRPT2-RPT2::loxp (reversed orientation) pSOK1-SOK1-loxp-KANMX-loxp (reversed orientation) ~13.5kbR_CEN4::tetOx224::URA3*
AMy27216	*MATa, cdc20::URA3::pMET-CDC20 Spc42-tdTomato::NAT leu2::tetR-GFP::LEU2 pMAF1-MAF1::loxp (reversed orientation) pPTC1-PTC1::loxp (reversed orientation) pRPT2-RPT2::loxp (reversed orientation) pSOK1-SOK1-loxp-KANMX-loxp (reversed orientation) ~4kbR_CEN4::tetOx224::URA3*
AMy27936	*MATa, cdc20::URA3::pMET-CDC20 PMAF1-MAF1::loxp (in opposite orientation) PPTC1-PTC1::loxp (reversed orientation) PRPT2-RPT2::loxp (reversed orientation) PSOK1-SOK1-loxp-KANMX-loxp (reversed orientation)*
AMy28477	*MATa, cdc20::URA3::pMET-CDC20 Spc42-tdTomato::NAT leu2::PURA3::tetR-GFP::LEU2 tetOx224-URA3 (tetOs ~23kb to right of CEN4)*
AMy28478	*MATa, cdc20::URA3::pMET-CDC20 Spc42-tdTomato::NAT leu2::PURA3::tetR-GFP::LEU2 tetOx224-URA3 (tetOs ~23kb to right of CEN4) MCD1-6HA PMAF1-MAF1::loxp (in opposite orientation) PPTC1-PTC1::loxp (reversed orientation) PRPT2-*

Strain	Relevant genotype
	RPT2::loxp (reversed orientation) PSOK1-SOK1-loxp-KANMX-loxp (reversed orientation)
AMy28726	*MATa cdc20::URA3::pMET-CDC20 Spc42-tdTomato::NAT leu2::PURA3::tetR-GFP::LEU2 tetOx224-URA3 (tetOs ~0.5kb to right of CEN3. INSIDE the boundary) MCD1-6HA PMAF1-MAF1::loxp (in opposite orientation) PPTC1-PTC1::loxp (reversed orientation) PRPT2-RPT2::loxp (reversed orientation) PSOK1-SOK1-loxp-KANMX-loxp (reversed orientation)*
AMy28787	*MATa ipl1-321 Spc42-tdTomato::NAT leu2::PURA3::tetR-GFP::LEU2 tetOx224-URA3 (tetOs ~4kb to right of CEN4)*
AMy28788	*MATa Spc42-tdTomato::NAT leu2::PURA3::tetR-GFP::LEU2 tetOx224-URA3 (tetOs ~4kb to right of CEN4)*
AMy28790	*MATa ipl1-321 MCD1-6HA Spc42-tdTomato::NAT PMAF1-MAF1::loxp (in opposite orientation) PPTC1-PTC1::loxp (reversed orientation) PRPT2-RPT2::loxp (reversed orientation) PSOK1-SOK1-loxp-KANMX-loxp (reversed orientation) leu2::PURA3::tetR-GFP::LEU2 tetOx224-URA3 (tetOs ~4kb to right of CEN4)*
AMy28791	*MATa MCD1-6HA Spc42-tdTomato::NAT PMAF1-MAF1::loxp (in opposite orientation) PPTC1-PTC1::loxp (reversed orientation) PRPT2-RPT2::loxp (reversed orientation) PSOK1-SOK1-loxp-KANMX-loxp (reversed orientation) leu2::PURA3::tetR-GFP::LEU2 tetOx224-URA3 (tetOs ~4kb to right of CEN4)*

Strain	Relevant genotype
AMy28792	*MET-CDC20::URA3 Spc42-tdTomato::NAT leu2::PURA3::tetR-GFP::LEU2 tetOx224-URA3 (tetOs ~4kb to right of CEN4) pURA3::ABIx2-V5::TRP1 (between RAD57 and MAF1 at chr IV RIGHT border, transcribed away from CEN4) pURA3::PYLx2-3FLAG::HisMX6 (between PTC1 and MED2 at chr IV LEFT border, transcribed away from CEN4)*
AMy28793	*MET-CDC20::URA3 Spc42-tdTomato::NAT leu2::PURA3::tetR-GFP::LEU2 tetOx224-URA3 (tetOs ~11.5kb to right of CEN4) pURA3::ABIx2-V5::TRP1 (between RAD57 and MAF1 at chr IV RIGHT border, transcribed away from CEN4) pURA3::PYLx2-3FLAG::HisMX6 (between PTC1 and MED2 at chr IV LEFT border, transcribed away from CEN4)*
AMy28794	*MCD1-6HA MET-CDC20::URA3 Spc42-tdTomato::NAT PMAF1-MAF1::loxp (in opposite orientation) PPTC1-PTC1::loxp (reversed orientation) PRPT2-RPT2::loxp (reversed orientation) PSOK1-SOK1-loxp-KANMX-loxp (reversed orientation) leu2::PURA3::tetR-GFP::LEU2 tetOx224-URA3 (tetOs ~4kb to right of CEN4) pURA3::ABIx2-V5::TRP1 (between RAD57 and MAF1 at chr IV RIGHT border, transcribed away from CEN4) pURA3::PYLx2-3FLAG::HisMX6 (between PTC1 and MED2 at chr IV LEFT border, transcribed away from CEN4)*
AMy28878	*MCD1-6HA MET-CDC20::URA3 Spc42-tdTomato::NAT PMAF1-MAF1::loxp (in opposite orientation) PPTC1-PTC1::loxp (reversed orientation) PRPT2-RPT2::loxp*

Strain	Relevant genotype
	(reversed orientation) PSOK1-SOK1-loxp-KANMX-loxp (reversed orientation) leu2::PURA3::tetR-GFP::LEU2 tetOx224-URA3 (tetOs ~13.5kb to right of CEN4) pURA3::ABIx2-V5::TRP1 (between RAD57 and MAF1 at chr IV RIGHT border, transcribed away from CEN4) pURA3::PYLx2-3FLAG::HisMX6 (between PTC1 and MED2 at chr IV LEFT border, transcribed away from CEN4)

Strains AMy22078 onwards were generated in this study.

Appendix III – ChIP-seq and Hi-C libraries generated in this study

Sample	Total unique reads (R1/R2)	Valid unique Hi-C pairs
WT - Tension	36 299 576 / 43 078 602	17 937 575
WT – No tension	34 921 366 / 42 352 447	17 779 189
chl4Δ - Tension	38 653 664 / 44 991 486	19 530 920
sgo1Δ – No tension	37 702 242 / 43 924 423	20 318 535
sgo1-3A – No tension	45 109 744 / 53 348 344	21 068 633
chl4Δ – No tension	64 306 395 / 70 848 109	62 060 500
Reoriented - Tension	70 760 639 / 76 584 915	76 278 472

ChIP-seq library	Total reads (M)	Unique reads (M)
Scc1-6HA *rad61Δ* Tension input	6.2	5.0
Scc1-6HA *rad61Δ* No tension input	5	4.2
Scc1-6HA *rad61Δ* Tension IP	30	11.4
Scc1-6HA *rad61Δ* No tension IP	27.4	11.9
Scc1-6HA Reoriented Tension Input	5.8	5.0
Scc1-6HA Reoriented No tension Input	5.4	4.7
Scc1-6HA Reoriented Tension IP	29.8	18.2
Scc1-6HA Reoriented No tension IP	28.8	13.9
Sgo1-6HIS-3FLAG Reoriented No tension Input	4	3.3

Sgo1-6HIS-3FLAG Reoriented No tension IP	29.6	15.0
Brn1-6HIS-3FLAG Reoriented No tension Input	0.4	0.4
Brn1-6HIS-3FLAG Reoriented No tension IP	4	3.3
Sgo1-6HIS-3FLAG No tension Input	5.2	4.2
Sgo1-6HIS-3FLAG No tension IP	28.8	13.9
Brn1-6HIS-3FLAG No tension Input	4.8	3.9
Brn1-6HIS-3FLAG No tension IP	30	15.1
Scc1-6HA WT Tension input	5.2	4.2
Scc1-6HA WT No tension input	5.4	4.3
Scc1-6HA WT Tension IP	27.8	17.1
Scc1-6HA WT No tension IP	27	14.7
Scc1-6HA *chl4Δ* Tension input	5.2	4.2
Scc1-6HA *chl4Δ* No tension input	4.2	3.4
Scc1-6HA *chl4Δ* Tension IP	24	12.3
Scc1-6HA *chl4Δ* No tension IP	24	11.5
Sgo1-6HA No tension Input	3.6	3.1
Sgo1-6HA No tension IP	5.2	3.6
Brn1-6HA No tension Input	3.2	2.8
Brn1-6HA No tension IP	7	3.9

Appendix IV – SacCer3 genome coordinates used to generate ChIP-seq and Hi-C pile-ups

Chromosome	Left border	CEN	Right Border
1	147806	151523	160211
2	235228	238265	244311
3	101301	114443	130517
4	440767	448766	456742
5	145845	152046	166000
6	143961	148569	154425
7	489446	496979	504623
8	100445	105645	109984
9	350183	355687	365766
10	431178	436366	440892
11	432938	440188	446723
12	134084	150888	161639
13	256267	268090	277501
14	616470	628817	638959
15	321621	326643	334818
16	550434	556015	560618

Chromosome	Left arm peak	Right arm peak
1	134298	166415
2	212364	284156
3	92933	139263
4	401066	477402
5	138610	189212
6	137306	172326
7	469180	531467
8	76328	119742
9	318507	377053
10	409512	453193
11	411713	458573
12	128912	168074
13	251386	294742
14	609784	648792
15	309510	367254
16	533727	577268